Steel and Industrial Edition

RHI Bulletin >1>2016

The Journal of Refractory Innovations

70th anniversary of RHI's Journal of Refractory Innovations

RHI Bulletin >1>2016

The Journal of Refractory Innovations

RHI Bulletin 1/2016
Steel and Industrial Edition

Published by:	RHI AG, Vienna, Austria
Chief Editor:	Stefan Schriebl
Executive Editors:	Markus Dietrich, Alexander Maranitsch, Alfred Spanring, Marcos Tomas
Raw Materials Expert:	Gerald Gelbmann
Lingual Proofreader:	Janine Pink
Project Manager:	Ulla Kuttner
Photography, Graphics and Production:	Markus Kohlbacher, Christoph Brandner
Design and Typesetting:	Universal Druckerei GmbH, Leoben, Austria

Contact: Ulla Kuttner
RHI AG, Technology Center
Magnesitstrasse 2
8700 Leoben, Austria
E-mail: bulletin@rhi-ag.com
Tel: +43 50213-5323
www.rhi-ag.com

The products, processes, technologies, or tradenames in the RHI Bulletin may be the subject of intellectual property rights held by RHI AG or other companies.

RHI worldwide

RHI Combines Caster Competence

Worldwide >> The constant development of RHI´s customers processes at steel plants, in terms of efficiency as well as diversification of the final product portfolio require a very specific knowledge of the application, especially of the continuous casting process. Consequently, RHI´s customers expect the corresponding know-how and application expertise, not only for the different refractory products, but also for the overall process of continuous casting. In order to address these requirements, as per July 1st, 2016, RHI has aligned the organization in the flow control marketing, combining the product managements "Tundish" and "Isostatic products" into the department "Continuous Casting". With establishing this new expert group, RHI will be able to service and support customers in all questions related to the transfer of liquid steel from ladle to mould including relevant process consultancy.

Training Opportunities

North America >> As a part of customer service RHI performed EAF training for the engineers and operators at the site regard "Electric arc furnace process and refractory control" in Gerdau Manitoba, Canada. The training addressed some practical and theoretical information for standard and non-standard operation practices include EAF metallurgy, process control, EAF refractory lining, and EAF maintenance. The training was very well received by the Gerdau management team. So much so that they have invited the trainer back to continue his efforts.

Tundish Technology and Processes: A New Road Map

Worldwide >> The RHI Bulletin editorial team regrets a typographical error in the METEC>1>2015 Steel Edition. In the paper titled "Tundish Technology and Processes: A New Roadmap" the upper and lower Al wt.% values are inverted in Figure 6: The blue line should represent 0.025 wt.% Al and the light grey line 0.015 wt.% Al.

Emergency Delivery — A new RHI GLASS Service

Europe >> RHI Glass has established a 24/7/365 Emergency Delivery Service for the glass industry and maintains appropriate emergency material, in various dimensions and packaging units for the most common hot repairs. RHI Glass guarantees delivery of refractory bricks, AZS, and refractory mixes within 24 hours for Germany and other selected European countries. For the customer this service creates free storage space and avoids capital being tied up in inventory. It also leads to reduced defect and follow up costs. RHI Glass provides expert advice before the repair and support in carry out hot repairs through its network of experts. The RHI GLAS emergency hotline is always available in case of an urgent risk of damage affecting the glass tank. It can also be contacted if the necessary refractory material for a repair is not on site or unavailable at short notice. The telephone number for the RHI GLAS emergency service is: +49 611 2365-222.

OMK Steel/FLS Contract: Life Time Record

Russia >> Within one year of signing the FLS contract with OMK Steel record parameters have been achieved. In June 2016 a ladle life time of 100 heats was reached, with specific consumption 3.73 kg/t of liquid steel. Successful development and optimization of the refractory concept was implemented with the support of Product Management Ladle, Marketing Service Metallurgy, and Production. The measures included following projects: qualitative improvements (COMPAC SOL technology, CN-bricks, third slag zone repair), "Clean Steel" project with metallurgical process reforming and the introduction of high quality RE brands.

Legislative Changes for the Ceramic Industry in 2017

Europe >> In 2017 the best available technology reference documents (BREFs) for the ceramics industry will be reviewed. The European Integrated Pollution Protection and Control Bureau (EIPPCB) organizes and co-ordinates the exchange of information between Member States, Non Governmental Organizations (NGOs) and the industries concerned on Best Available Techniques (BAT). The EIPPCB produces BAT reference documents (BREF) and BAT conclusions. The BAT conclusions are adopted through committee procedures by the European Commission and the emission limits of these conclusions are legally binding.

It is of utmost importance that the limit values are not excessive. To ensure the consideration of the industry input, Cerame Unie has established a taskforce to work on the definition of "best available technique" and realistic limit values for the ceramic industry. The task force is composed of BREF experts from all ceramic sectors. RHI is chairing this working group. Initial steps were to develop a comprehensive questionnaire to describe the the current status of the ceramic industry. This status will provide the baseline to establish the best available technique in the sector. Further meeting are planned with all stakeholders, after which the IPPC Bureau will issue a draft of the document. The draft will be discussed in a series of meetings in Seville, after which the final negotiations to adopt the official text of the BREF will take place. The results of which will have a significant impact on future development and investment decisions in the refractory industry.

RHI worldwide

RHI at Metal & Metallurgy China

China >> RHI Raw Materials Sales presented for the first time at "Metal & Metallurgy China", which took place 17–20 May in Beijing, China. Metal & Metallurgy unifies the trade fairs "China International Foundry Expo", "China International Metallurgical Industry Expo", "China International Industrial Furnaces Exhibition", and "China International Refractories and Industrial Ceramics Exhibition" under one roof. It is the largest trade fair of the metal processing industries in China and the second largest in the world, with approximately 1300 exhibitors and 85000 visitors attending each year.

RHI and Tata Steel–KPO Cooperation Project.

India >> Tata Steel commissioned the Kalinganagar Project (KPO) in March 2016, using RHI refractories in the primary melting and secondary metallurgy units. Unique in this project was that the entire spectrum of activities, from material selection, supplies, material handling on shop floor, installation, and maintenance is carried out by RHI. RHI also presented a workshop "Achieving Excellence in Refractories through Continuous Improvement", which was well attended by steelmaking, ironmaking, refractory, and procurement personnel from Tata Steel–KPO.

First Heat of El-Marakby Steel

Egypt >> El-Marakby Steel (MKS), recently celebrated the initial heat of the new EAF. RHI is the sole refractory supplier for this new plant. With a capacity of 350000 tonnes per year, it will feed the existing rolling mill with square billets for rebar production.

Egyptian Steel is also expecting another start up, with a new Danieli built Consteel plant, with a capacity of 800000 tonnes per year. This will be the second plant in the region to operate with this technology. RHI is also the main refractory supplier for this plant.

RHI Participates at "PetroCem 2016"

Russia >> The 9th "PetroCem" conference and exhibition was held in St Petersburg, Russia, from the 24–26th April. The conference traditionally targets the cement sector of the CIS, however the scope is continually growing. RHI has been a regular participant at this conference in the past. This year RHI was a general sponsor of "PetroCem 2016", made the presentation "Requirements on Basic Refractory Material in Operation of Cement Rotary Kilns", which demonstrated the superiority of RHI hercynite bricks, and had a booth at the associated exhibition. There was significant audience interest in the RHI booth and the conference also provided the opportunity to sign a supply contact for magnesia hybrid spinel bricks to JSC "Asia Cement".

Customer Workshop: Special Waste Incineration

Worldwide >> Operators of special waste incinerators often face the problem of variable operating conditions, the storage of hazardous waste is very strictly controlled and operators need to remove waste in very short time periods. This influences not only the lifetime of the bricks, premature wear of the refractory material is only one reason for shutdowns or maintenance work. As a competent partner in refractory materials, not only a refractory producer, RHI assists customers to increase the lifetime of refractory material.

Recently several customers have taken advantage of this help and professional knowledge. RHI has provided workshops for customers and their staff. Experts from Marketing, Sales, and R&D provide a through overview of basic refractory knowledge, the major factors of influence, and the wide range of products and linings. Customers benefit from a growth in knowledge of refractories, of greater benefit are longer operation times, fewer shut downs and longer lifetime of the refractory material. Reducing the costs of shut downs and maintenance work. RHI produces not only refractory products; it also provides technological services and expert advice.

S Gate Conversions in USA

USA >> The newest ladle slide gate from the Flow Control group has been successfully introduced to the US Marketplace. This year, starting in January, the S Gate has been successfully commissioned in into four steel plants, with an additional steel plant in the midst of commissioning and another scheduled for September.

Gerdau, Beaumont was converted to the S2 ladle gate in January of this year and immediately increased their refractory life. Carpenter, Latrobe was converted to the S2 Gate in January/February and significantly increased their refractory life. Gerdau, Jackson was converted to a S2 (horizontal version) in February/March and saw a dramatic increase in refractory life. Nucor, Hickman was converted in March/April and also increased refractory life. The Nucor, Yamato conversion is in process and the first hot run should begin in August. Another start-up is scheduled at Nucor, Auburn in September to the S2 Slide Gate. The combined efforts of engineers, technicians, training personnel, and sales all helped ensure the success of these projects.

New EBT Taphole Lifetime Record

Qatar >> In the scope of a series of trials at Qatar Steel, a new lifetime record of 308 heats was achieved using RHI patent protected CFD optimized taphole design in combination with the highest performance grade bricks ANKERTAP YY. The average lifetime prior to these trials was 178 heats.

Upcoming Trade Fairs in 2016

Worldwide >> RHI is pleased to be participating in the Metal-Expo, the 22nd International Industrial Exhibition, taking place 8–11 November, 2016 in Moscow, Russia. 570 companies from 34 countries and 28000 visitors are expected to participate.

RHI will also be present at the Aluminium 2016, the 11th World Trade Fair & Conference, which will take place 27th November until 1st December, 2016 in Düsseldorf, Germany. The biennial event brings together more than 1000 exhibitors from more than 50 countries and approximately 27000 trade visitors. We look forward to see you there.

RHI at China Glass Exhibition in Shanghai

China >> The 24th "International Congress on Glass" took place from April 7–11, 2016 in Shanghai. More than 800 delegates from 33 countries and regions attended this meeting. RHI attended as a Silver sponsor. ICG is a significant event in the international glass industry. Glass scientific and technical staff from all over the world attended this meeting and exchanged the latest research results and understanding of the development trend of glass industry.

The 27th "China International Glass" exhibition was held from April 11–14 in Shanghai. More than 880 exhibitors and approx. 22000 visitors from 65 countries attended the trade fair.

Advancements in Impregnation Technology for MagCarbon Bricks

Worldwide >> For many years RHI has used the technology of impregnating MagCarbon bricks to decrease the porosity of bricks and to increase the carbon content in the matrix. However this technology has come under pressure from REACH regulations, prohibiting the use of coal tar pitch and other substances containing elevated amounts of Benzo-a-Pyrene (BaP). RHI's Technology Centre in Leoben was tasked with developing a REACH conforming, health, and eco-friendly alternative. This new process was also required to improve the efficiency and versatility of the impregnation process. Both tasks have been successfully completed. The new impregnation plant in Radenthein is operating flawlessly with higher pressure and optionally under a protective atmosphere. R&D Leoben identified a new, eco-friendly impregnation medium (aliphatic hydrocarbons) with typical BaP content <0.1 ppm, which increases the carbon content of the matrix and lowers porosity to 0.7% (by volume). Due to the extremely low BaP content of the impregnated MagCarbon bricks it is no longer necessary to include hazard and precautionary statements in the material safety data sheets.

RHI Participates at AISTech 2016

USA >> AISTech 2016, the Iron and Steel Technology Conference and Exposition, took place from May 16–19 at the David L. Lawrence Convention Center in Pittsburgh (USA). North America's most important steel trade and conference, the exhibition spanned two levels making it the largest AISTech yet with a total of 542 exhibiting companies. This year 45 countries were represented from the 7764 participants.

RHI participated in the technical sessions, presenting multiple topics including, BOF refractory maintenance practices, using modeling and simulation tools, soft bubbling technology, dry setting tundish mixes, and energy efficiency. AISTech 2017 will take place at the Music City Center, Nashville, from May 8–11.

MagForum 2016

Austria >> The inaugural MagForum 2016 was held May 9–11, 2016 at the Melia Hotel in Vienna. The biennial conference for the development, supply, processing, logistics, and market application of magnesium minerals was founded by IMFORMED (Industrial Mineral Forums & Research Ltd). The congress brought high profile international raw material experts together in the Austrian capital for three days. More than half of the participants visited the RHI Veitsch facility, which has 135 years of industrial magnesite processing history. The factory tour provided the participants interesting insights into production at the facility.

New BOF Taphole System at ArcelorMittal Gent

Europe >> The commissioning phase of the BOF tapping system HYFLO-C and TBD at ArcelorMittal Gent, Belgium, has been successfully completed. The tapehole area was updated using the HYFLO-C, resulting in a lifetime increase from 70 to 120 heats. The taphole break out device was replaced by the latest TBD-400CSH generation, an essential part of the system for fast and efficient changes of the HYFLO-C tapholes. The taphole design has been optimized and specially adapted for the slag retaining system PSS (Pneumatic Slag Stopper) of Primetals and for the highest vessel lifetime demands. ArcelorMittal Gent is the first customer within the ArcelorMittal group to introduce the RHI HYFLO-C and TBD.

www.rhi-ag.com EXCELLENCE
IN REFRACTORIES
RHI

Editorial

We are very proud that this year marks the 70th anniversary of RHI's Journal of Refractory Innovations. Formerly titled the Radex-Rundschau and the Veitsch-Radex Rundschau, it was relaunched in 2003 as the RHI Bulletin: A technical refractories journal focusing on our innovative products and services. Previously published biannually, the Steel and Industrial editions will now typically be consolidated into one edition each year, available as a digital version. This not only provides ecologically benefits, regarding paper consumption and shipping resources, but will also enable efficient and timely delivery.

The first of twelve articles in this edition describes multiple customer advantages that can be realized using the RADEX DPP gas purging system during high-alloyed and stainless steelmaking, including cost savings and increased process safety. This is followed by an overview of the metallurgical and process benefits achieved in converters at Jindal Steel Works with inert gas bottom purging: Through a partnership with RHI, careful slag maintenance strategies have been implemented that improve gas purging efficiency and availability. The various demands on refractories for travelling grate iron ore pelletizing furnaces are detailed in the next paper, which discusses technical approaches that are used to select materials that increase lining performance and reliability. In the fourth article the sources of CO_2 emissions arising from secondary metallurgy practices in the steel ladle are presented as well as approaches to reduce this environmental impact. Inert gas purging is an essential state of the art process step in ladle secondary metallurgy and in the next paper a water modelling study compares three different plug designs and demonstrates the optimal gas purging results that can be achieved with the hybrid plug design. The sixth article provides an overview of RHI's customer tailored solutions to ensure high-quality steel production, focusing on approaches to minimize the risk of gas pick-up during ladle to mould transfer. This is followed by a comprehensive overview of zirconia nozzles for tundish applications and a paper describing methods to investigate zirconia phase transformations in postmortem slag band samples from isostatically pressed continuous casting products.

In the ninth article, the complex refractory wear processes mediated by zinc attack are elucidated; this is relevant to multiple sectors as zinc is a by-product of many metallurgical processes. In the next paper a study is reported that combines the results of hot-stage microscopy and thermodynamic analysis to understand corrosion mechanisms occurring between magnesia refractories and molten slags used in ferroalloy smelting. This is followed by a detailed explanation of the advantages provided by the resonant frequency ratio method to determine the Young's modulus, thereby enabling cylindrical samples to be effectively selected for round robin testing. The last paper in this edition is the summary of an article discussing various approaches to examine the depletion potential of mineral resources, which was published in the International Journal of Life Cycle Assessment.

In closing, once again I would like to wholeheartedly thank all the authors and editorial team for their valued contributions to this edition.

Yours sincerely

Stefan Schriebl
Corporate Research and Development
RHI AG

Contents

8 Benefits from Improved Bath Agitation with the Radex DPP Gas Purging System During EAF High-Alloyed and Stainless Steel Production

14 BOF Bottom Purging Efficiency and the Impact of Slag Maintenance with a Case Study from Jindal Steel Works in India

20 Refractory Applications in Iron Ore Pelletizing Plants—Travelling Grate Furnaces

28 Evaluation of the Potential for Reduction of CO_2 Emissions at the Secondary Metallurgy

35 A Water Modelling Comparison of Hybrid Plug, Slot Plug and Porous Plug Designs

39 Tundish Technology and Processes: Ladle to Mould Systems and Solutions (Part I)

45 RHI Zirconia Nozzles in Tundish Application

51 Characterization Methods to Investigate Zirconia Phase Transformations in Slag Bands

57 Zinc and Refractories

62 Experimental Study of Refractory Wear Mechanisms Caused by Molten Slags

68 Young's Modulus Determination of CCS Cylinders by the Resonant Frequency Method as a Basis Investigation for Round Robin Tests

74 Life Cycle Impact Assessment and Raw Materials

Subscription Service and Contributions

We encourage you, our customers and interested readers, to relay your comments, feedback, and suggestions to improve the publication quality. Furthermore, to receive the RHI Bulletin free of charge or contribute to future editions please e-mail your details (name, position, company name, and address) to the Subscription Service:

E-mail: bulletin@rhi-ag.com
Phone: +43 50213-5323

RHI Bulletin > 1 > 2016, pp. 8–13

Marcus Kirschen, Reinhard Ehrengruber and Karl-M. Zettl

Benefits from Improved Bath Agitation with the Radex DPP Gas Purging System During EAF High-Alloyed and Stainless Steel Production

Modern production processes of high alloyed and stainless steel grades are subject to the cost-optimized production of raw steel or molten metal combined with high flexibility. Excellent mixing of the steel melt helps to improve mass and heat transfer in the EAF, in order to accelerate the melting of heavy scrap and alloys, decarburization, homogeneous superheating, alloy distribution, and to avoid skull formation and solid remainders that may obstruct tapping. The RADEX DPP system generates customer benefits by improving EAF processes during high-alloyed stainless steel making. The most important effect of the enhanced steel bath mixing besides improved heat transfer and decarburization is a decreased chromium oxidation. Firstly, chromium oxidation is decreased by improving the homogeneous distribution of carbon and chromium in the melt. Secondly, build-up of chromium-containing solids in the EAF hearth and skull formation is decreased by stronger melt movement. The cost savings of both effects economically justify the application of gas purging in EAF stainless steelmaking. Case studies are presented demonstrating the advantages.

Application of Gas Purging for Stainless Steelmaking in EAF

The production of high alloyed and stainless steel grades covers approx. 2.5% of total steel production for many years, i.e., 41.5 million tonnes in 2015. The standard production process is based on melting of steel scrap and alloys in the EAF and subsequent decarburization and refinement of the molten metal in the AOD converter or, rarely, by VOD treatment.

At modern high productivity levels in steel plants and minimills with electric arc furnaces, even small improvements of the EAF process provide considerable cost savings. Such improvements can be realized, for example, by efficiently increasing mass and energy transfer in the EAF. Therefore, optimizing flow patterns in the steel bath is important for efficient scrap and ferro-chromium melting and high melt homogeneity [1, 2, 5, 6, 7]. By far the most efficient movement of the entire steel melt is generated by gas purging, where columns of bubbles rise through the steel bath (Figure 1).

Metallurgical Constraints to Alloyed and Stainless Steelmaking

Additional constraints apply to the production of alloyed or high-alloyed chromium or Cr-Ni molten metal in the EAF. As carbon and chromium oxidation occurs in the molten metal at very similar oxygen activities, special care is taken to minimize chromium loss during oxygen injection in the EAF. A homogeneous distribution of carbon, chromium, and oxygen in the molten metal significantly helps avoid concentration gradients and improves yields.

A low FeOx content and a high chromium oxide content in the EAF slag often inhibits efficient slag foaming during stainless steel production. This is due to the low Cr_2O_3 solubility in basic EAF slag that results in precipitation of Cr_2O_3 bearing solids and a higher slag viscosity. A high oxidation of chromium in the EAF is in most cases caused by carbon deficiency in the molten metal area that is affected by the oxygen injector (Figure 2).

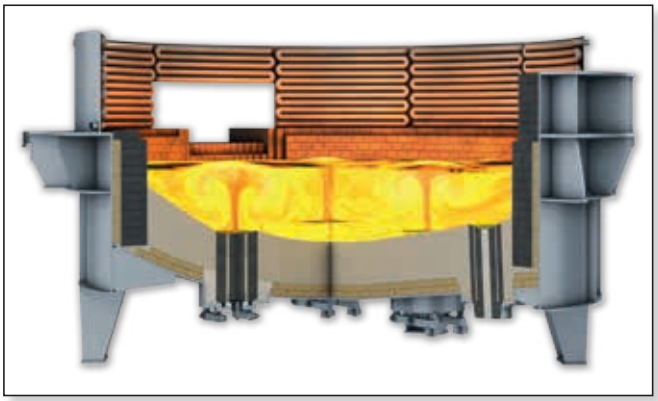

Figure 1. *Efficient mixing throughout the steel melt using 3 gas purging plugs in the EAF hearth (Figure based on computational fluid dynamic (CFD) modelling of steel flow pattern).*

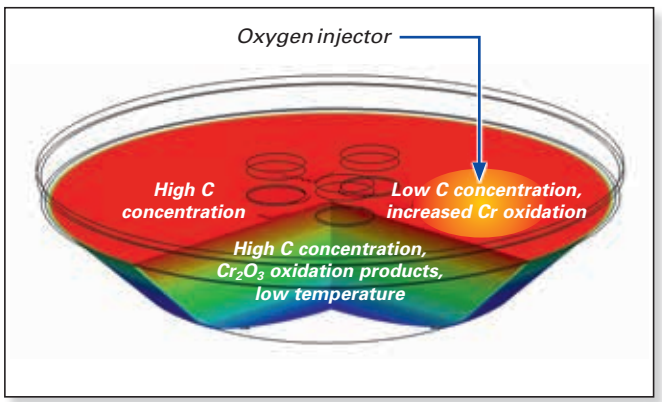

Figure 2. *Increased Cr oxidation in stainless steelmaking due to low mixing of the metal volume, i.e., low mixing of C-rich melt with C-deficient melt where Cr oxidation occurs. A sufficiently high C content minimizes unwanted Cr oxidation.*

The unwanted effects are:

>> Cr losses to the slag, decreasing the Cr yield.
>> Impaired slag foaming due to:
Highly increased slag viscosity resulting from high levels of Cr_2O_3 containing solid particles.
Low levels of O_2 gas injection result in low levels of CO gas generation.

The usual EAF operations implemented to avoid these disadvantages are:

>> Minimum use of oxygen in the EAF.
>> Oxygen injection as late as possible, in order to refine a high carbon containing melt.
>> Reduction of Cr_2O_3 by adding FeSi to the slag before or during tapping.
>> Tapping the molten metal with a specific content of Si together with the Cr_2O_3-rich slag in order to reduce the Cr_2O_3 in the slag and thereby increase Cr levels in the steel during tapping:

$$2\ Cr_2O_3 + 3\ Si \rightarrow 4\ Cr + 3\ SiO_2$$

As a consequence of these EAF operations during stainless steelmaking, mixing of the molten metal by the oxygen injectors is lower than during usual EAF operations. As a result other disadvantages occur:

>> A high carbon content in the molten metal is difficult to oxidize over the full volume of the EAF molten metal due to poor mixing.
>> Mixing of C-rich volumes with C-poor metal volumes is very restricted resulting in higher than necessary Cr oxidation near the injectors.
>> Late reaction of O-rich metal volumes with C-rich metal volumes during tapping results in retarded CO boiling of the melt that may require interruption of the tapping.
>> Due to poor movement of the molten metal, Cr_2O_3-containing solids (chromites, spinels, see Table I) with high melting points are enriched in the EAF hearth and can increase the bottom thickness, decreasing the EAF volume and affecting tapping.

Increased movement and mixing of the molten metal using the RADEX DPP system (Figure 3) is the most efficient measure to:

>> Improve the Cr yield in stainless steelmaking.
>> Decrease bottom buildup.
>> Avoid sudden CO boiling due to unbalanced reactions between dissolved C and O.

In foundries, metallurgical fine tuning of the molten metal is often performed in the EAF. The yield of ferroalloys is dependent on the activity of the metal alloy in the steel melt and the activity of its oxides in the slag. Compositional gradients in the molten metal lead to higher alloy oxidation than necessary. Stirring the melt using DPP's increases homogeneity of the melt and improves the yield.

Efficient decarburization of the molten metal to low values with minimum oxidation of metal alloys requires decreased CO partial pressure that is realized either by introducing argon or nitrogen gas at atmospheric pressure in the AOD converter or in a vacuum in the VOD.

EAF Bottom Gas Purging Technology

Currently, gas purging systems with a multi-hole design of the purging plug for gas injection to the steel melt represent the majority of bottom purging systems in EAFs in the steel industry worldwide; for example the RHI direct purging plug (RADEX DPP) series. Nitrogen and/or argon gas is applied depending on availability and metallurgical necessity.

Oxidation products	Melting temperature
Cr_2O_3	2400 °C
Al_2O_3	2050 °C
$(Mg,Fe)Cr_2O_4$	> 1850 °C
$MgAl_2O_4$	2135 °C

Table I. *Melting temperatures of various oxidation products.*

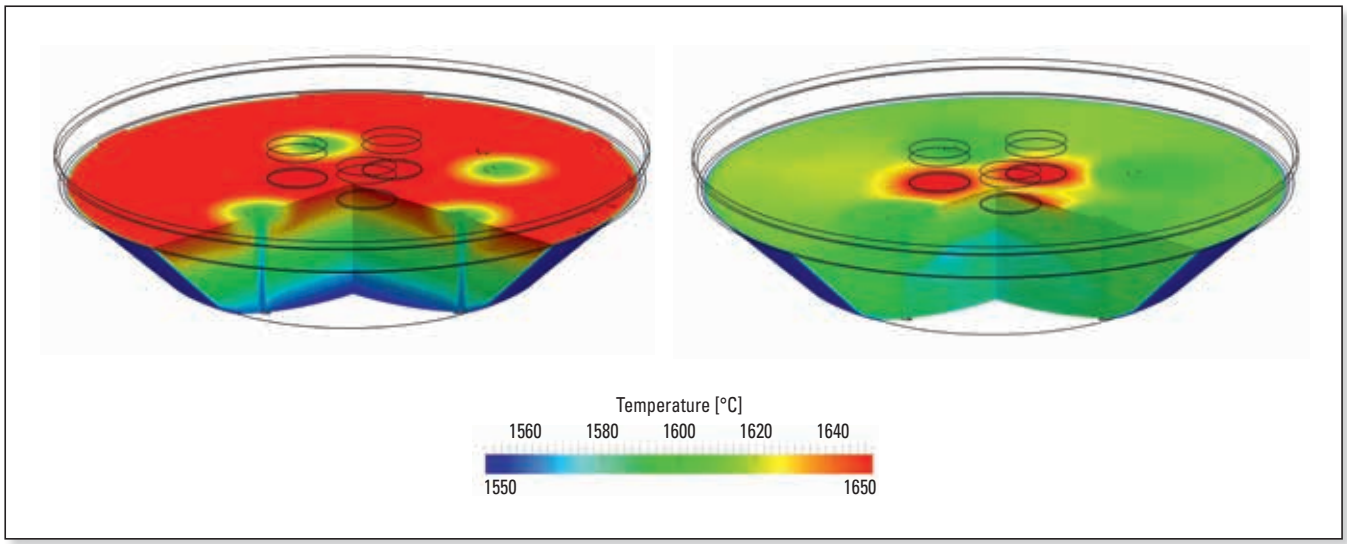

Figure 3. *The RADEX DPP system increases mixing and reduces the metal volume with a low temperature and high levels of oxidation products in the EAF bottom during stainless steelmaking.*

Safety of EAF Gas Purging System

Gas purging plugs are installed into the EAF hearth through a channel comprising of surrounding blocks (Figure 4), thus firstly facilitating exchange of the purging plug in the EAF hearth and secondly increasing safety standards as the hearth ramming mix is installed, deaired, compacted, and sintered without interfering with the purging system. The remaining gap around the purging plug is filled with two special filling mixes, optimized for the special sintering behaviour required near the purging plug (Figure 4). By using this standardized lining strategy, the highest safety requirements are fulfilled and breakout incidents have become obsolete.

Gas is supplied to the steel bath through numerous steel tubes (Figure 5). By providing multiple small holes, infiltration of the brick by melt or slag at low gas flow rates is restricted to the upper few millimetres of the plug. The reopening of blocked tubes, by melt movement caused by gas ingress through neighbouring tubes, occurs and is reported as common during RADEX DPP gas purging operations. In contrast, single-hole purging plugs typically remain blocked after deep infiltration of the one tube.

A wear indicator in the purging plug is based on a pressurized gas line. A pressure drop through the opened wear line indicates a remaining minimum brick length and the purging plug can be closed safely by interrupting the gas supply.

In small EAF's used in foundries for example, very low gas flow rates are applied to avoid an open eye in the steel melt, due to the decreased slag thickness. Sometimes only one purging plug is installed and high reliability of gas purging is needed. Very low gas flow rates require precise gas control to avoid infiltration and blocking. RADEX DPP purging plugs with an optimized number of gas tubes and unique hybrid plugs have performed very well in small EAF's when operated at very low gas flow rates.

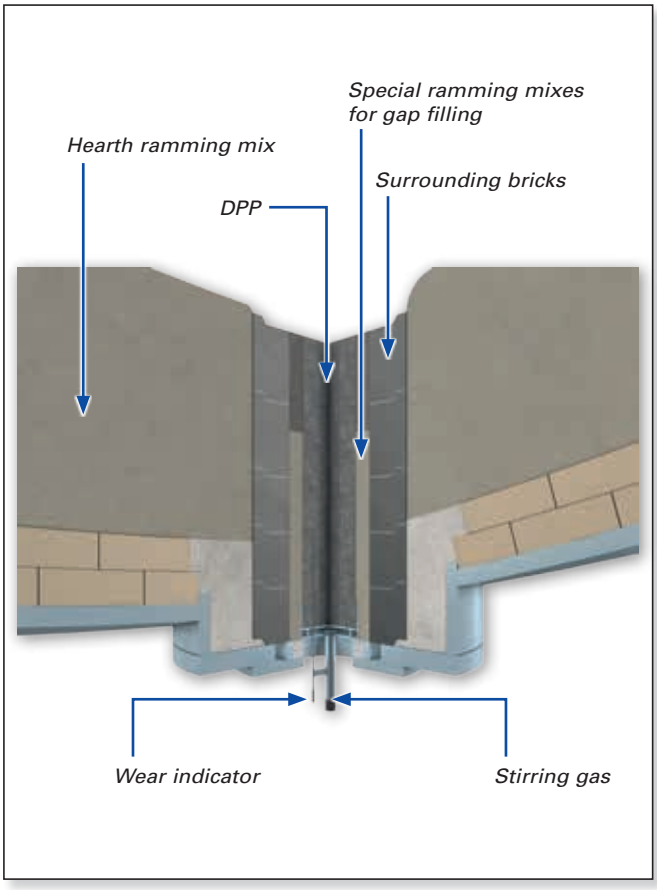

Figure 4. *Schematic sketch of an installed RADEX DPP in the EAF hearth lining, showing the surrounding brick channel, central purging plug, and special gap-filling ramming mixes.*

Gas Control Unit for BOF Converters, EAF and Secondary Metallurgy (Ladle, AOD, etc.)

RHI provides an entire gas purging system comprising the refractory bricks and mixes, installation procedure, process support, and the gas control unit. The gas control unit was newly developed by INTERSTOP/RHI based on decades of experience with gas purging [3].

A typical gas control station to supply 1–6 RADEX DPP purging plugs in the EAF is shown in Figure 8. Each plug is controlled separately. Nitrogen and/or argon is used. The gas flow rates can be regulated independently of the EAF control, by using particular EAF operating parameters, or by incorporating it into the EAF control system.

The RHI RADEX DPP gas purging system increases significantly the availability and reliability of gas purging during the entire EAF campaign by supplying the complete gas purging system with top technological solutions. Technical advantages of the state-of-the-art gas purging systems from INTERSTOP/RHI are:

>> Modular, maintenance-friendly design (Figure 6).
>> 100% leak-free system due to O-ring sealed standard blocks instead of pipes.
>> Possibility to control the stirring efficiency.
>> Visualization of all input and output signals on customer demand.
>> Error report with failure detection.
>> Process data availability through embedding into existing IT infrastructure for data transfer and processing.
>> Program language Siemens Step 7/WinCC flexible or TIA Portal.
>> Accurate and individual flow control for multi-plug purging systems.
>> Typical guaranteed parameters of a INTERSTOP/RHI system are:
  – 100 % leak-free system
  – Accuracy of +/-3%
  – Setting time <500 ms

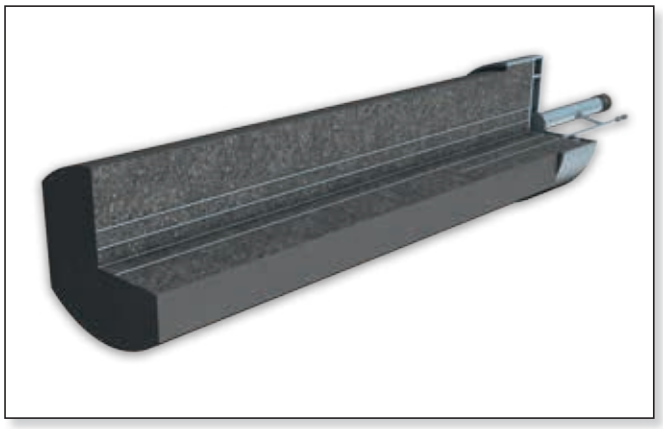

Figure 5. *RADEX DPP direct purging plug for EAF gas stirring.*

The general characteristics of the INTERSTOP/RHI gas purging systems for EAF and secondary metallurgy are:

>> Holistic, state-of-the-art EAF gas purging solution. Control of the entire gas purging technology from refractory to valve control and purging strategy.
>> Integrated solution from gas supply and control, purging plug, and metallurgical know-how.
>> One-stop project management for systems and refractories.
>> Technical support by experts with process knowledge.
>> Combined excellence of top suppliers. INTERSTOP gas control systems and RHI refractories.
>> Full integration in customers' process control system at Level 0 to Level 2.
>> Simple and cost-effective serviceability due to modular design.
>> Highly precise mass flow control, latest generation of mass flow controller (MFC's).
>> Quick response of flow rate to set value.
>> User-friendly intuitive control panel and visualisation.
>> Very compact design requires very little space (Figure 7).
>> Customer-specific software solutions.
>> Exact adjustability of purging gas type and flow rate over entire heat cycle.
>> Programmable gas flow rates for distinct steel grades or production programs.

Benefits for EAF Process and Refinement of Stainless Steel Production

The EAF process benefits realized using direct gas purging systems are related to an overall increased steel bath movement as well as intensified mixing between the lower and upper steel melt volumes. The specific reported benefits of RADEX DPP bottom gas purging systems for stainless steel production include:

Increased thermal and temperature homogeneity in the steel melt:

>> Decreased melting time of scrap and alloys.
>> Increased heat transfer during the superheating period.
>> Increased efficiency of power transfer.
>> Decreased specific electrical energy demand.
>> Decreased deviation between the measured steel temperature in the EAF and the ladle furnace.
>> Avoidance of skull formation or debris in the EAF hearth after tapping, decreased or prevented build-up of EAF hearth ("clean furnace").

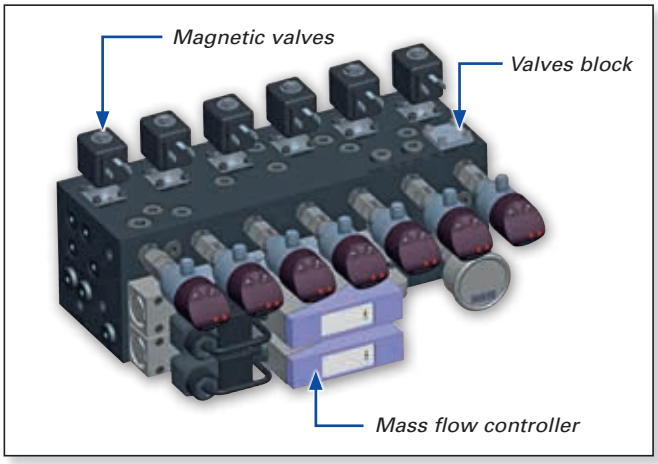

Figure 7. *Compact block of RHI/INTERSTOP gas control unit [3].*

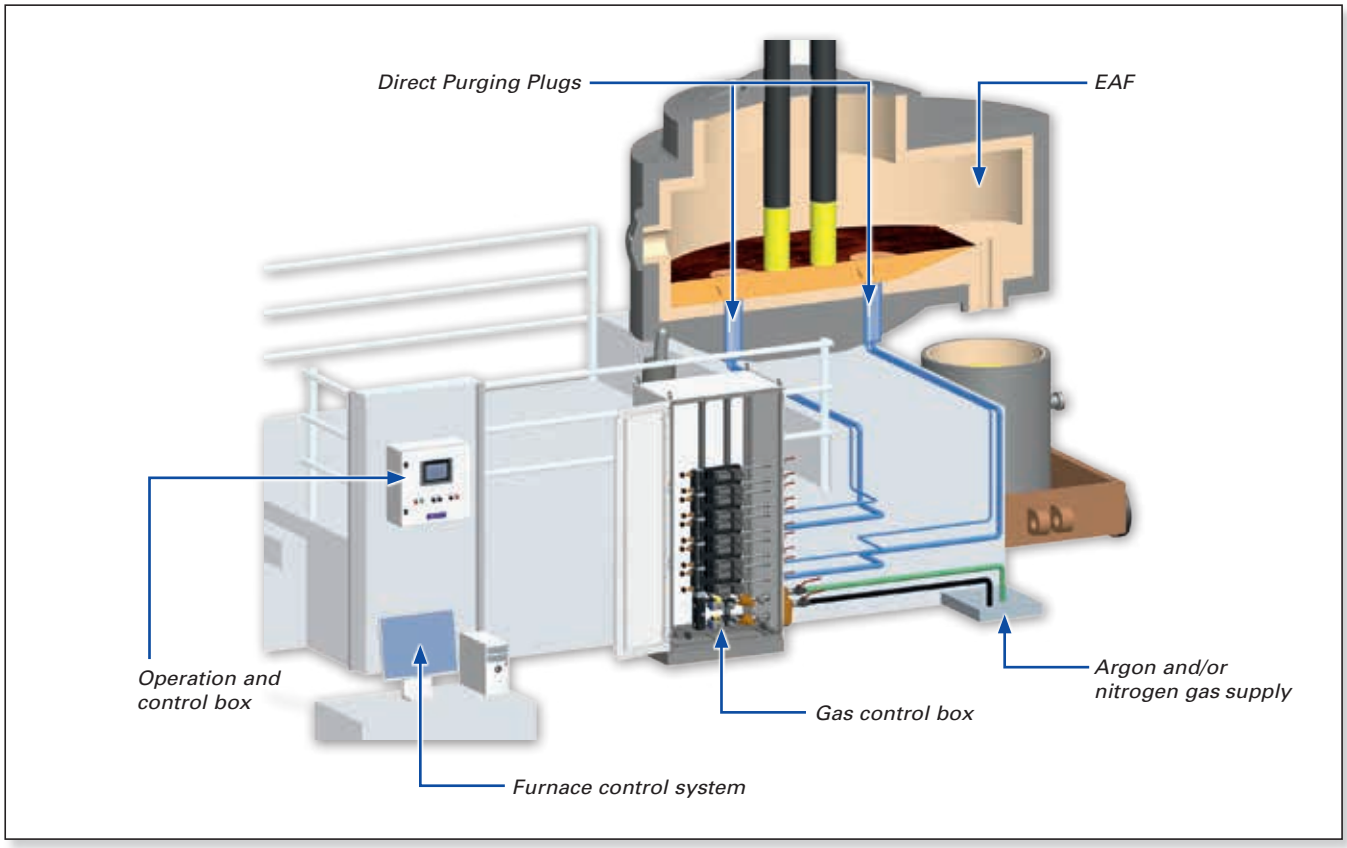

Figure 6. *Setup of a gas control station and supply of the gas purging plugs in the EAF [3].*

Increased chemical homogeneity in the steel melt:

>> Increased metal yield.
>> Decreased variation in steel analysis, better process control.
>> Increased yield from alloy addition.
>> Decreased Cr_2O_3 content of slag.
>> Increased rate of carbon oxidation.
>> [C] x [O] levels closer to equilibrium conditions, resulting in less alloy addition, better alloy prediction, and more stable ladle furnace operations.
>> Improved dephosphorization.
>> Improved efficiency of oxygen injection.

Generation of gas bubble columns in the steel melt:

>> Avoidance of instantaneous or retarded CO boiling in the steel melt

Case Studies of Process Benefits by Gas Purging in Stainless Steel Production

DPP gas purging systems have been installed in EAF's used for stainless and special steel production as well as in foundry EAF's. For these applications, the EAF bottom gas purging systems rapidly proved to be sustainable EAF technology for the customers:

100 tonne EAF in Asia:

>> 100 tonne AC EAF for stainless steel production via the AOD process.
>> Three DPP's.
>> Gas flow rate per plug from 50–110 l/min.
>> Tapping via a launder.
>> 1000 heats lining life per campaign.
>> Charge: 65% steel scrap, 15% FeCr, 10% FeNi, 10% internal scrap.
>> 1.5% decrease of Cr_2O_3 in slag, i.e., minimum 1.1 kg Cr/t saving.
>> Overall yield increase: +0.5%, i.e., 5 kg/t (Table II).
>> Productivity increase of 0.5 heats per day.

Slightly lower tapping temperature at the EAF with the same temperature at the AOD indicates higher thermal homogeneity of the metal volume in the EAF with the DPPs during the temperature measurement.

50 tonne EAF in Europe:

>> 50 tonne AC EAF for alloyed and stainless steel production, special products.
>> Moderate use of oxygen by a door lance.
>> Lifetime of hearth lining and DPP plugs is approx. 800–1000 heats.
>> Three DPP's (two near the electrodes, one DPP in EBT area), due to technical reasons one EAF campaign only with one DPP in EBT area.
>> Set-points of gas flow rates were decreased to 25 l/min in the past with no reports of blockage of DPP purge plugs.
>> Data from four EAF campaigns were assessed (Table III).

The RADEX DPP system decreased the tap-to-tap times, firstly due to shorter power-off times because of decreased sudden CO reaction, degassing and boiling, and secondly because the Al and FeSi addition to the residual melt for removal of solids and build-ups in the EAF bottom was decreased. The operation of all three DPP's decreased the overheating of upper steel melt with a higher thermal homogeneity of steel melt. The EAF energy efficiency increased significantly (lower specific electricity and oxygen consumption), -17 kWh/t equivalent.

Other DPP Case Studies:

>> Three DPP purging plugs were installed in a 140 tonne EAF used for stainless steel production and operated at a constant gas flow rate of 100 l/min. By increasing the bath agitation and thermal exchange, the electrical energy transfer efficiency was increased and the oxygen consumption was significantly decreased by 10 m^3/t. The most important result of the decreased oxygen input was the 4.5% yield increase and a reduction in the tap-to-tap time of 9 min. With a decrease in Cr deslagging, the lime requirement was reduced by 2 kg/t.
>> The application of a single DPP bottom gas purging system in a 6 tonne foundry EAF used for specialty steel and high-alloyed steel products resulted in a significant yield increase from the alloy addition. A 10 l/min gas flow rate was applied.
>> The installation of a DPP system in a 120 tonne EAF increased the metal yield by more than 2% and decreased the electical enegy demand by 17 kwh/t, FeSi addition was decreased by 23%.

100 tonne EAF	EAF process data		
	without DPP	with 3 DPP	difference
Charged weight [t]	100	100	0.0
Tap weight [t] and yield [%]	93.5	94.0	+0.5
Tap-to-tap [min]	95	93	-2.0
Power-on time [min]	50	48	-2.0
Energy [kWh/t]	385	380	-5.0
Oxygen [m^3/t]	11.5	11.0	-0.5
C content before tapping [%]	1.8	1.8	0.0
Temperature at EAF tap [°C]	1545	1543	-2.0

Table II. *Process improvements by EAF gas purging.*

50 tonne EAF	EAF process data		
	with 1 DPP	with 3 DPP	difference
Charged weight [t]	52.38	51.80	-0.58
Tap weight [t]	49.98	50.12	+0.14
Yield [%]	95.40	96.10	+0.70
Power-on time [min]	36.30	37.70	+1.40
Power-off time [min]	38.20	32.00	-6.20
Tap-to-tap time [min]	74.50	69.70	-4.80
Tap temperature [°C] (*)	1615	1599	-16.00
Oxygen [m^3/t]	9.10	8.62	-0.48
Energy [kWh/t]	558.50	543.40	-15.10

Table III. *Process improvements by EAF gas purging.*
(*) Indicating higher thermal homogeneity of the molten metal.

>> The installation of four DPP purging plugs in an 150 tonne EAF for stainless steel production resulted in a 2 min lower tap-to-tap time, 15 kWh/t lower specific electrical energy demand and, in combination with other measures, a clear production increase. EAF gas purging has become standard operation [6].
>> One DPP purging plug was installed at a 30 tonne EAF for high alloyed and stainless steel production. Metallic yield increased by 3%, yield of alloys by 8%. Power-on time was reduced by 7 min.

Cost Savings

From numerous case studies in the last few years, RHI can claim that the minimum process benefits are approximately 5–15 kWh/t lower electrical energy demand, 0.5–0.7% increased metal yield, 2–4 min lower tap-to-tap time. The corresponding overall cost savings were customer-specific, depending on raw material costs and product price levels (Table IV). Increased process safety is not taken into account. Bottom gas purging systems are claimed to have the shortest payback time compared to other measures that increase EAF energy efficiency [4]. A typical example for a 60 min tap-to-tap time, 120 tonne EAF, 3 DPP, shows a payback time of the RADEX DPP gas control system comprising refractory and the gas control unit in the range of few campaigns.

Conclusions

For the EAF process in stainless steel making, inert gas purging from the bottom provides cost benefits by increasing bath homogeneity, oxygen efficiency, decarburization, and consequently improving the yield from alloying elements, as well as decreasing electrical energy demand. The additional advantage of this technology includes a more homogeneous melt, enabling improved process monitoring and control. Control of Cr_2O_3 content in the slag is improved. Process safety is increased by less sudden discharge and boiling of CO gas due to retarded mixing and oxidation reaction. RHI has several references of EAF's with RADEX DPP gas purging systems in stainless steel production.

Inert gas systems have become crucial tools as the quality and cost requirements for steel production have increased. These systems not only offer simple gas flow control, but are also capable of complex operations and provide a high-level operator interface when improved controllers, PLC's, and HMI's are added. In addition, a consolidated system approach is key to achieve the desired metallurgical results with advantageous cost savings due to the highest degree of process control.

It is also very important not to separate the gas regulation system and the functional refractory purging products, but to consider the gas purging system, refractory purging elements, and maintenance concept holistically. The approach offered by RHI and INTERSTOP for BOF or AOD converters, EAF, and secondary metallurgy (ladle etc.) results in an improved overall process control and cost savings due to the multiple advantages described.

Process improvement		
Electrical energy demand	5–15 kWh/t	
Increased metal yield	0.5–0.7%	(5–7 kg/t)
Lower tap-to-tap time	2–4 min	
Better process control		
Total, depending on raw material costs and product price levels		

Table IV. *Process improvements of the RADEX DPP system installed in an EAF based on minimum values for process improvements for high alloyed and stainless steel making.*

References

[1] DeSantis, M., Copola, J. and Ferro, S. Enhanced Plug Stirring Policies for EAF Bath Homogenisation, 1st European Steel Application Days, Paris, France, April 7–8 2014, pp. 380–381.

[2] Dong, K., Zhu, R. and Liu, W. Bottom—Blown Stirring Technology Application in Consteel EAF, *Advanced Materials Research*, Vol. 361-363, 2012, pp. 639–643.

[3] Ehrengruber, R. Excellence in Inert Gas Control Systems for the Steel Industry, 8th European Continuous Casting Conference, Graz, June 23–26, 2014, pp. 1080–1091.

[4] Jones, D.L. Available and Emerging Technologies for Reducing Greenhouse Gas Emissions from the Iron And Steel Industry, U.S. EPA, Office of Air Quality Planning and Standards, Sector Policies and Programs Division, 2012, https://www.epa.gov/sites/production/files/2015-12/documents/ironsteel.pdf.

[5] Kazakov, S.V., Gulyaev, M.P. and Filippov, V.V. Hydrodynamics of Electric Arc Furnace Bath at Stirring with Inert Gases, 21st International Conference on Metallurgy and Materials, Brno, Czech Republic, May 23–25, 2012, pp. 1–12.

[6] Niemi, T., Vallo, K. and Kotzschmar, A. Pohjahuuhtelun vaikutus valokaariuunin energia- ja tuotantotehokkuuteen (Impact of gas stirring to the energy and production efficiency of the electric arc furnace; in Finnish). *Materia*, No. 5, 2015, pp. 36–37.

[7] Ricci, M., Waterfall, S. and Sun, S. Optimization of Bottom Stirring in the 165 t Electric Arc Furnace at ArcelorMittal Dofasco. *RHI Bulletin.* 2008, No. 1, pp. 22–28.

Authors

Marcus Kirschen, RHI AG, Steel Division, Vienna, Austria.
Reinhard Ehrengruber, Stopinc AG, Hünenberg, Switzerland.
Karl-Michael Zettl, RHI AG, Steel Division, Vienna, Austria.
Corresponding author: Marcus Kirschen, marcus.kirschen@rhi-ag.com

Return to Content

RHI Bulletin > 1 > 2016, pp. 14–19

Matthäus Haider, Gerald Gutschier, Andreas Schretter and Marcus Kirschen

BOF Bottom Purging Efficiency and the Impact of Slag Maintenance with a Case Study from Jindal Steel Works in India

Jindal Steel Works (JSW) in Toranagallu, India, focuses on steelmaking technologies to be able to utilise iron ores of varying grades for the production of high quality steel grades. In the converters, for example, bottom gas purging is applied together with slag splashing maintenance technology in order to achieve the required high quality of tapped steel with minimum conversion costs. To meet this target a partnership between JSW and RHI was successfully created comprising an implementation team from JSW and a continuous site supervision from RHI. The realized metallurgical and process benefits due to gas purging in combination with intensive slag splashing maintenance of the converter are described below.

Introduction

Combined BOF blowing is currently applied in more than 50% of the installed BOFs worldwide, applying inert gas purging at the BOF bottom together with the top blowing oxygen lance (Figure 1) [1]. In rare cases, oxygen is also injected from the bottom with concentric double tube tuyeres together with shrouding gases to control the temperature at the tuyere outlet and the wear of the bottom (Figure 1). However, as inert gas purging provides generally higher control of wear, lifetime of the purging elements, and the bottom, the majority of converters with bottom stirring are equipped with gas purging plugs.

A major benefit of BOF bottom purging is the increase of mixing energy especially at the end of blow, when the bath movement is reduced by decreased {CO} formation and degassing. Improved bath kinetics increase mass transfer between steel and slag, reduce process time, and increase process efficiency, namely the following process improvements [1, 2, 3]:

>> Improved decarburization, i.e., lower [C] x [O] product at tapping.
>> Increased dephosphorization.
>> Decreased (FeO) content in the slag at tapping.
>> Decreased losses of [Mn] to the slag before tapping.
>> Decreased rate of reblowing.
>> Decreased tap-to-tap time.

Increased dephosphorization capacity is of increased importance for economic steelmaking today and in the future, when using iron ores with varying phosphorus content [1].

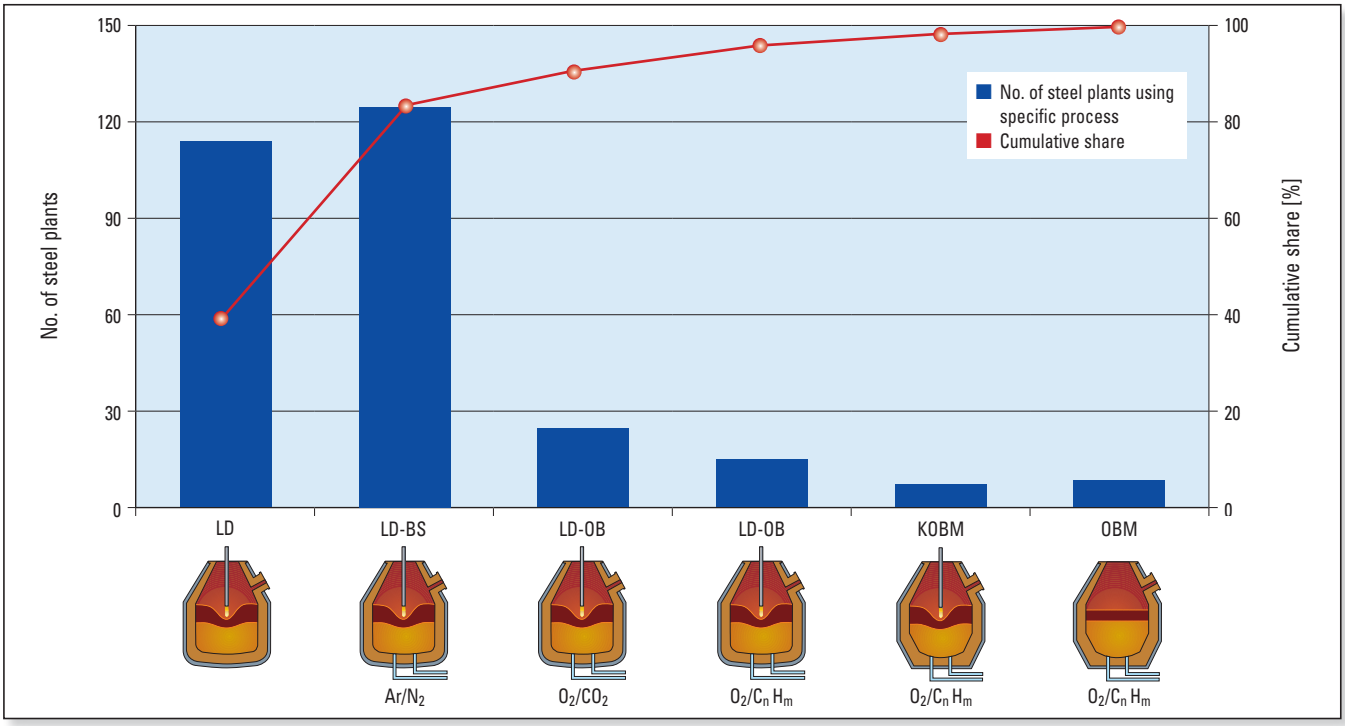

Figure 1. *Variety and application frequency of oxygen steelmaking processes worldwide. Abbrevations Linz-Donawitz (LD), Linz-Donawitz bottom stirring (LD-BS), Linz-Donawitz oxygen bottom (LD-OB), Klöckner oxygen bottom Maxhütte (KOBM) and oxygen bottom Maxhütte (OBM) [1].*

The applied process strategy and converter technology depends on a successful combination of bottom gas purging technology with slag maintenance strategies for maximum purging efficiency at minimum refractory cost.

BOF Slag Maintenance and Bottom Purging Availability

Today, the strategy for a BOF process with or without bottom gas purging is driven by minimum conversion costs of the available raw materials. Long BOF lifetimes with minimum idle times for relining and refractory costs are achieved for example by the intense use of slag splashing up to approximately 20000 heats, whereas typical lifetimes of BOF linings with bottom purging are in the range of 2000 to 5000 heats [3].

Slag splashing is a very cost effective maintenance method for the BOF bottom without purging plugs. However, slag splashing is a disadvantage when using bottom purging, in that it is very adhesive, (MgO) oversaturated slags cause bottom build-up and clogging of the purging plug thus reducing the bottom purging availability.

In the case of slag maintenance of the converter lining with bottom purging, careful adjustment of the gas purging technology and the converter maintenance is mandatory. The arrangement of the plugs, the design of the purge plug, details of the gas supply, control system, and the slag maintenance have a serious impact on the bottom purging availability and metallurgical results:

Design of Purging Plug

Single Hole Plug (SHP)

>> Availability: A high minimum gas flow rates per pipe is required over the entire process time to reduce the probability of slag clogging for the one pipe of a SHP.
>> Purging characteristic: The jetting regime of the gas flow above the single hole decreases a homogeneous distribution of a large number of gas bubbles and therefore purging efficiency (Figure 2).
>> Reopening: If the SHP is clogged, the probability of plug reopening is small due to deep infiltration and reduced or zero melt movement around the plug. An increase in the set point of gas flow does not help in the case of flow controlled outlet lines, because the system pressure of the gas purging system has already been applied and the gas flow cannot be increased in a clogged plug.

Multi Hole Plug (MHP)

>> Availability: The minimum gas flow rate is lower than for a SHP for the same range of purging gas capacity because of the much smaller open diameter of the tubes. If partial clogging occurs in a modern flow controlled gas supply system, the gas pressure and flow increases automatically in the remaining open pipes of the MHP and prevent further clogging of the MHP.
>> Purging characteristic: The higher specific surface of the gas bubbles above the multiple pipes increases the purging efficiency (Figure 3). The large volume of small

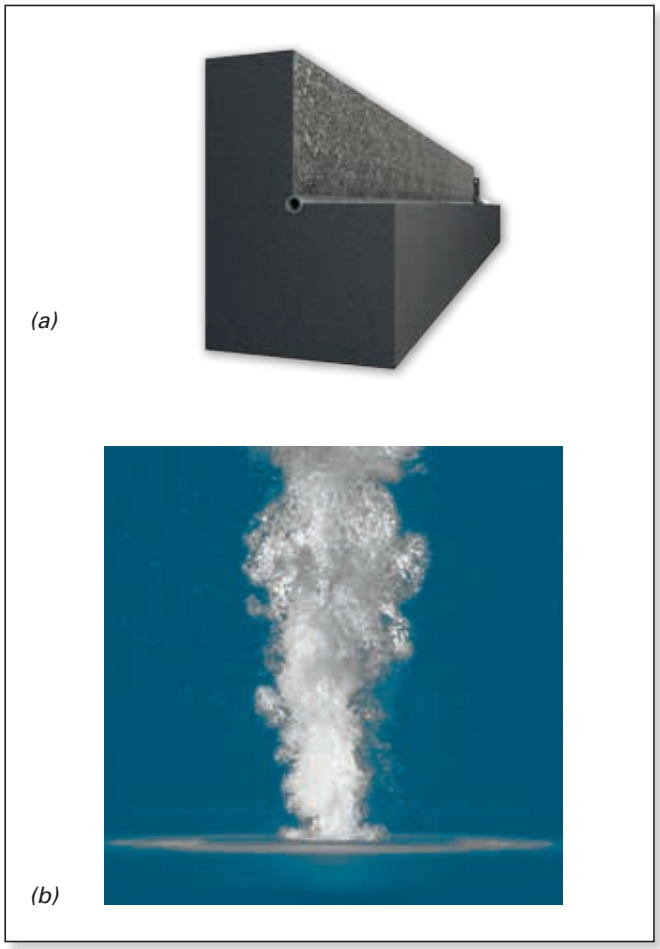

Figure 2. *Single-Hole Plug (SHP) showing (a) design and (b) gas bubble evolution in the water model.*

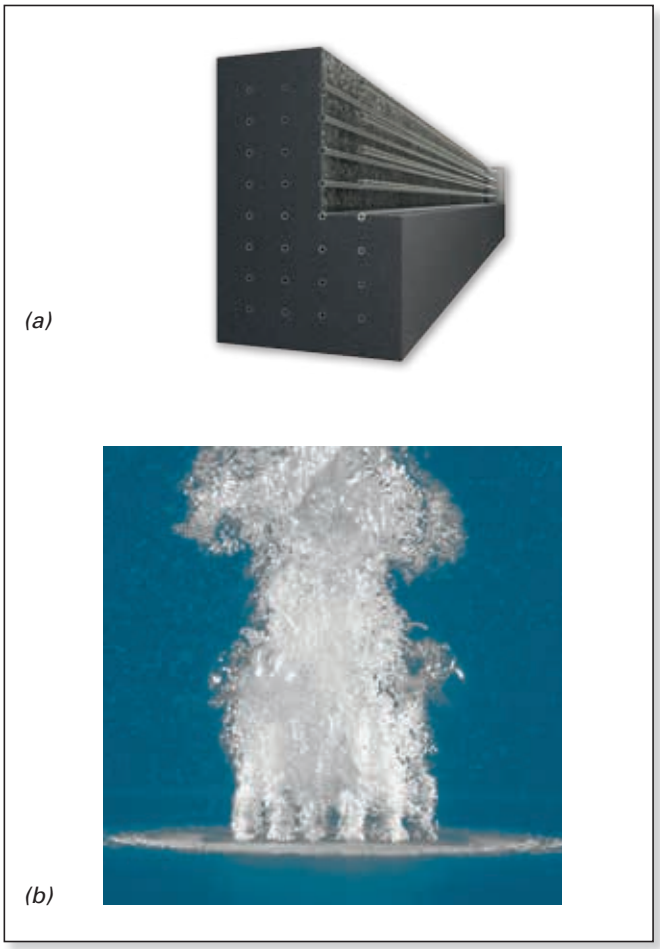

Figure 3. *Multi-Hole Plug (MHP) showing (a) design and (b) gas bubble evolution in the water model.*

bubbles support diffusion processes into the unsaturated gas phase and introduce a higher mixing energy due to the higher specific interface between steel and gas.

>> Reopening: The low infiltration depth of the pipes with small open diameters enables easy plug reopening.

Gas Supply and Control

>> Stability: Stable flow regulation at low gas flow rates through precise mass flow controllers is mandatory. In the case of valve swinging, pressure loss increases the probability of the clogging of the purging plug. This is especially critical during slag splashing and deslagging, because in most of the BOFs, minimum gas flow rates are applied during these process steps to save gas consumption.

>> Quick gas switch over: If the pressure drop of the purging gas during gas switch-over times is minimized, e.g., to < 0.5 seconds, the tendency of blocked purging plugs by steel infiltration decreases significantly.

>> Response time: Rapid response times of the gas control system increase the periods of high gas flow rates during blowing time significantly. A high gas flow enhances the plug reopening and improves metallurgical results. It has been observed, that older gas purging systems require a few minutes until the new flow rates are reached. This significantly reduces the time of high gas flow for each blowing phase and therefore increases the risk of blocked plugs.

>> Gas control by pressure: Pressure-controlled inlet lines of the gas purging system are often applied to extend the flow range of the gas supply valves to high gas flow rates. For low gas flow rates on contrary, a reduced system pressure is applied. Low gas pressure is critical when dealing with partly clogged plugs, because the probability of the purging plug reopening decreases. Further clogging of the plug until complete blockage is often the consequence.

Slag Maintenance

>> Bottom build-up must be avoided in order to maintain the converter volume and required BOF lifetime. When bottom build-up is visible, the slag maintenance rate or the amount of slag conditioner must be decreased.

BOF Process Efficiency With and Without Bottom Purging at Jindal Steel Works, India

Jindal Steel Works (JSW) in Toranagallu, situated in the Bellary-Hospet iron ore belt in India, focuses on technology to be able to utilise iron ores of varying grades. In addition to two blast furnaces of 3.2 million tonnes capacity each, JSW Steel processes sinter fines in its Corex plant in Vijayanagar with capacity of 1.6 million tonnes of hot metal. Seven converters are installed in two meltshops resulting in a capacity of approximately 10 million tonnes of crude steel. The product portfolio comprises quality steels, flat and long products, for use in high end applications such as oil exploration, automotive steel, and infrastructure etc.

Metallurgical Benefits of Bottom Gas Purging

The Jindal Steel Works steel plant 2 (JSW II) applies bottom gas purging on all four converters with tapping weights of 170 tonnes each. The average lifetime of the MHP purging plugs is currently 3300 heats with a total campaign length of 3450 heats. Resulting in a purging plug availability of 95.6% throughout the campaigns. Therefore, the metallurgical results with and without bottom gas purging could be assessed for a series of converter campaigns. The influence of raw material quality and composition on metallurgical results was small due to the regular sequence of heats with gas purging and heats without gas purging at the end of converter campaigns. The slag splashing frequency was in general between 70–80%, i.e., slag maintenance after 70–80% of all heats during the entire campaign.

Oxygen levels at tap were systematically below 1000 ppm (Figure 4). The [C]x[O] product with BOF bottom purging was on average 30% below the [C]x[O] product without BOF bottom purging (Figures 4 and 5). The average [C]x[O] product with bottom purging was 21.5 in comparison with 29.9 without bottom purging. During the converter campaigns evaluated, the [C]x[O] product decreased from campaign to campaign from 22.4 to 19.9 whereas the period without gas purging in each converter campaign maintained [C]x[O] products of approximately 29.9 (Figure 5). This positive result was only possible due to the very accurate control of bottom build-up during slag maintenance.

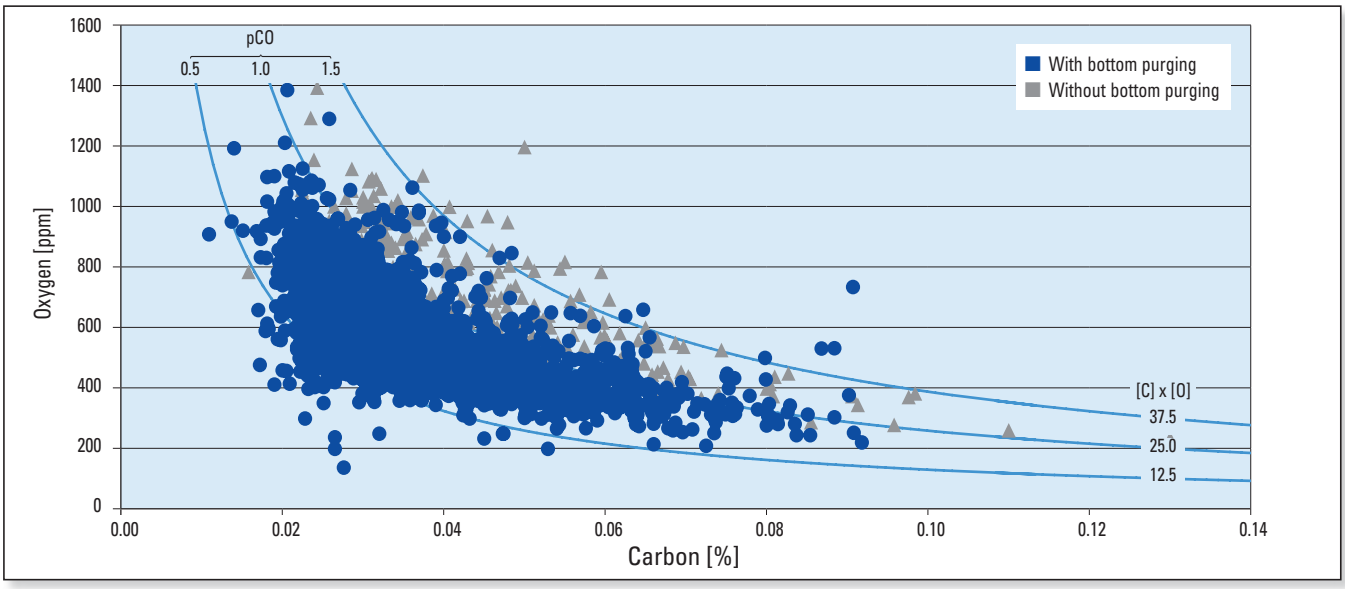

Figure 4. *Steel [C]x[O] product with BOF bottom purging (blue) and without BOF bottom purging (grey).*

Without bottom gas purging higher oxygen consumption was needed to achieve an acceptable carbon content at tapping. It was evident that steel grades with a 20% lower carbon at tapping were produced at decreased specific oxygen consumption with BOF bottom purging (Figure 6). The corresponding savings of bottom gas purging were decreased blowing time, oxygen consumption, and decreased alloy addition for steel killing.

The average (FeO) content of the slag increased from 23.1% with gas purging to 24.5% without gas purging. The mean values of (FeO) concentration of the slag are shown in relative units in Figure 7. The increased Fe loss to the slag without gas purging was consistent although the slag volume varied between 80 and 120 kg/t due to dephosphorization and other reasons for slag conditioning.

The dephosphorization efficiency was especially enhanced through the increased mass transfer between the slag and the steel melt with bottom gas purging. The required viscosity and (CaO) activity of the slag was mainly influenced by the (FeO) concentration during blowing: low (FeO) levels in the slag ("dry slag") caused lower dissolution rates of lime and low mass transfer from steel to slag at end of blow. However, the distribution of phosphorus between slag and steel melt, $(P_2O_5)/[P]$, was improved in the heats with gas purging although phosphorus levels changed with the hot metal compositions during the assessed time period (Figure 8). The phosphorus distribution between slag and steel bath was 15% higher with bottom purging than without bottom purging.

Manganese is often added in secondary metallurgy to Mn steel grades to compensate Mn oxidation losses during decarburization in the BOF. The manganese distribution between slag and steel melt, (MnO)/[Mn], i.e., [Mn] loss was on average 13% lower with gas purging compared to heats without gas purging due to improved mass transfer between steel melt and slag (Figure 9). However, when low [Mn] values at the end of the blow are the target for particular steel grades, the gas flow rates were adapted to lower values for these heats.

The process results at JSW show the systematic and clear benefits of bottom gas purging to the metallurgical results comprising [C] x [O] product, [Fe] loss to the slag, dephosphorization, and yield of [Mn] (Figures 4–9). The high availability of the purging plugs is mandatory for these process improvements and mainly influenced by the wear of the plugs at JSW, currently at a mean level of 96% for the entire converter campaigns. Adapted purging patterns and monitoring procedures for the slag maintenance were implemented as a crucial factor for maximum availability of the purging plugs.

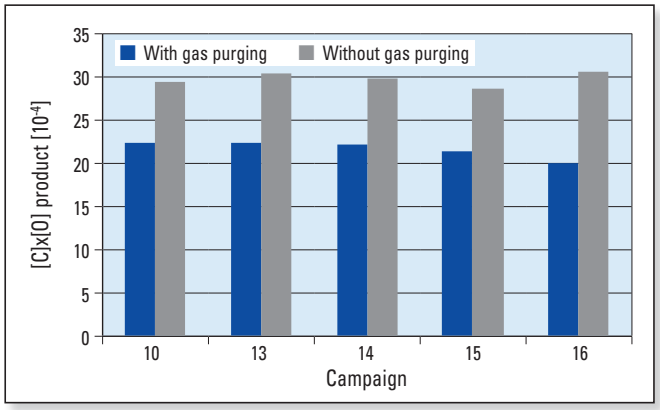

Figure 5. *Improved mean [C]x[O] product with BOF bottom purging.*

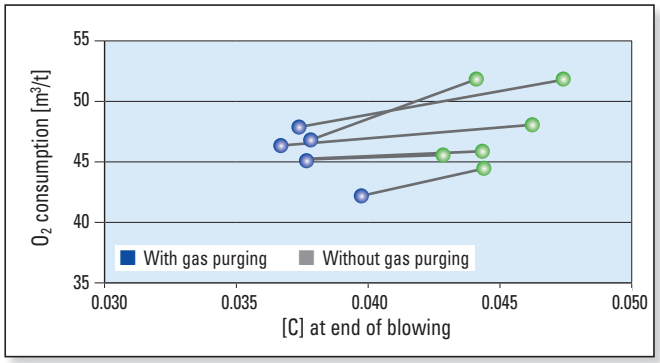

Figure 6. *Improved mean values of [C] at end of blowing for heats with gas purging in 6 different BOF campaigns.*

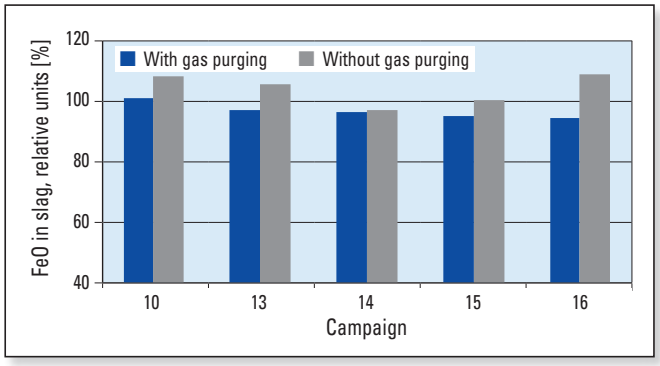

Figure 7. *Improved average slag (FeO) with BOF bottom purging.*

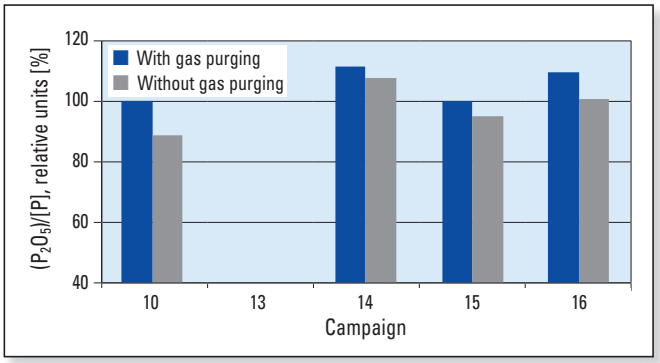

Figure 8. *Improved dephosphorization efficiency $(P_2O_5)/[P]$ with gas purging. (Insufficient data available for campaign 13).*

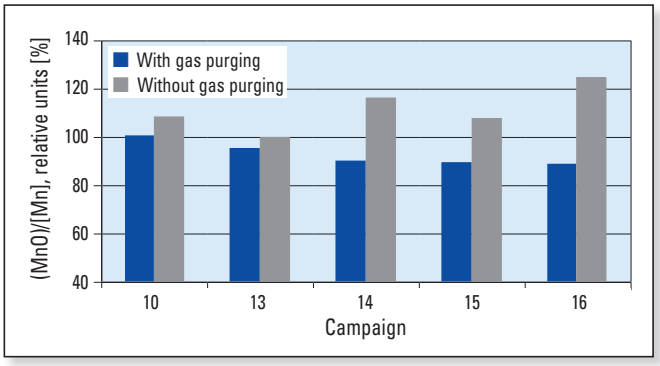

Figure 9. *Improved manganese distribution (MnO)/[Mn] with gas purging.*

Influence of Slag Splashing Frequency to Metallurgical Benefits

JSW II focuses strongly on purging plug availability together with the slag splashing frequency between 50–100% with a current mean value of 75%. Bottom build-up is avoided through different measures, e.g., adapted amount of slag conditioner, iron ore addition, and careful oxygen blowing. Despite the relatively high availability of gas purging, a high slag splashing frequency decreases the [C]x[O] product (Figure 10), [Mn] yield (Figure 11), and dephosphorization (Figure 12).

The metallurgical benefits of gas purging decrease especially at the end of the converter campaign where the slag splashing rate was higher due to lining conditions, and 1–3 of the 8 plugs were shutdown due to wear. After 1000 heats, JSW was applying a 100% slag splashing rate with fully operational gas purging indicated by low [C]x[O] provided the bottom build-up was under control. Optical inspection of the purging plugs after tapping ensured, that the purging plug was only covered by a thin slag layer. When, for example, large amounts of slag were in the BOF, the BOF was not kept in vertical position in order to avoid bottom build-up around the purging plugs.

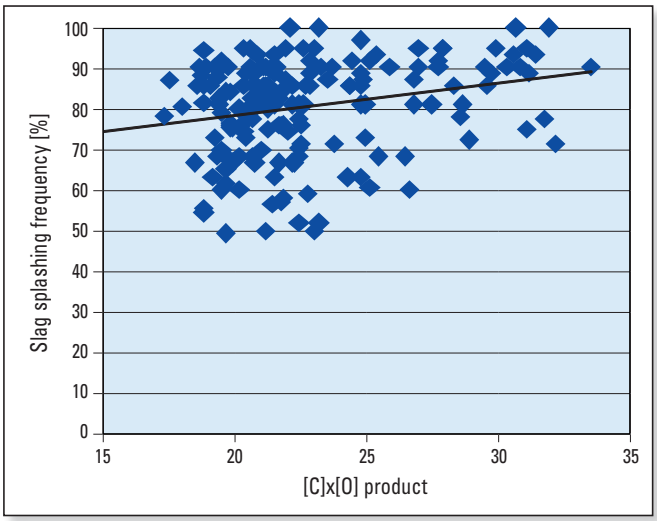

Figure 10. *Decreasing decarburization efficiency (increasing [C]x[O] product) with increasing slag splashing rate.*

Systematic Improvement of BOF Operation and Purging Availability at JSW

The improvement of the purging system efficiency and availability has been based on a partnership contract between JSW and RHI consisting of an implementation team from JSW and continuous site supervision from RHI (as per a separate service contract). After fact-finding to define the potential for improvements, the following major steps were applied:

>> Training of blowers/BOF operators for purging, slag maintenance practice.
>> Standardized operating practice (SOPs) rules for slag maintenance.
>> Automated customized splashing patterns for different BOF wear scenarios.
>> Seamless monitoring of plug wear, bottom build-up, and [C]x[O] product.
>> Plug installation and leak test procedure.
>> Daily maintenance meeting with operation personnel to plan sufficient slag work at highest productivity level.
>> Adaptation of purging patterns to metallurgical needs and continuous improvement.
>> Continuous monitoring and improvement of operating conditions through:
- Evaluation of laser scans (to define the wear speed of plugs) vs. maintenance practice vs. purging patterns.
- Flux monitoring vs. wear speed vs. dephosphorisation along with bottom stirring.

Conclusions

The successful combination of bottom gas purging with slag maintenance of the converter lining at JSW provided a cost-effective optimisation to process raw materials with variable compositions, e.g., phosphorus content, with minimum refractory costs. Metallurgical improvements in the order of 15–20% due to gas purging were clearly observed.

Slag maintenance at a high slag splashing frequency was carefully controlled in order to achieve maximum availability of the purging plugs. Purging programs were adapted accordingly. An example of process benefits due to the combination of slag splashing and gas purging from an integrated steel plant, JSW in India, has been shown.

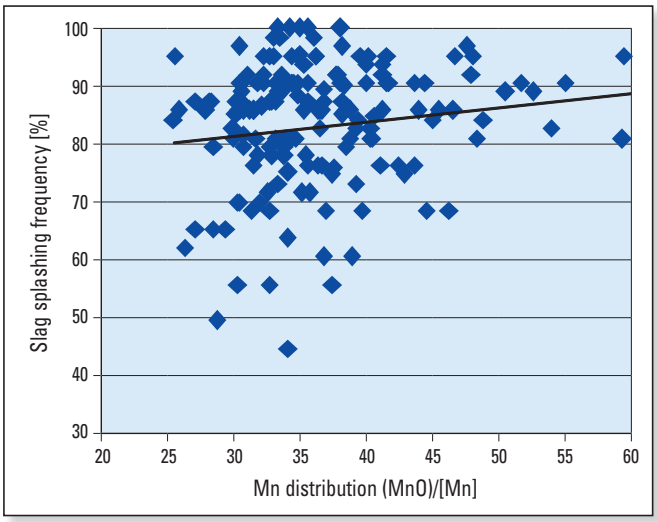

Figure 11. *Increasing loss of [Mn] to the slag, (MnO)/[Mn], with increasing slag splashing rate.*

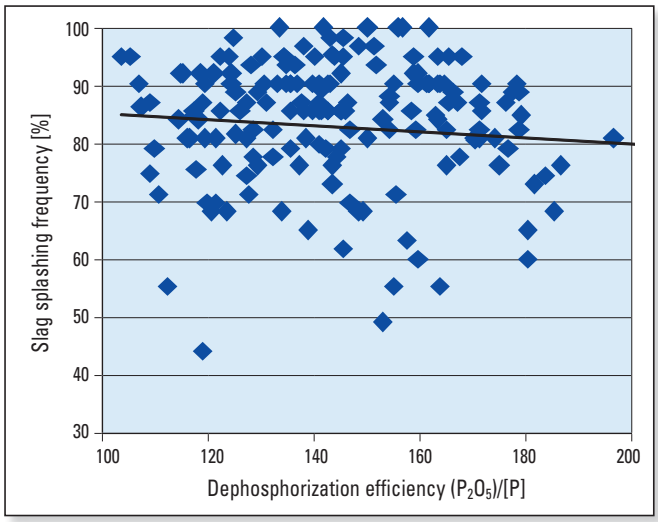

Figure 12. *Decreasing dephosphorization efficiency, (P_2O_5)/[P], with increasing slag splashing rate.*

The preconditions for efficient bottom purging are:

>> Appropriate slag maintenance practice.
>> A purging plug design which provides reliable plug reopening.
>> An appropriate gas purging pattern, especially for realizing gas savings through minimum flow rates during process and slag maintenance.
>> A state-of-the-art gas control system which helps to prevent plug blockage and supports reopening of the purging plug in case of blockage.

Acknowledgements

The authors would like to thank Jindal Steel Works in Toranagallu, JSW II, for sharing large sets of process data, for the permission to prepare a case study, and to publish the most important results within the RHI Bulletin.

References

[1] Kollmann, T., Jandl, C., Schenk, J., Mizelli, H., Höfer, W., Viertauer, A. and Hiebler. M. Comparison of Basic Oxygen Furnace Bottom Gas Purging Options. *RHI Bulletin* 2012, No. 1, pp. 8–15.

[2] Hüsken, R., Fechner, R. and Cappel. J. Use of Hot Metal With High Phosphorous Content in Combined Blowing BOF Converters. *Iron & Steel Technology*, 2011. pp. 46–58.

[3] Kollmann, T. and Jandl, C. Basic Oxygen Furnace Benchmarking—Maintenance and Process Considerations. *RHI Bulletin* 2013, No.1, pp. 29–32.

Authors

Matthäus Haider, RHI AG, Steel Division, Vienna, Austria.
Gerald Gutschier, RHI AG, Steel Division, Radenthein, Austria.
Andreas Schretter, RHI AG, Steel Division, Radenthein, Austria.
Marcus Kirschen, RHI AG, Steel Division, Vienna, Austria.
Corresponding author: Marcus Kirschen, marcus.kirschen@rhi-ag.com

Return to Content

RHI Bulletin > 1 > 2016, pp. 20–27

César G. J. Nader, Maycon Athayde, Hans Ulrich Marschall, Gerald Hebenstreit and Bruno Wilhelmi

Refractory Applications in Iron Ore Pelletizing Plants—Travelling Grate Furnaces

Blast furnaces do not operate properly with fine grained iron ore. To make use of it, it must be processed efficiently into pellets in large scale travelling grate pelletizing plants. Such furnaces are lined with thousands of tonnes of refractories that play an important role in operation stability and energy efficiency. This paper describes, based on the most important process conditions, the best solutions for refractory applications for the travelling grate induration furnaces, also called pelletizing furnaces. Additionally it shows how advanced refractory engineering and materials can be used to increase lining performance and reliability, enabling improved operational and maintenance costs, energy efficiency, plant availability, and productivity.

Introduction

The process routes to obtain metallic pig iron are based on the reduction of lump or fine grained iron ore. However, the commercial availability of high grade coarse ore has decreased significantly in the past 30 years, therefore a solution is needed to exploit fine grained iron ore reserves. This can be achieved through producing artificial lumps, i.e., pellets from powder finer than 45 µm, as shown in Figure 1.

Additionally the state-of-art of the reduction technology requires a pretreatment of the ores to increase the concentration of iron oxide to enable an economical and productive process. The concentration processes often leads to very fine grained iron ore that must be turned into pellets. A feasible way for processing high volumes of fine grained concentrated iron ore is through the travelling grate pelletizing technology. The German company, Lurgi Gesellschaft, which in 2001 became Outotec, originally developed it 60 years ago. Didier-Werke AG, now part of the RHI Group, has delivered large volumes of refractories for such plants in the past. Outotec has delivered pelletizing furnaces to many countries such as Brazil, Iran, China, Russia, and India with capacities from 1 up to 9.25 million metric tonnes of iron ore pellets per year, the largest pelletizing plant in the world. RHI Dinaris was involved in most of the recent pelletizing projects through refractory engineering, deliveries for selected refractory high wear areas, or by taking over the complete refractory project, consisting of full refractory engineering, material production, delivery, and supervision.

The induration of pellets, i.e., hardening of pellets, is a high temperature and energy intensive process, therefore requiring refractories for an efficient and stable operation. The continuous pressure to improve operational and maintenance costs, energy efficiency, plant availability, and productivity requires continuous improvements of refractory designs, installation techniques, maintenance, and quality material selection.

Travelling Grate System

The pelletizing process begins with the agglomeration of iron ore fines into sphere-like rotating discs through the addition of water, binders, and coal. The agglomerates require enough strength to be transported overseas and to be processed inside the reduction reactors (direct reduction and blast furnaces) without disaggregating. This is possible through a heat treatment at very high temperatures in travelling grate furnaces. The thermal treatment is conducted through three process zones named: drying, firing, and cooling. These processes enable maximum quality of the pellets and higher throughput rates.

The travelling grate pelletizing technology is a high-temperature process that consists in drying and sintering spherical iron ore agglomerates at temperatures up to 1300 °C using hot gases through a packed bed of pellets. The temperature varies through the process, as shown in Figure 2, and can reach temperatures more than 1600 °C inside the burner chambers that releases heat to the process. Depending on the iron mineral involved, coal, or coke can be added to the agglomerates in order to improve the heat distribution across the bed.

The furnace consists of a rolling conveyor grate covered by a hood, where the air is insuflated to cool down the pellets and then used in the rest of process for firing and drying the pellets. Figure 3 shows a typical heat recovery diagram in a travelling grate furnace. The travelling grate pelletizing is a continuous process with very little downtime and where

Figure 1. *Picture of iron ore pellets after treatment. (Courtesy of Outotec GmbH & Co. KG).*

the temperature is usually kept constant during idle times. Longer downtimes are very undesirable and can be expected once a year for preventive maintenance of the refractory lining. Some plants opt to run without cold shutdowns for as long as possible, adopting major refractory repairs every 5–10 years.

Drying Zones

Modern furnaces operate with the drying zone divided into two steps: updraft (UDD), and downdraft (DDD) drying. The refractory linings in the UDD and DDD are much less challenged as the process temperature is lower than 100 °C and 300 °C, respectively. Nevertheless, the dew point of combustion products from the firing zone such as sulphur, alkalies, and moisture content should be observed. In both zones iron ore dust can be an issue, however pellet fragments are very unlikely. The lining design for the drying zones should be reliable and well insulated, as these zones are expected to require very low maintenance and the heat losses should be minimised.

Firing Zone and Combustion Chambers

The most demanding areas for refractory linings are the firing zones, where the process temperatures are higher. Although the pellets are sintered between 1200–1300 °C, the temperatures inside the chambers are much higher. Figure 4 shows the general design of a section of a furnace section in the firing zone in 3D and the simulated temperature profiles of the firing zone in a furnace cross section. The combustion with the high O_2 content and primary hot air from down comers leads to adiabatic flame temperature of 1800–2200 °C, depending on the fuel used. Furthermore, air velocities are relatively high and can reach 75 m/s in the stream between the combustion and the grate [1].

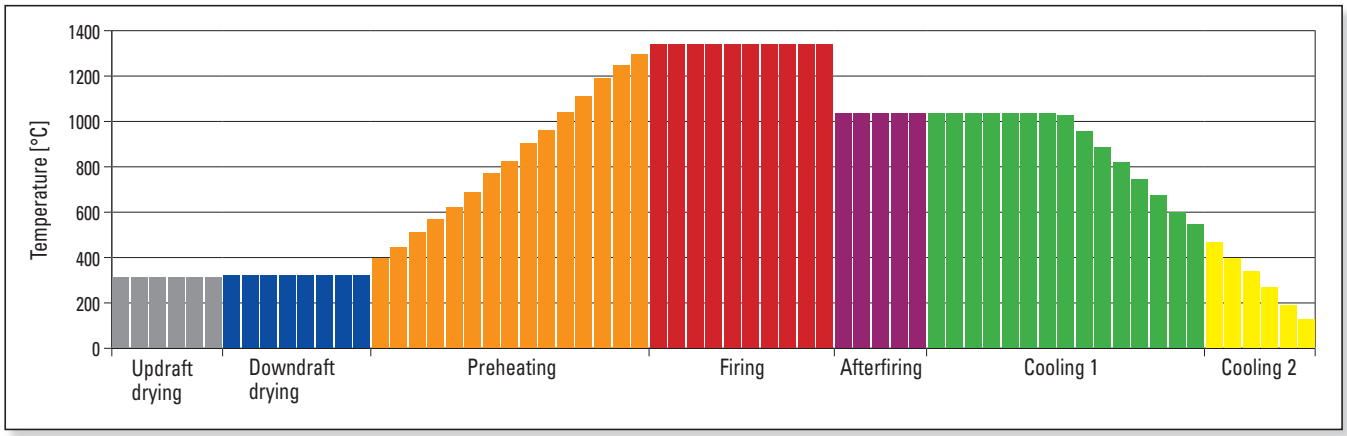

Figure 2. *Heating profile of travelling grate furnace, (Courtesy of Outotec GmbH & Co. KG).*

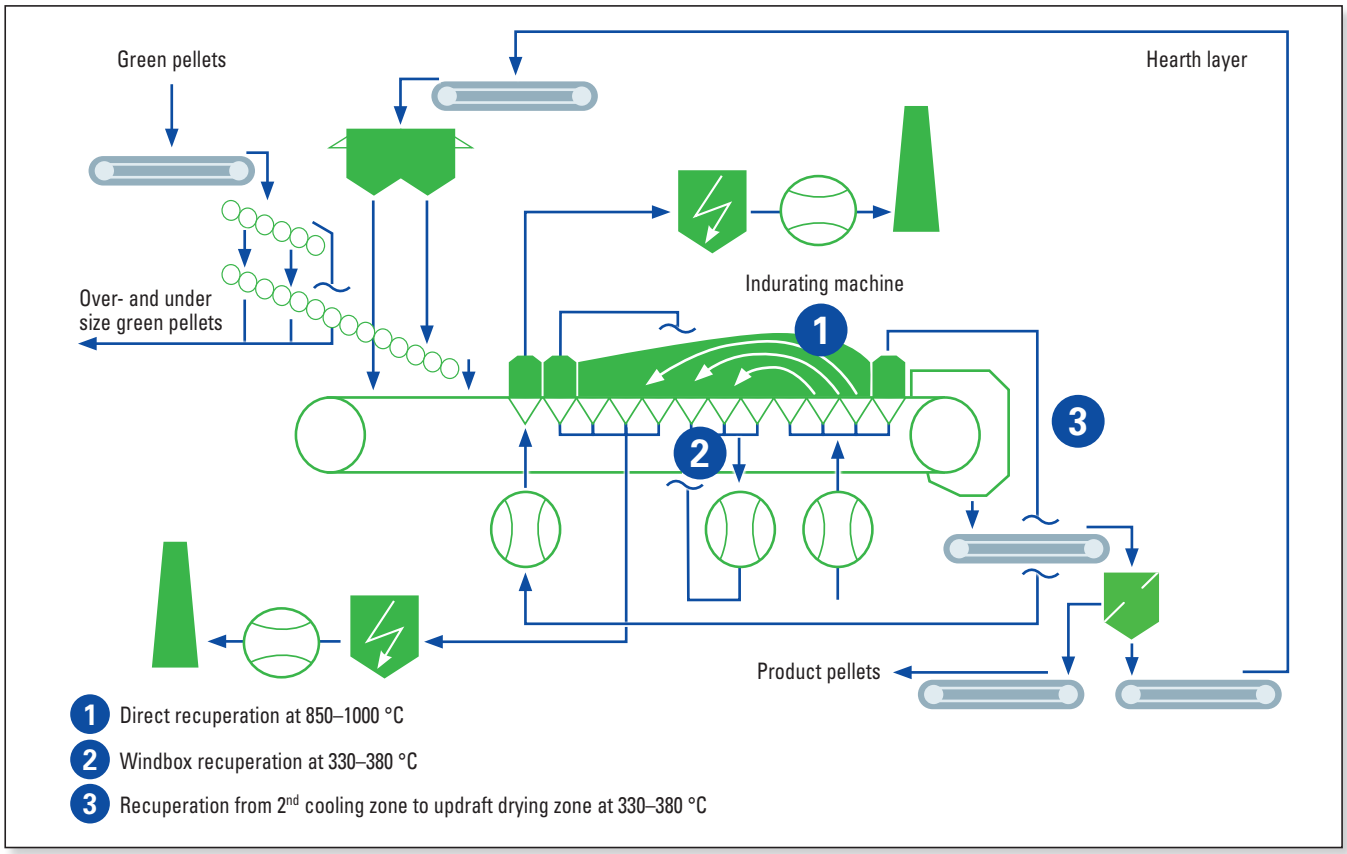

Figure 3. *Typical heat recovery design in a travelling grate furnace. (Courtesy of Outotec GmbH & Co. KG).*

In some operations, iron ore dust may drop into the combustion chamber from recovered air from the cooling zone through the direct recuperation duct and down comers. The dust may build up (Figure 5) and lead to clogging if a cleaning procedure is not conducted properly. Additionally, the flame may be switched on and off during operation, which can lead to thermal cycling within the chamber.

Therefore thermal shock resistance properties are very important for the reliability of the working lining.

Due to such conditions, the combustion chambers (Figure 6) are the hottest and most demanding application in a pelletizing furnace, where temperatures may reach more than 1600 °C on the refractory surface. As shown in Figure 7,

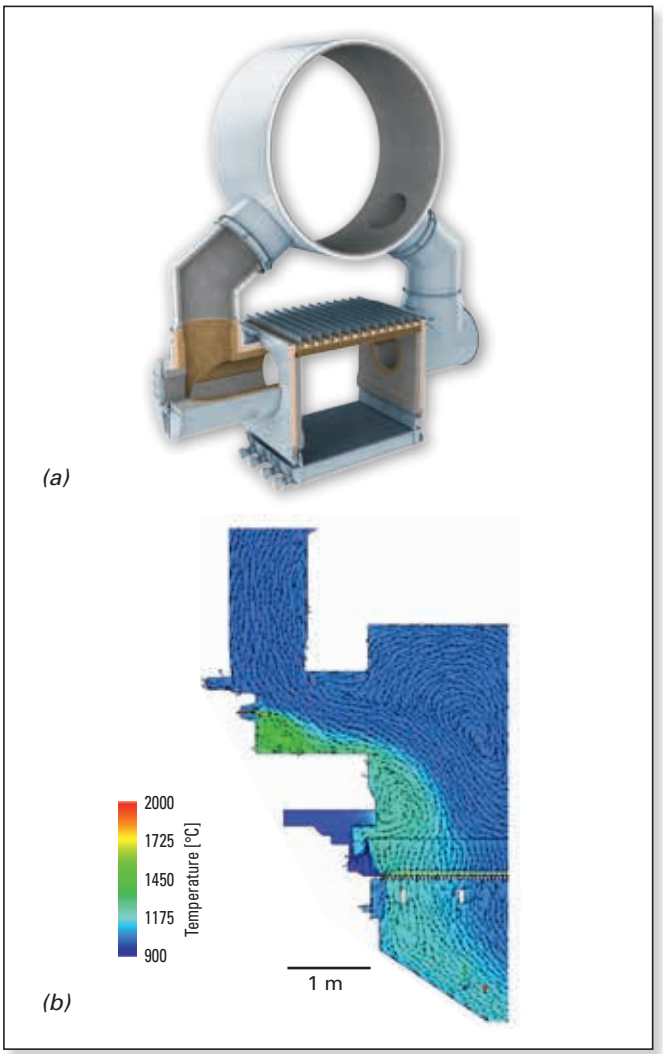

Figure 4. *Showing (a) 3D model of a typical firing zone showing burner chambers, sidewalls, roof, direct recuperation duct, down-comers lined with refractory materials, and metallic grate car and (b) Temperature contours computational fluid dynamics simulation at a furnace cross section [1].*

Figure 5. *Build up of iron ore dust and melt within a combustion chamber.*

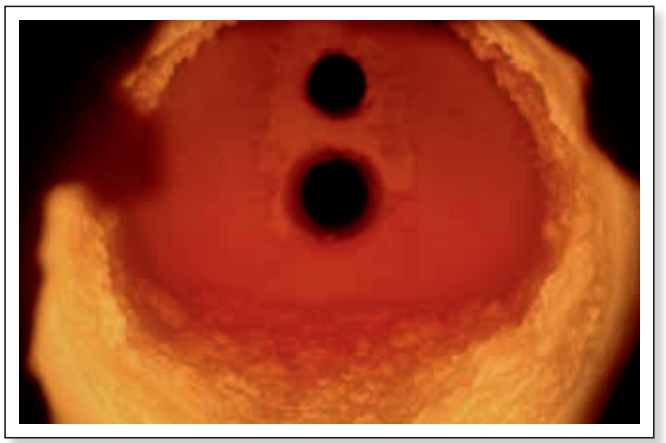

Figure 6. *Picture of combustion chamber interior. Iron ore dust and slag accumulates on lower parts demanding high grade refractories to avoid corrosion.*

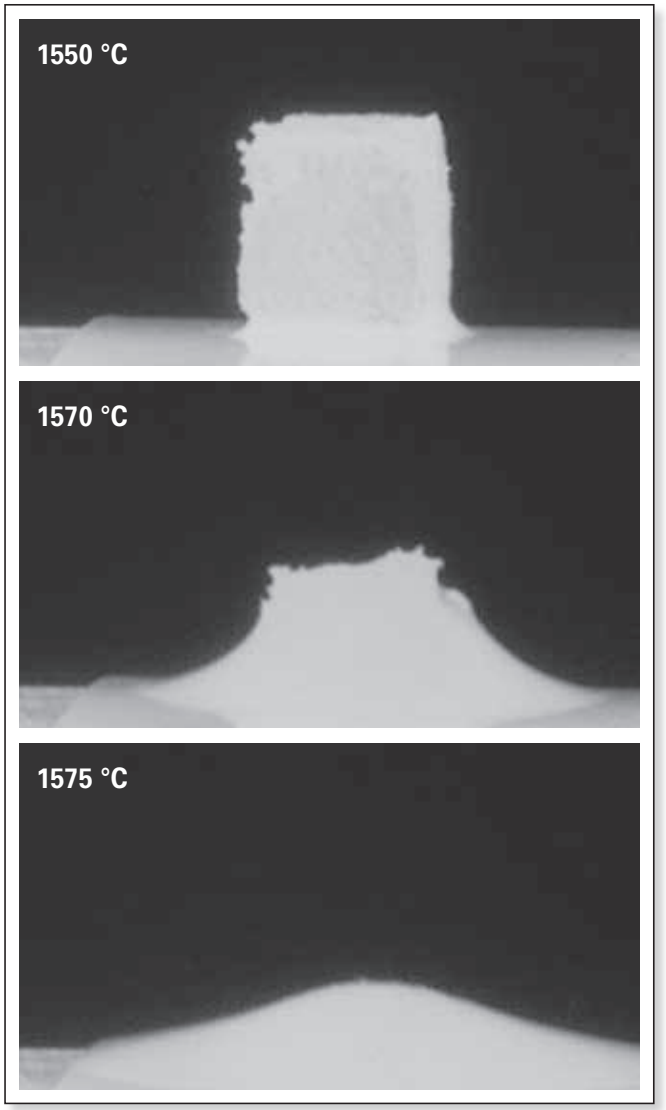

Figure 7. *Hot stage microscopy of hematite rich iron ore pellet feed sample.*

hematite (Fe_2O_3) rich iron ore melts at this temperature, forming an iron oxide rich slag that is highly corrosive to refractory lining. The iron oxide reacts with refractory lining forming new phases such as hercynite ($FeO.Al_2O_3$), spinels, and low melting iron silicates such as fayalite ($2FeO.SiO_2$).

The chemical and dimensional stability of the working refractory lining to the attack of the molten phase is the key to the success of the chamber operation. The most modern equipment apply cylindrical high alumina bricks fired at temperatures of more than 1600 °C, which combine such properties.

Cooling Zones and Heat Recuperation

The process ends at the cooling zone where temperatures decrease from 1000 °C to 300 °C at the discharge point of the grate. The selected refractory in the working layer must develop sufficient strength at low temperatures. Otherwise refractory linings in this zone may be susceptible to erosion due to the flow of air and particles at approximately 10 m/s. Spalling resistance is also desirable due to possible temperature variations. Frequent thermograph inspections of the cold face are important, as this zone may have incidence of hot spots and require emergency repairs, which can lead to downtimes. Normally these zones are lined with conventional dry gunned castables because of reduced installation time when compared with vibration casting. However it is also possible to increase performance while keeping installation costs and time low by installing special materials, designs, and applying special installation techniques.

Sidewalls

A typical travelling grate furnace has a length of more than 120 meters. This is equivalent to more than 500 m² of vertical walls that must be lined with engineered refractories suitable to the service conditions in each process zone. There are a whole range of possibilities for lining concepts and installation methods, with different characteristics as shown in Table I.

The furnace walls of the most modern plants built by Outotec use the refractory lintel technique instead of the water cooled lintel. This development saves energy and increases the plant availability.

Advanced Refractory Engineering and Materials for Pelletizing Plants

In order to fulfil customer requirements for these applications, RHI Dinaris GmbH provide a full range of specialized services and high quality materials to achieve the most reliable and cost effective solutions for the challenging applications in pelletizing furnaces.

During inspections and discussions at the customer´s site, RHI experts identify “weak points” of the refractory lining and suggest unique material selections and professional designs for areas of severe load. In this way it is possible to avoid lining failures as shown in Figure 8, where the highlighted region requires an individual refractory design and material selection. Severe localized corrosion of this lining was observed after 9 months of operation.

Figure 8. *Evaluation of severe localized corrosion of the lining below combustion chamber of a pelletizing furnace after 9 months of operation. The highlighted region requires an individual refractory design and material selection.*

Material / Technique	Advantages	Disadvantages
Special shaped fired bricks (RESISTAL™, DURITAL™)	Fast installation Cost effectiveness High performance	Requires customized engineering
Prefabricated parts (URBLOCK™, ANKOFORM™)	Ease installation Reliability	Additional costs for mould building
Conventional dry gunning (COMPRIT™, LEGRIT™)	Simple and flexible installation	Lower performance compared to casted materials
Low cement dense gunning (DIDURIT DG™)	Low porosity Abrasion resistant	Requires special gunning nozzle
SOL bonded gunning (COMPAC SOL™)	Spalling resistant Fast heat-up	Requires special additive
Wet gunning (shotcasting) (COMPAC SHOT™)	High volume of installation Good physical properties	Requires specialized machinery and workforce
Vibration casting (DIDURIT™, COMPAC SOL™)	Reliability	Time consuming mould work Expensive installation

Table I. *Overview of possible lining concepts/techniques for sidewalls in iron ore pelletizing plants.*

In order to solve these issues, RHI Dinaris GmbH involved the RHI R&D and Technology Centre in Leoben, Austria, a highly advanced technology centre for specialized services to support the refractory engineering. They offer:

>> Complete material characterization and investigations.
>> Mineralogical investigations and post mortem wear studies.
>> Corrosion tests and other practical simulations.
>> Thermodynamic simulations.
>> Thermomechanical simulations by finite element method (FEM).

Material Investigation for Combustion Chambers

To provide the best solutions, extensive laboratory investigations were undertaken to develop and select the most resistant refractory materials against iron oxide for the hottest combustion chambers in iron ore pelletizing plants.

In order to evaluate the most suitable refractory materials, brands were tested for corrosion resistance by rotary slag testing with iron ore pellets from the client [2]. In order to obtain relevant results, the materials were submitted to extremely severe conditions. The test was performed at 1700 °C in a small rotary kiln lined with samples, with slag changes every 30 minutes for 5 hours. The samples were evaluated macroscopically to quantify wear and infiltration depths. Then microscopic chemical and mineralogical investigations were performed on samples reaction zones, as illustrated in Figure 9. Physical properties like permanent linear change (PLC) at 1700 °C, refractoriness under load (RUL), and thermal shock resistance (TSR) were also evaluated. A summary of most the relevant results are presented in Table II.

All the chrome containing bricks showed significant corrosion resistance, although RESISTAL RKM08 showed the best results, the only brick brand without macroscopic detectable infiltration. From the chrome free bricks,

Brand	Rotary furnace test 1700°C				Microscopy		PLC 1700°C		TSR Water		Refractoriness under Load		Ranking
	Wear depth		Infiltration depth								$T_{0.5}$		
Unit	mm		mm				Lin%		Cycles		°C		
Standard							ABNT NBR 6225		ABNT NBR 13202		DIN EN ISO 1893		
RESISTAL RK10	8.5	+	9.0	+	+	2	0.10	+	> 20.0	+	> 1705	+	1
RESISTAL RKM08	6.0	+	0.0	+	+	1	-0.20	+	10.0	-	> 1700	+	2
DURITAL E92	7.0	+	25.0	-	Ø	3	0.06	+	20.0	+	> 1705	+	2
RESISTAL RK05	7.0	+	35.0	-	+	2	-0.10	+	17.0	-	> 1710	+	3
DURITAL E90	14.0	-	27.0	-	Ø	3	-0.20	+	> 20.0	+	> 1700	+	4
RESISTAL KSP 95-1	11.5	Ø	7.0	+	+	1	1.30	-	11.0	-	> 1700	+	5
ANKOFORM 204	9.0	+	14.0	+	Ø	3			9.0	-			6
ANKOFORM 94MG	16.0	-	24.0	-	Ø	3			20.0	+			7
URBLOCK MA2 0-6	12.0	Ø	19.0	+	-	4	-0.85	-	17.0	-	> 1700	+	8

Table II. *Summary of most relevant results of material investigation for combustion chambers.*

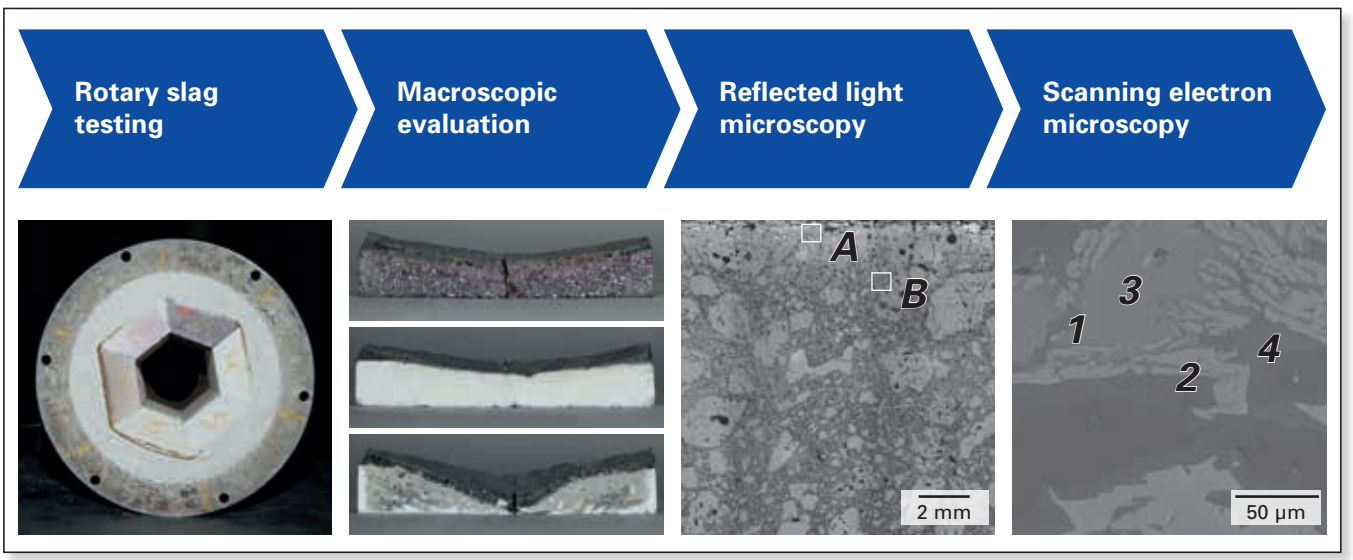

Figure 9. *Illustration of materials investigation procedures.*

RESISTAL KSP95-1 showed very good corrosion resistance and interesting microscopic behaviour due to very low iron penetration depth. DURITAL E92 was selected as the best chromium free brick brand due to a combination of very low erosion depth, excellent dimensional stability, and thermal shock resistance.

The tests were also performed also on high grade refractory castables used for prefabricated parts: ANKOFORM 204, ANKOFORM 94MG and URBLOCK MA2-6. Although with very low silica contents, their corrosion test performance were, in general, inferior to the fired bricks. This leads to the conclusion that high grade fired bricks are more suitable for the most severe regions of combustion chambers.

Finite Element Simulations

The design of the new type of partition walls has been supported by thermomechanical simulations with the method of finite element analysis (FEA). Based on the complex material behaviour of refractory materials including plasticity, visco-plasticity, and relaxation and the challenges to describe them in FEA simulations, the predicted values for stresses and forces will be higher than those observed in reality. Nevertheless a comparison of different stress patterns will lead to reasonable conclusions, higher stresses result in a higher risk of failure.

Thermomechanical simulations have been used to compare the stresses in a conventional partition wall with the stresses in a new arch design proposed by RHI Dinaris GmbH. This comparison is shown in Figure 10 using the maximum principal stress to visualize the most critical tensile stresses.

In both figures, areas influenced by an insufficient description of the boundary conditions are shown as uniform coloured areas, the model of the arch only covers the material in between the first and second arch as the second arch will carry the load of the material above it. In both models similar stresses are predicted. However, the formation of a horizontal crack in the double T shaped bricks will result in a failure of the wall while the arch will maintain its stability even with horizontal cracks due to the wedge shape of the arch-bricks.

Refractory Castables Selection

Recent outstanding performance references of RHI's new technology SOL bonded materials in cement plants opened the path for introducing COMPAC SOL into other applications as an evolution of low cement castables (LCC) [3, 4]. The advantages of sol-bonded mixes over cement bonded castables mainly result from the substitution of cement binder by a liquid binder containing high purity silica nano particles dispersed in water and include [5]:

>> Easy, fast, and safe heat-up: the lack of cement hydrates allows the material to be virtually water free after drying at 150 °C. See standard heat-up schedule in Figure 11.
>> Higher refractoriness: the lack of cement inhibits formation of low melting compounds expected in the system $CaO\text{-}Al_2O_3\text{-}SiO_2$
>> Chemical resistance: Nano scale SiO_2 particles dispersed in a matrix, improved chemical resistance towards alkali, sulphur, and acid attacks.
>> Ultra fine porosity: the liquid binder fills the porosity reinforcing it with nano particles leading to an optimized particle packing with ultra fine pore size distribution, improved physical properties, and infiltration resistance.

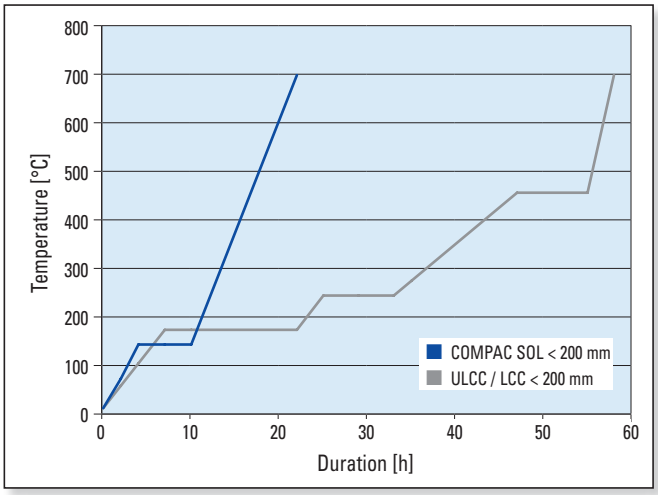

Figure 11. *Standard heat-up schedules for sol bonded mixes and low/ultra low cement castables [6].*

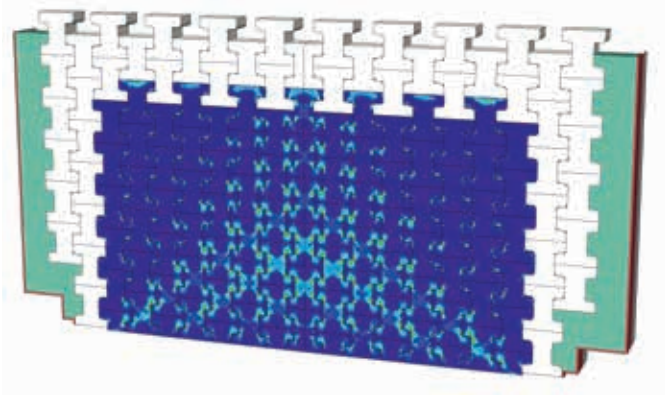

(a)

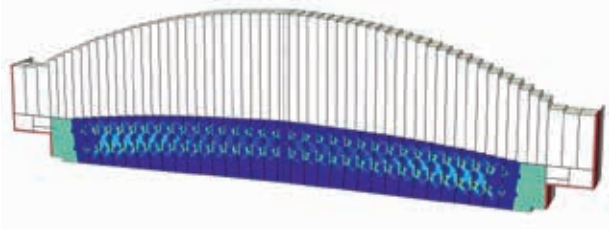

(b)

Figure 10. *Thermo mechanical simulations used to compare the stresses of (a) conventional partition wall, with (b) those on new design proposed by RHI Dinaris with self supporting bricks arrangement.*

>> Excellent thermal shock resistance: SOL bonded materials are considered to be spalling resistant (low crack formation) due to its increased fracture toughness.
>> Extremely high abrasion resistance: Due to optimized particle packing and increased bonding strength of SiO_2 nano particles, SOL bonded materials develops very high strength.
>> High performance dry gunning: Since the liquid binder has low viscosity and high solid content, properties are not severely affected by over dosage of binder, enabling a high performance lining even with gunning techniques.
>> Longer shelf life: The absence of hydratable compounds other sensitive additives allows storage for more than 18 months.
>> Reliable workability: setting time and flow characteristics are not heavily dependent on environmental conditions.

Low cement castables are commonly selected for applications in iron ore pelletizing furnaces, which are less severe than the combustion chambers. Such as prefabricated sections and casting in the sidewalls of the firing and cooling zones, have shown good results. Therefore to support the selection of SOL bonded castables for pelletizing plants chemical resistance against iron oxide must be compared with LCC and show similar or better results. It is also important to evaluate and define maximum allowable temperatures for the materials in contact with iron oxide, i.e., the maximum temperature in which process infiltration is not observed. This way it is possible to select the most cost-effective material for each process zone. In order to evaluate such parameters for proper materials selection, crucible tests were conducted with LCC and SOL bonded materials samples at the highest expected application temperatures [1]. Table III shows the selected brand products. The crucibles were charged with standard hematite rich green milled pellets and held for 10 hours at testing temperature. Table III shows the crucible test parameters and main results. Pictures of tested samples are shown in Figure 12.

COMPAC SOL F53-6 / 1200 °C

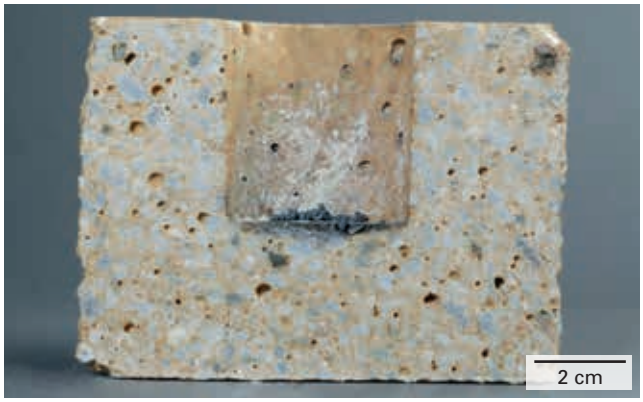

COMPAC SOL B87-6 / 1500 °C

COMPAC SOL M64-6 / 1500 °C

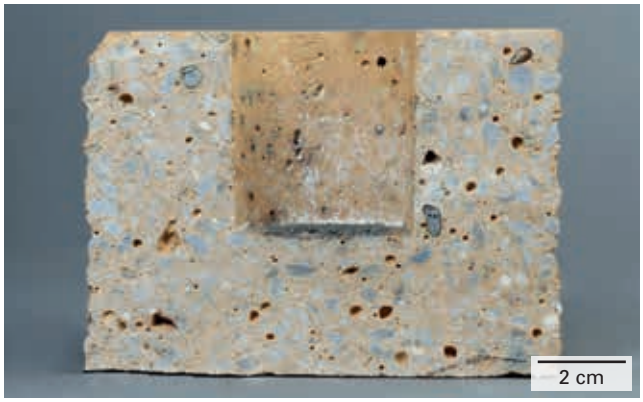

DIDURIT B83-6 / 1500 °C

DIDURIT M60-6 / 1500 °C

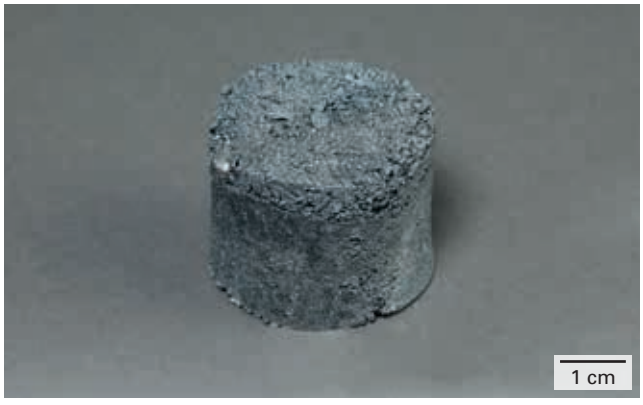

Figure 12. *Showing tested samples and residue after firing. SOL bonded castables and low cement castable equivalent shows very similar corrosion resistance against iron ore on crucible tests.*

Brand	Bonding system	Main raw material	Testing temperature (x 10h)	
			1200 °C	1500 °C
COMPAC SOL F53-6	Sol bonding	Fireclay	++	
DIDURIT M60-6	Low cement	Mullite rich		++
COMPAC SOL M64-6	Sol bonding	Mullite rich		++
DIDURIT B83-6	Low cement	Bauxite		++
COMPAC SOL B87-6	Sol bonding	Bauxite		++

Table III. *Crucible tests parameters and results.*

Conclusions

Travelling grate pelletizing furnaces requires a wide range of refractory applications with various specific design, materials, quality, and installation techniques requirements, with the combustion chamber being the most challenging. As the production output of these plants is very high, the operation must be stable and shutdowns must be kept as short as possible. Hence, reliable refractory designs and materials that allow quick installation techniques and fast dry-out procedures will be the future refractory engineering solutions. RHI relies on a set of tools to offer the best solutions to fulfil these requirements. Customer focus, specialized engineering, technical assistance, high-end laboratory support, finite element analysis, high quality, advanced materials, and customized solutions make RHI a reliable partner for refractory applications.

Acknowledgements

The authors would like to acknowledge the permission of Outotec GmbH & Co. KG, Agglomeration – Pelletizing and SAMARCO-Mineração S.A. for allowing this work to be published.

References

[1] Athayde, M., Tavares, P. R., Nunes, S. F. and Fonseca, M. C. Evaluation of Flow Distribution in the Pelletizing Furnace through CFD and Experimental Validation at Samarco. Tecnol. Metal. Mater. Miner. 2014, Oct/Dec, Vol. 11, No. 4, pp. 340–345.

[2] RHI internal investigations, Leoben, Austria, unpublished results, 2013–2016

[3] Fritsch, P., von der Heyde, R. and Krischanitz, R. COMPAC SOL—Operational Experiences with the Easy, Fast Heat-Up No Cement Castable. *RHI Bulletin*. 2011, No. 2, pp. 42–45.

[4] Schneider, U., Krischanitz, R., and Fritsch, P. No-Cement Sol Mixes Achieve Service Life Records at Solnhofer Portland-Zementwerke. *RHI Bulletin*. 2015 No. 2, pp. 40–43.

[5] Blajs, M., von der Heyde, R., Fritsch, P. and Krischanitz, R. COMPAC SOL—The New Generation of Easy, Safe and Fast Heat-Up No Cement Castables. *RHI Bulletin*. 2010, No. 1, pp. 13–17.

[6] Wenzl, C., Handle, B., Meza, D. and Garcia, N. Technical Aspects for the Proper Design of Refractory Concepts Applied to Ferronickel Rotary Kilns. *RHI Bulletin*. 2015, No. 2, pp. 9–19.

Authors

César G. J. Nader, RHI Brasil, Industrial Division, Belo Horizonte, Brazil.
Maycon Athayde, Outotec GmbH & Co. KG, Agglomeration - Pelletizing, Oberursel, Germany.
Hans Ulrich Marschall, RHI AG, Technology Center, Leoben, Austria.
Gerald Hebenstreit, RHI Dinaris GmbH, Industrial Division, Wiesbaden, Germany.
Bruno Wilhelmi RHI Dinaris GmbH, Industrial Division, Wiesbaden, Germany.
Corresponding author: César Nader, cesar.nader@rhi-ag.com

Return to Content

RHI Bulletin > 1 > 2016, pp. 28–34

Andrey Gerasev, Philip Bundschuh, Johannes Schenk, Peter Reisinger, Roman Rössler, Bernd Trummer, Andreas Viertauer and Gregor Arth

Evaluation of the Potential for Reduction of CO_2 Emissions at the Secondary Metallurgy

Policies all over the world encourage the high energy efficiency of processes and the reduction of greenhouse gas (GHG) emissions, classified as direct and indirect. Iron and steelmaking is energy intensive industry, which also contributes 30% of the direct global CO_2 emissions (2007), triggered through the industrial processes [1]. This article focuses on the verification of the CO_2 emissions distribution for the secondary steelmaking. The potential for reduction of these emissions depends on the key factors of ladle logistics and temperature losses under consideration of the steel contact time, additions during tapping, treatment at the ladle furnace to compensate temperature losses, and ladle preheating.

Introduction

The global problem of climate change requires also a global solution. In fact, 30% of all direct CO_2 emissions from the global industrial processes are caused by the iron and steelmaking industry. It is 7% of the global man-made GHG. At the same time this industry consumes approximately 5% of the world´s total energy [2].

In general, there are two main routes to produce steel (Figure 1). The integrated route (IR) is based on the steel production from iron ore. The recycling route (RR) uses scrap as the main raw material, but can be supplemented with the use of direct reduced iron ore (DRI). The RR consumes about 80% less energy than the IR and produces five times less CO_2 emissions [3].

The calculations of the current study are based on the ladle treatment for the recycling production route, comprising the transfer of crude steel from the electric arc furnace (EAF) via the ladle furnace (LF) to the continuous casting machine (CCM). The detailed model and calculations are described in the master thesis of Mr. Gerasev carried out at the Montanuniversitaet Leoben in 2015/2016 [6].

Tapping from EAF represents the initial point of secondary metallurgy. The main tasks for common treatment at secondary steelmaking facilities are:

>> deoxidation, alloying and desulphurization (depend on the requirements),
>> homogenisation of steel temperature and chemistry by means of heating and inert gas purging,
>> enhancing steel cleanliness,
>> logistic buffer between BOF/EAF and casting installation [4].

The main influences for the verification of the CO_2 emissions contribution are the additions during tapping, logistics of the ladle and ladle treatment at the LF. These three influences were selected as the most important for the following estimation of the potential savings and reduction of CO_2 emissions.

Estimation of CO_2 Emissions Generated in the Secondary Metallurgy

In general, GHG emissions, associated with the industrial processes, can be divided into three scopes (Figure 2) [5].

In terms of the secondary refinement, Scope 1 includes the direct emissions, which are generated by:

>> yield loss of carbon alloying,
>> decomposition of carbonates, used for a slag generation,
>> electrode consumption in the process of LF treatment, and

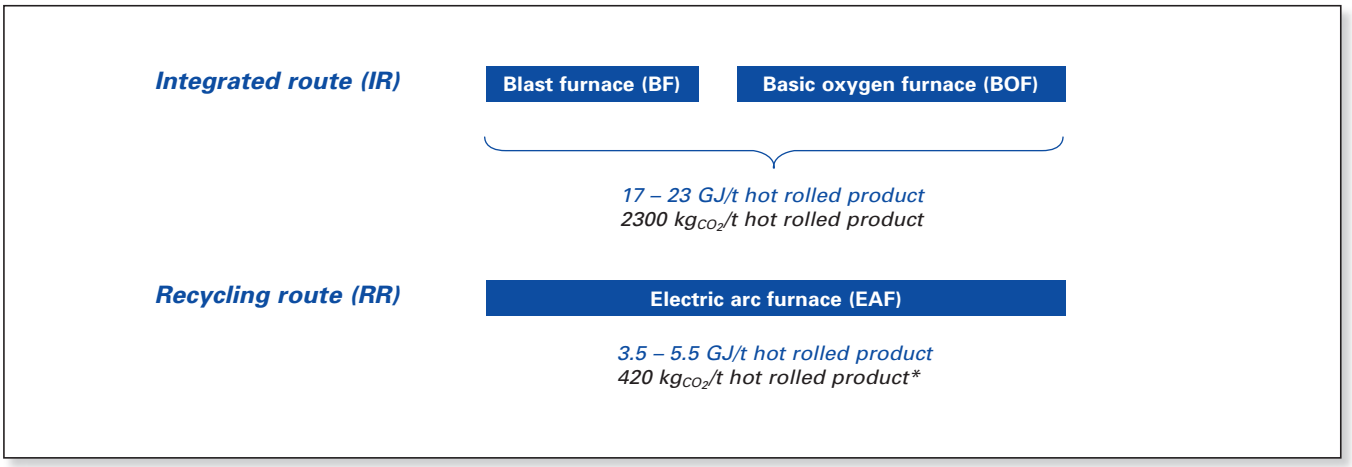

Figure 1. *Energy efficiency and CO_2 emission in the iron and steel industry [3]. * Value is based on own calculation.*

>> combustion of natural gas during preheating of a new lined ladle [6].

Scope 2 includes indirect emissions related to the purchasing of electricity for LF treatment. Scope 3 includes indirect emissions associated with the production of materials such as alloying agents, slag formers and refractory materials etc.

It is necessary to correlate all the following values of this study with the estimated production route, including all technological aspects. The current alloying concept represents the production with the following compositions of crude steel tapped from EAF, treated at the LF and casted at CCM (Table I) [6].

The amount of solid additives is specified for alloying of 170 tonnes crude steel with the use of lime, raw magnesite or doloma lime and alumina for slag generation. The consumption of electrodes during the preheating of steel at the LF was set as 6 g/kWh. The lifetime of lining was determined 110 heats with no hot repair performed. The preheating of a new lined ladle was fixed with 8 hours [6].

At the same time an increase of energy efficiency means the reduction of indirect CO_2 emissions from Scope 2. All temperature losses have to be compensated during the treatment at the LF. The estimated heating rate of LF is on average 4 °C per minute. The duration of treatment was determined with 40 min [6].

It is a fact, that each country has different conditions of primary energy resources to generate electric energy. The British company "Ecometrica", which bundles up sustainability, environment, and business management with geospatial intelligence, has specified a table of CO_2 emission coefficients for each country. Some of which are included in Table II [7].

	C	Si	Mn	P	S	Al
	[wt.%]					
EAF	0.04	–	0.10	0.020	0.01	–
CCM	0.12	0.20	0.80	0.022	0.01	0.030

Table I. *Compositions of steel tapped at EAF and casted at CCM [6].*

Countries	[t_{CO_2}/MWh]
Austria	0.18
IEA Europe (*)	0.45
China	1.00

Table II. *Emission coefficients for Scope 2 [7].*
(*) IEA – International Energy Association

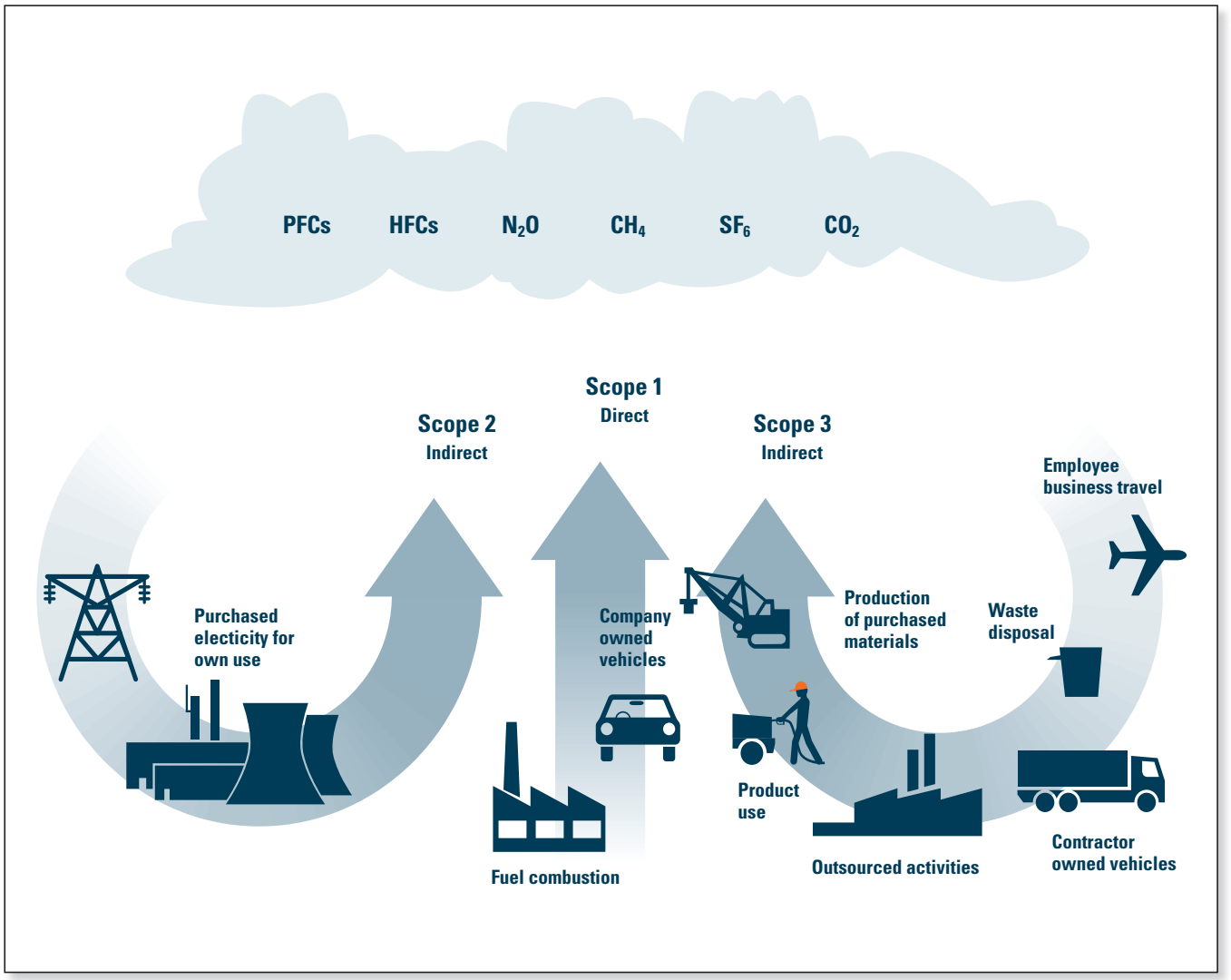

Figure 2. *Greenhouse gas emissions associated with industrial processes [5].*

Nevertheless the emissions from Scope 3 comprise the largest proportion of total emissions at secondary metallurgy. All the additions were separately estimated according to the emission coefficients from [8–11]. The raw magnesite value was assessed for a raw material with no external processing (extraction and transport only). Table III includes the coefficients for different alloying agents and slag formers.

Emission coefficients (Scope 3)						
[t_{CO_2}/t]						
FeSi [8]	FeMn [8]	Lime [9]	R.Magn. [10]	Dolomite [9]	Alumina [11]	Al [8]
3.80	1.45	0.95	0.02	1.1	0.39	1.65

Table III. *Emission coefficients for production of alloying agents and slag formers (Scope 3) [8–11].*

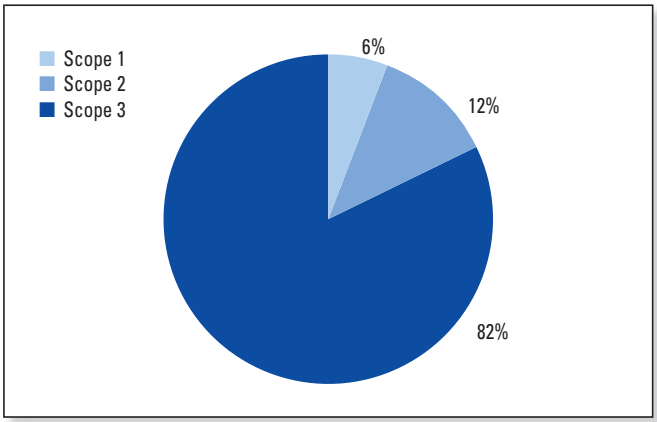

Figure 3. *Distribution of total CO_2 emissions per one heat due to three scopes for RR route [6].*

The calculated distribution of CO_2 emissions, due to these three scopes, is illustrated in Figure 3. The following values are based on the previously mentioned experience data of a steel plant, located in Austria. Potentially, the part of Scope 2 can extremely range according to emission coefficients (Table II). Thus, a medium coefficient for International Energy Association (IEA) Europe was used for Figure 3. However, the biggest contributor of total CO_2 emissions in secondary metallurgy is associated with Scope 3.

The total amount of CO_2 emissions generated during the recycling route (RR), including EAF, secondary metallurgy, casting and hot rolling is 420 $kg_{CO_2}/t_{hot\ rolled\ product}$ (Figure 1). Thus, calculation showed that, only ~10% of the CO_2 emissions are related to secondary metallurgy, 47 kg of 420 kg_{CO_2}/t_{ls} (ls - liquid steel). The value of 47 kg_{CO_2}/t_{ls} is an average calculated value that has been used for the assumptions, described below.

Evaluation of Ladle Logistic and Potential Savings

A potential to reduce steel temperature losses is to analyse the ladle logistics. This article describes for:

>> time after EAF tapping and before start of LF treatment waiting time - 1 (WT-1), and
>> time after LF treatment is completed and casting started waiting time - 2 (WT-2) [6].

The steel temperature tapped from EAF was assumed as 1645 °C. In cases of "good" logistics (assumptions A1 and A2 in Figure 4) time segments WT-1 and WT-2 were set at 20 and 15 minutes respectively. In cases of "poor" logistics they were set at 90 and 30 minutes.

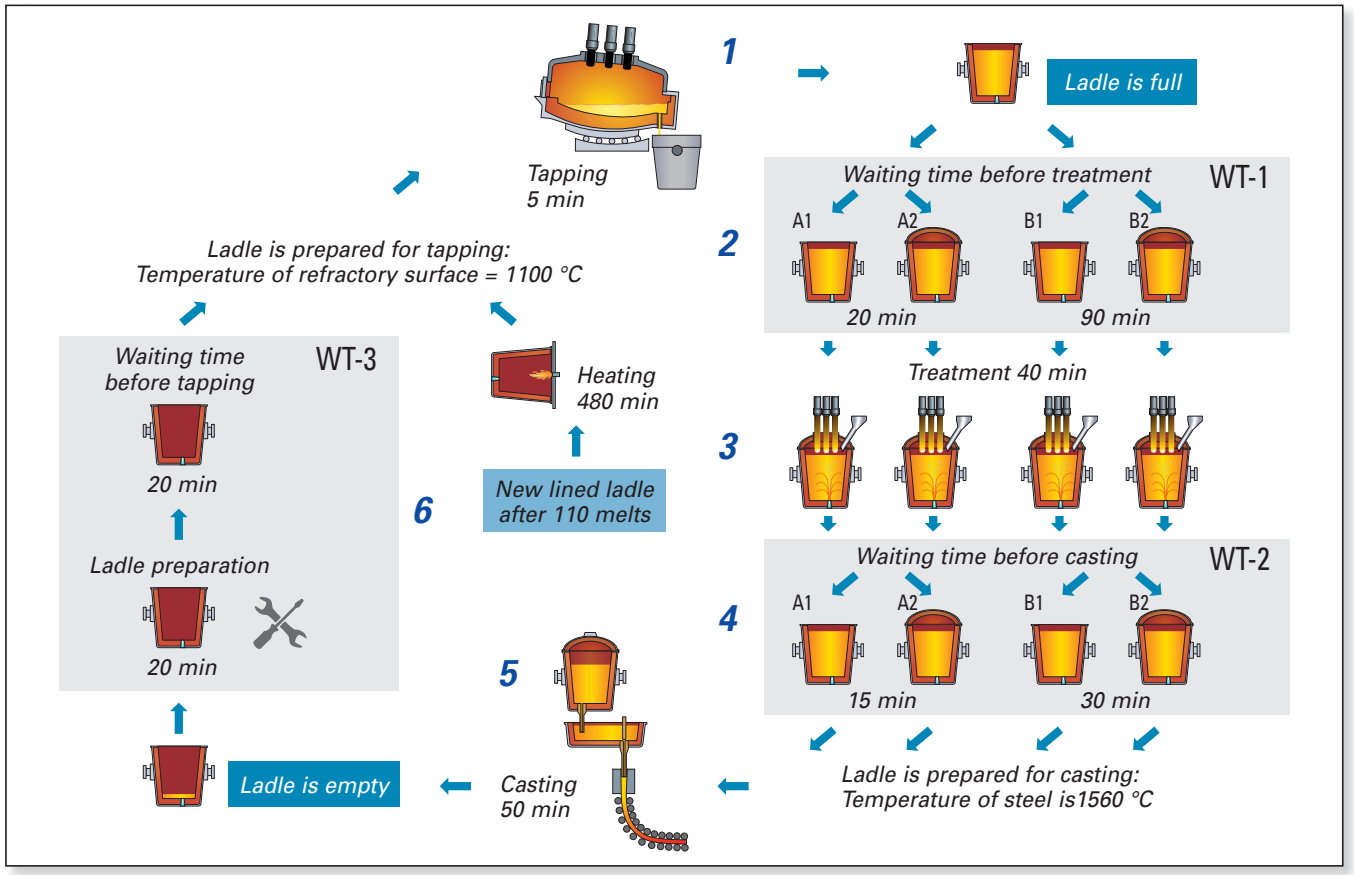

Figure 4. *Schematic structure of logistical assumptions [6].*

In addition, it was decided to evaluate the potential of the decreasing heat losses through the use of a ladle cover (assumptions A2 and B2 in Figure 4) during these two time segments. All the geometry dimensions and lining configurations of the ladle are based on the internship protocol, provided by the steel plant [6].

Thus, four logistical assumptions were determined for the model calculations (Figure 4):

>> A1 "good" logistic, no cover.
>> A2 "good" logistic, with cover.
>> B1 "poor" logistic, no cover.
>> B2 "poor" logistic, with cover.

The waiting time after casting until the next tapping was designated as WT-3. The duration of this segment was set as 40 minutes for all four logistical cases.

These logistic assumptions aim to evaluate the quantity of the electric energy for the LF-treatment, to compensate the sum of losses during WT-1, WT-2 and WT-3. The potential of the energy savings during treatment thus represents the savings of indirect emissions (Scope 2).

All the heat loses during the secondary refinement (steel contact time) were divided in two groups:

>> losses caused by alloying, and
>> losses caused by ladle parameters.

The mass and heat balances were calculated considering the steel and slag chemistry. The alloying concept and the mass and energy balances were developed considering the basics of thermodynamics and industrial operation practice.

Furthermore, the possibility of using raw magnesite or doloma lime for MgO saturation is also taken into account.

Thus, for all logistic assumptions two concepts were investigated:

>> Concept with raw magnesite (RM).
>> Concept with doloma lime (DL) [6].

The calculations for the production cycle for the two cases with good logistic (with and without cover) and alloying concept with raw magnesite (RM-A1 and RM-A2) are illustrated in Figure 5. In the upper section of Figure 5 the temperature time trends of these assumptions are depicted. These trends are respectively correlated with the two lines in the middle of Figure 5, symbolizing the duration of each production step, additionally marked with arrows. Temperature time trend and production step line are connected with the scales at the bottom, illustrating the amount of CO_2 emissions.

The highest temperature losses at secondary metallurgy are associated with tapping. From the moment when the ladle is completely filled, two trends RM-A1 (no cover) and RM-A2 (with cover) illustrate the benefit of a ladle cover during waiting time before treatment WT-1. At the end of this segment LF-treatment starts with synchronous heating and purging. Temperature losses during WT-1 as well as predicted losses during WT-2 have to be compensated during LF treatment. After the required temperature has been achieved, treatment will be continued only with purging. The required temperature at the end of heating is calculated according to the required casting temperature 1560 °C.

It is obviously clear, that during WT-1 and WT-2, a ladle cover reduces temperature loss and furthermore the heating duration, due to lower radiant heat loss. The comparison of assumption RM-A1 (no cover) and temperature time trend of RM-A2 (with cover) demonstrates a temperature loss of 22 °C, due to the absence of a ladle cover. The compensation has thus to be done at the LF.

Figure 5 shows that the dominate portion of CO_2 emissions is related to the charging materials settled in the ladle during tapping (Scope 3). Consequently the savings using a cover for these two cases account 1.7 kg_{CO_2}/t_{ls}. It represents ~5% of the total amount (Figure 3).

The same logistic assumptions for alloying concept doloma lime (DL) are represented in Figure 6. It is important to note, that the reduced temperature losses by tapping are referred to smaller heat requirements of slag saturation. Temperature after tapping for concept RM is 1563 °C, and for concept DL 1574 °C (Figures 5 and 6). Thus, using doloma lime, only during tapping 11 °C can be saved.

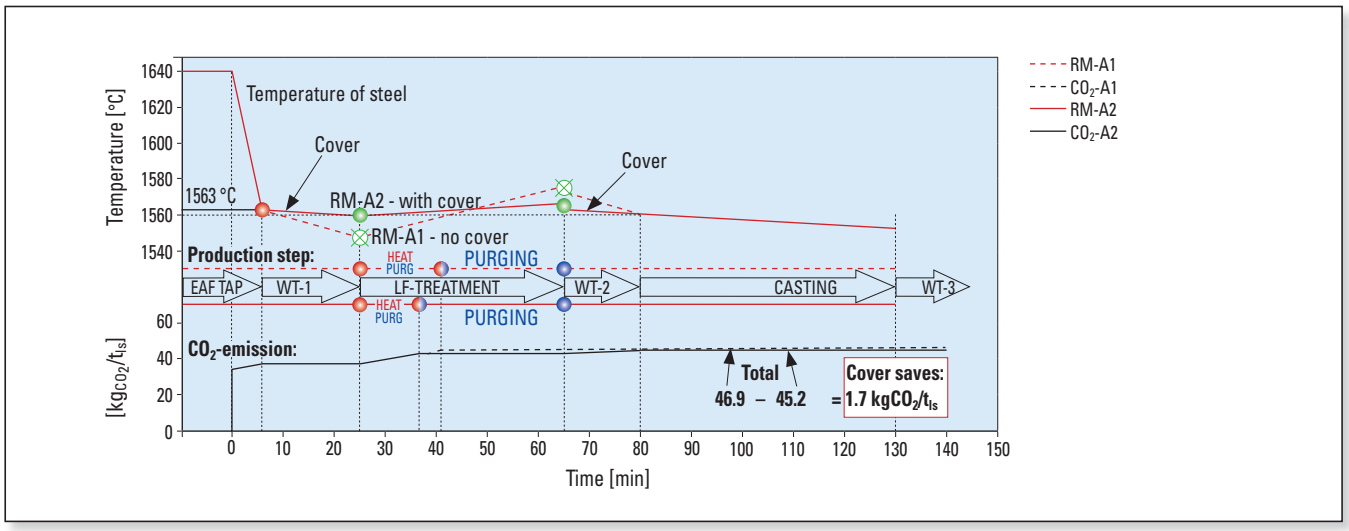

Figure 5. *Time-temperature charts and CO_2 emissions during one heat for cases RM-A1 and RM-A2 due to the corresponding production step [6].*

Other logistic assumptions for "poor" logistics were analogically calculated to evaluate the significance of time. Results are illustrated in Figure 7. It is crucial to note, that assumption "B1" (no cover) were not included in the common estimation, because theoretically the steel temperature drops below the liquidus temperature.

To summarise all the calculations it was decided to illustrate the final results for doloma lime (DL) and raw magnesite (RM) in a graph with four scales and three gradients (Figure 8).

Addition Gradient

The addition of raw magnesite (RM) is compared with doloma lime (DL) in kg/t_{ls}. The values differ due to the different amounts of alloying materials required to obtain the same desired MgO saturation. The addition of raw

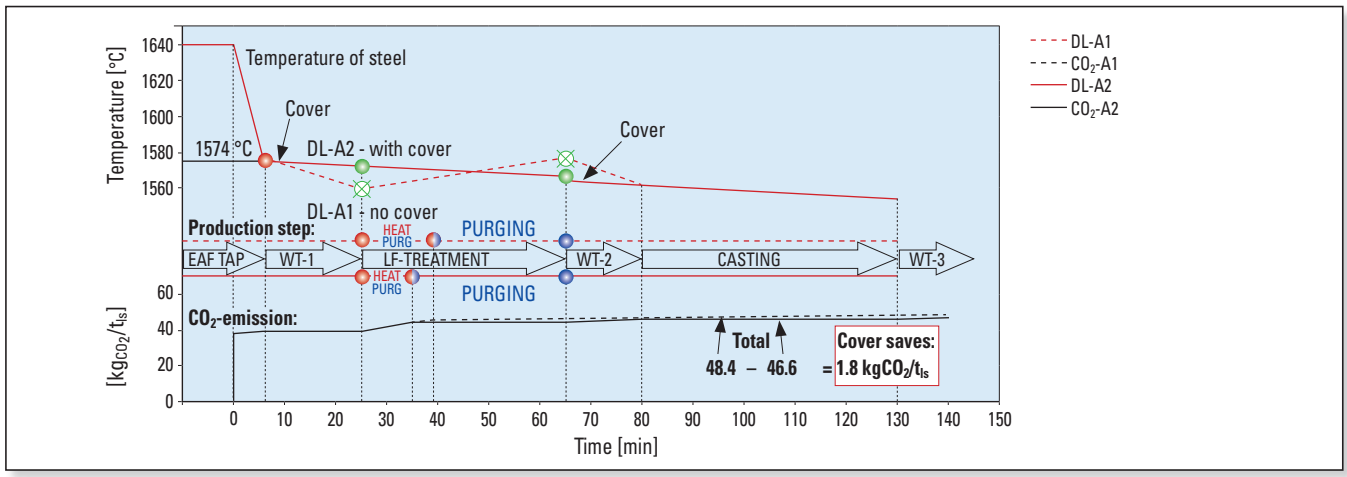

Figure 6. *Time-temperature charts and CO_2 emissions during one heat for cases DL-A1 (doloma-lime, no cover) and DL-A2 (doloma lime, with cover) due to the corresponding production step [6].*

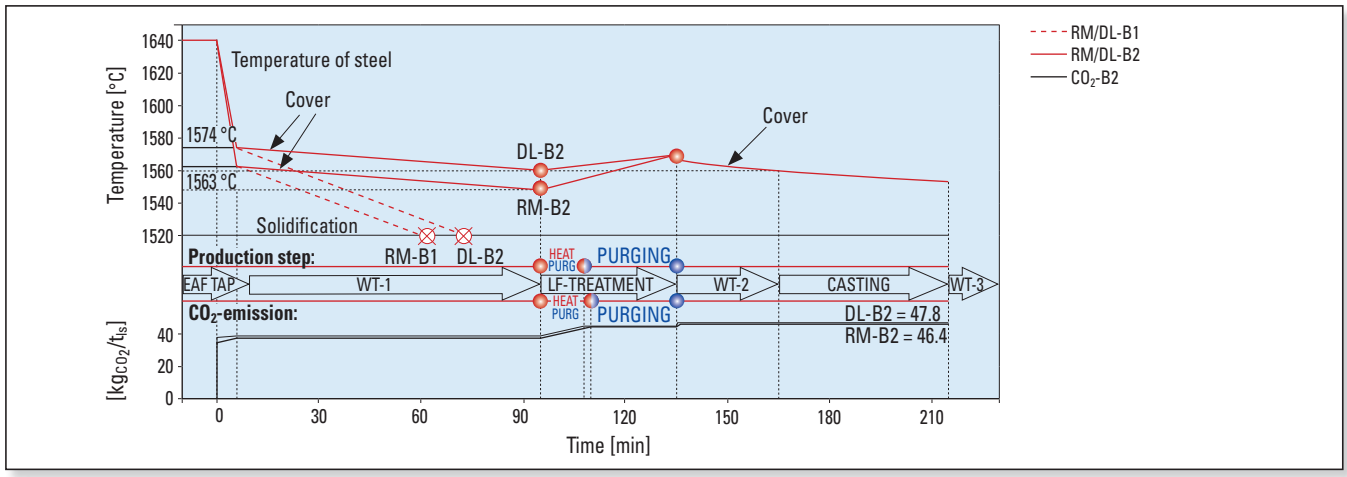

Figure 7. *Time-temperature charts and CO_2 emissions during one heat for cases RM-B1 (raw magnesite, no cover), RM-B2 (raw magnesite, with cover), DL-B1 (doloma lime, no cover) and DL-B2 (doloma lime, with cover) due to the corresponding production step (poor logistics) [6].*

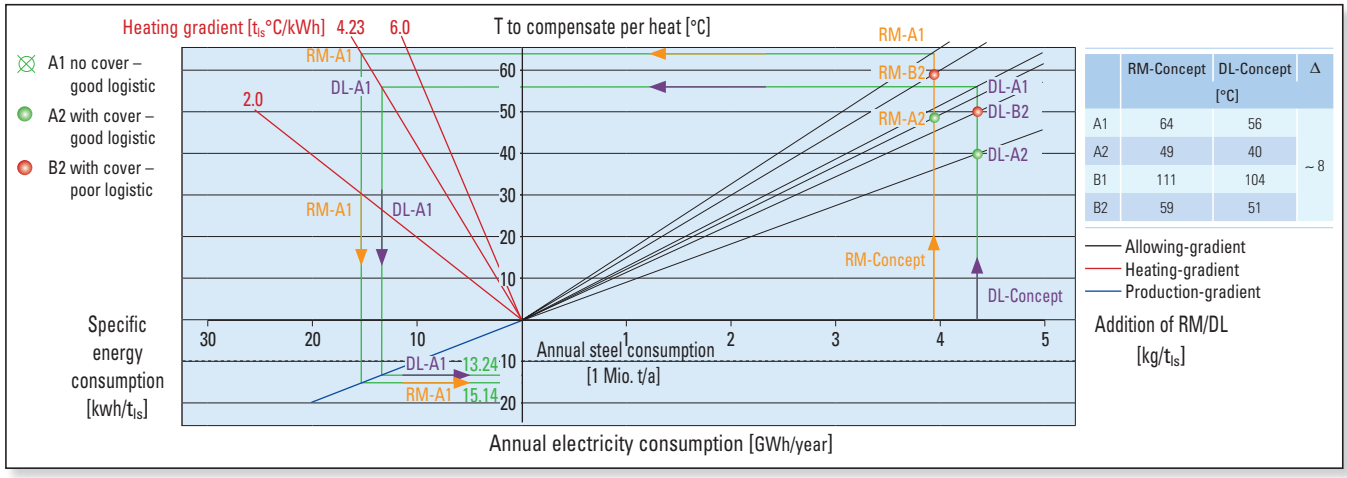

Figure 8. *Star diagram, which compares the alloying concepts and logistic cases with specific energy consumption and annual electricity consumption [6].*

magnesite was ~4 kg/t_{ls}, addition of doloma-lime was ~4.4 kg/t_{ls}. Each of these concepts was then correlated with the three logistical assumptions. These assumptions are the sum of all estimated temperature losses per heat, presented in the table within Figure 8. Thus, the temperature difference between RM and DL for two identical assumptions A1 (good logistics, no cover) is in average 8 °C.

Heating Gradient:

Temperature losses to be compensated during LF treatment were correlated with the amount of required electricity in kWh/t_{ls}. The gradient of 4.23 t_{ls}°C/kWh is based on technical configurations respective to LF and heat size (170 tonnes). In other words, this gradient shows the number of kWh that is required to preheat 170 tonnes of steel by 1 °C respective to the corresponding LF configurations [6].

Production Gradient

The specific energy consumption was recalculated to annual energy consumption (10^6 kWh/t_{ls} = 1 GWh/a) based on annual steel production (1 million tonnes) and heat size (170 tonnes). Thus annual electricity consumption for case of good logistic by RM concept is 15.14 GWh/a, by DL concept 13.24 GWh/a.

The difference between RM and DL concepts for these cases amounts to a total of 1.9 GWh/a, or €169860, (based on 1 KWh= €0.0894) [12] [6].

Direct Emissions in the Secondary Metallurgy

The estimation of the emission distribution showed, that direct emissions account for approximately 5% of the total amount (Figure 3). The substitution of raw magnesite by doloma lime can potentially reduce direct emissions twice, because no decomposition occurs through alloying. Also the slag saturation with MgO by doloma lime requires less extra heat than using raw magnesite.

As it was mentioned previously in this article, combustion of natural gas is the main source of direct emissions. According to the real operation practice in secondary metallurgy, it was decided to estimate the amount of direct emissions regarding different preheating durations. Table IV shows a simplified comparison of the CO_2 emissions for ladle preheating for 8, 9 and 10 hours after relining. The quantity of required ladle preheating treatments per year is based on ladle life time (110 heats), size of each heat (170 tonnes) and annual steel production for the calculation was determined with 1 million tonnes. Amount of CO_2 by each treatment is calculated based on natural gas flow of 350 Nm^3/h, aiming on a ladle temperature of 1100 °C. Taking into account these values and parameters, each regular additional hour of ladle preheating causes 36.6 t_{CO_2}/year [6].

Summary

The distribution of the total CO_2 emissions per heat due to three scopes for all estimated assumptions is summarised in Figure 9, using the average calculated value of 47 kg Co_2/t_{ls}.

Scope 1 includes the direct emissions, which are generated by:

>> yield loss of carbon alloying,
>> decomposition of carbonates, used for a slag generation,
>> electrodes consumption in the process of LF treatment, and
>> combustion of natural gas during preheating of a new lined ladle.

Scope 2 includes indirect emissions related to the purchasing of electricity for LF treatment.

Scope 3 includes indirect emissions associated with the production of materials such as alloying agents, slag formers, and refractory materials etc. [6].

Conclusions

Due to logistical improvement and use of a ladle cover it is possible to reduce the total CO_2 emissions by 2%. The dominate proportion (up to 80%) of the total emissions in secondary metallurgy is related to indirect emissions from scope 3.

The potential for savings is more tangible in terms of electricity consumption. Using the improvements in Table V, it is possible to decrease the annual electricity consumption and reduce production costs [13] [6].

Nevertheless, these improvements will contribute not only to the financial profit due to energy savings but also to reduced CO_2 emissions at the secondary metallurgy.

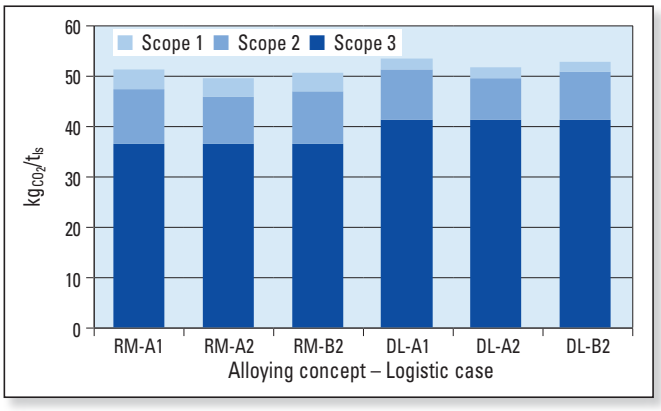

Figure 9. *Estimation of total CO_2 emissions during one heat according to alloying concept and logistic case [6].*

Duration of ladle preheating treatment [h]	Annual data by steel production 1 million tonnes		
	Number of heats	Number of preheating operations	Direct CO_2 [t]
8	5882	53	293
9			329
10			366
Emission, caused by additional hour of ladle preheating treatment			37

Table IV. *Influence of a new ladle's preheating duration on the amount of direct CO_2 emissions per year [6].*

Estimated improvements	Potential annual savings					
			[mio.tCO_2] per Scope			
	[GWh]	[€]	1	2	3	Sum
Substitution of raw magnesite by doloma lime	2.00	170100*	+1.83	+0.89	-4.14	-1.42
Usage of ladle cover before and after LF- treatment	3.70	327600*	-	+1.67	-	+2.81
Logistic improvement of 85 minutes (~30%)**	2.40	217800	-	+1.10	-	
Decreasing ladle preheating treatment by 1 hour	-	4500	+0.04	-	-	
Total	8.10	720000	1.40			

Table V. *Influence of estimated improvements on annual electricity consumption for 1 million tonnes steel/a, the price of electricity was assumed to be €0.09 per KWh. The price of natural gas was assumed to be €0.34 / Nm^3 [6].*
** - excluding investments costs*
*** - difference between logistic assumptions "poor" and "good" logistic for corresponding route.*

References

[1] Brown, T., Gambhir, A., Florin, N. and Fennell, P. Reducing CO_2 Emissions from Heavy Industry: A Review of Technologies and Considerations for Policy Makers. Grantham Institute for Climate Change, Briefing paper No 7, 2012. https://www.imperial.ac.uk/media/imperial-college/grantham-institute/public/publications/briefing-papers/Reducing-CO_2-emissions-from-heavy-industry—Grantham-BP-7.pdf

[2] Laplace Conseil. Impacts of Energy Market Developments on the Steel Industry. Presented at 74th Session of the OECD Steel Committee, Paris, France, July 1–2, 2013. http://www.oecd.org/sti/ind/Item%209.%20Laplace%20-%20Steel%20Energy.pdf

[3] Energy Efficiency and CO_2 Reduction in the Iron and Steel Industry. SETIS https://setis.ec.europa.eu/system/files/Technology_Information_Sheet_Energy_Efficiency_and_CO_2_Reduction_in_the_Iron_and_Steel_Industry.pdf

[4] Lachmund, H. Bedeutung und Aufgaben der Sekundärmetallurgie. Vortrag am 24.März 2014 on AG der Dillinger Hüttenwerke, Dillingen.

[5] Daviet, F. Designing a Customized Greenhouse Gas Calculation Tool. World Resources Institute, Washington, June 2006. http://pdf.wri.org/GHGProtocol-Tools.pdf

[6] Gerasev, A. Evaluation of the Potential for Reduction of CO_2 Emissions at the Secondary Metallurgy, Master Thesis, Monanuniversitaet Leoben, 2016.

[7] Brander, M., Sood, A., Wylie, C. Haughton, A. and Lovell, J. Technical Paper; Electricity-specific emission factors for grid electricity. Ecometrica, 2011. http://ecometrica.com/assets/Electricity-specific-emission-factors-for-grid-electricity.pdf

[8] IPCC Guidelines for National Greenhause Gas Inventories, Volume 3: Industrial Processes and Product Use, Chapter 4, 2006. http://www.ipcc-nggip.iges.or.jp/public/2006gl/pdf/3_Volume3/V3_4_Ch4_Metal_Industry.pdf

[9] World steel Association. CO_2 Emission Data collection. User guide, Version 6. https://www.worldsteel.org/dms/internetDocumentList/downloads/steel-by-topic/Data-collection-user-guide_v6/document/Data%20collection%20user%20guide.pdf

[10] Private communication with Professor J.Schenk, Chair of Ferrous Metallurgy, Monanuniversitaet Leoben, 2015.

[11] Methodology for the Free Allocation of Emission Allowances in the EU ETS post 2012. Sector report for the aluminium industry. November, 2009. http://ec.europa.eu/clima/policies/ets/cap/allocation/docs/bm_study-project_approach_and_general_issues_en.pdf

[12] Data from EuroStat website, title „Strompreise nach Art des Benutzers", code: ten00117 http://ec.europa.eu/eurostat/tgm/table.do?tab=table&plugin=1&language=de&pcode=ten00117

[13] Internal discussion between MUL and RHI, 2015.

Authors

Andrey Gerasev, Chair of Ferrous Metallurgy, University of Leoben, Austria.
Philip Bundschuh, Chair of Ferrous Metallurgy, University of Leoben, Austria.
Johannes Schenk, Chair of Ferrous Metallurgy, University of Leoben, Austria.
Peter Reisinger, voestalpine Steel Division AG, Austria.
Roman Rössler, voestalpine Steel Division AG, Austria.
Bernd Trummer, RHI AG, Steel Division, Vienna, Austria.
Andreas Viertauer, RHI AG, Steel Division, Vienna, Austria.
Gregor Arth, RHI AG, Steel Division, Leoben, Austria.
Corresponding author: Andreas Viertauer, andreas.viertauer@rhi-ag.com

Return to Content

RHI Bulletin > 1 > 2016, pp. 35–38

Bernd Trummer, Wolfgang Fellner, Andreas Viertauer, Leopold Kneis and Gernot Hackl

A Water Modelling Comparison of Hybrid Plug, Slot Plug and Porous Plug Designs

Introduction

Inert gas purging is an essential state of the art process step in ladle secondary metallurgy with the following main objectives: Homogenization of the steel melt (temperature, analysis), desulphurization if required and separation from non metallic inclusions (NMI) in order to fulfil steel cleanliness requirements [1, 2, 3, 4]. Whereas proper homogenization requires high gas flow rates, purification is carried out at very low gas flow rates in a process step called "soft bubbling". Due to the importance of this process step research has already been carried out for a long time [1].

A large number of purging plug types and designs are available on the market and comprehensive overviews have been published [5, 6]. This paper presents the results of a water model investigation comparing the bubbling behaviours of a hybrid plug, a slot plug and a porous plug at very low flow rates.

Implications on soft stirring in the ladle are presented and conclusions regarding the purging efficiency of hybrid plug versus slot plug and porous plug designs are given.

Experimental Procedure

A hybrid plug (porous part cross section: 60x60 mm), a standard slot plug with 24 slots (slot dimensions: 16 mm long and 250 µm wide and a porous plug (round porous part with cross section 120 mm) were installed in a water model. Details of the plug characteristics are given in Table I. The 1000 litre capacity water modelling tank was 1000 mm high. Sufficient tank height was necessary in order to observe the gas behaviour as it permeated through the water.

The plugs were fed with compressed air at ambient temperature via a pressure valve with a mass flow controller (range 0–10 l/min), which allowed a precise adjustment and a constant mass flow in the range of 0.5 l/min up to 10 l/min. A digital high speed camera was used to take images of the water model at a rate of 50 frames/second for bubble counting. The bubbles were counted in a defined field 222 mm high and 192 mm wide. A representative bubble number was determined by averaging the counts from 500 individual frames. Thereby, overlapping bubbles rising in the three dimensional water tank were statistically eliminated. The two-dimensional areas, πr^2, (i.e., great circle) of all the bubbles in the 500 individual frames were determined automatically by the software. Subsequently, the surface area, S, of an equivalent spherical bubble was calculated using the equation:

$$S = 4\pi r^2 \quad (1)$$

Water Modelling Results

Already pictures of bubble formation taken with standard phototographic equipment showed differences among hybrid plug, porous plug and slot plug (Figures 1, 2 and 3).

	Hybrid plug	Porous plug	Slot plug
Slot number	–	–	24
Slot dimensions [mm]	–	–	16x0.25
Porous part [mm]	60x60	Round, 120 mm cross section	–
Open porosity [vol.%]	27	27	12
Bulk density [g/cm^3]	2.7	2.6	3.1
Raw material basis	Al_2O_3	MgO	Al_2O_3

Table I. *Geometric and physical characteristics of the hybrid, porous and slot plugs examined in the water model investigation.*

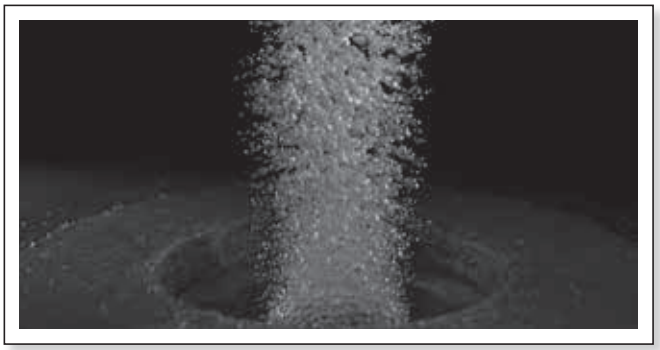

Figure 1. *Bubble formation from a hybrid plug at a flow rate of 10 l/min.*

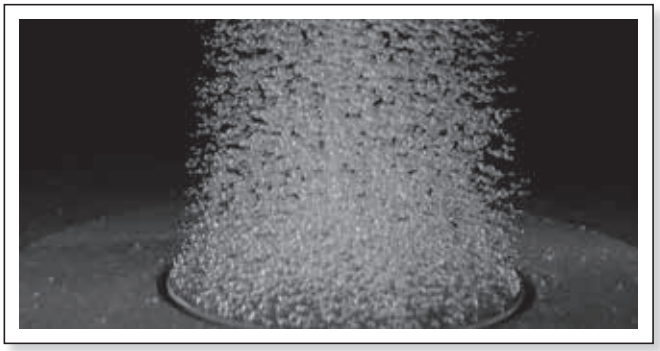

Figure 2. *Bubble formation from a porous plug at a flow rate of 10 l/min.*

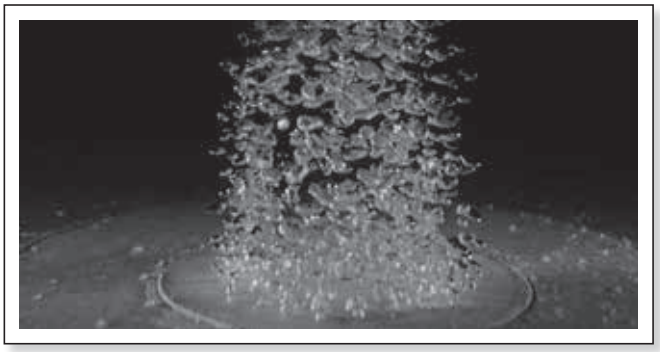

Figure 3. *Bubble formation from a slot plug at a flow rate of 10 l/min.*

However, for quantitative investigations high speed photography and automated image processing were required. By evaluating individual frames (Figure 4) single bubbles were resolved and their size as well as their number was determined.

Flow Characteristics

All three plug designs – hybrid plug, porous plug and slot plug – showed very linear flow characteristics in the investigated low flow regime (Figure 5). The hybrid plug had a rather steep slope of the relationship between the back pressure and flow rate which allowed easy controllability of the flow rate. The slope of the porous plug was more flat compared to the hybrid plug. However, still very good controllability of the flow rate was possible. Contrary to hybrid plug and porous plug, the slot plug had a gradient of the direct relationship between back pressure and the flow rate which was almost zero. Since an incremental increase in the applied pressure resulted in a significant flow rate increase, control and correct adjustment of the slot plug in such a low flow regime presented considerable difficulties.

Bubble Formation Characteristics

Hybrid Plug

The bubble size distributions determined at increasing flow rates are given in Figure 6. The areas of all bubbles in the 500 frames are included to provide minimum and maximum values.

The actual bubble size was rather constant, with the majority of bubbles having a cross-sectional area in the range of 1.5–2.5 mm^2, irrespective of the flow rate (Figure 7). This corresponds to a bubble diameter of 1.4–1.80 mm. With increasing flow rates, the relative number of larger bubbles increased. However, even at 10 l/min the area of hardly any bubbles reached 10 mm^2 or more, which was equivalent to a bubble diameter of ~ 3.6 mm.

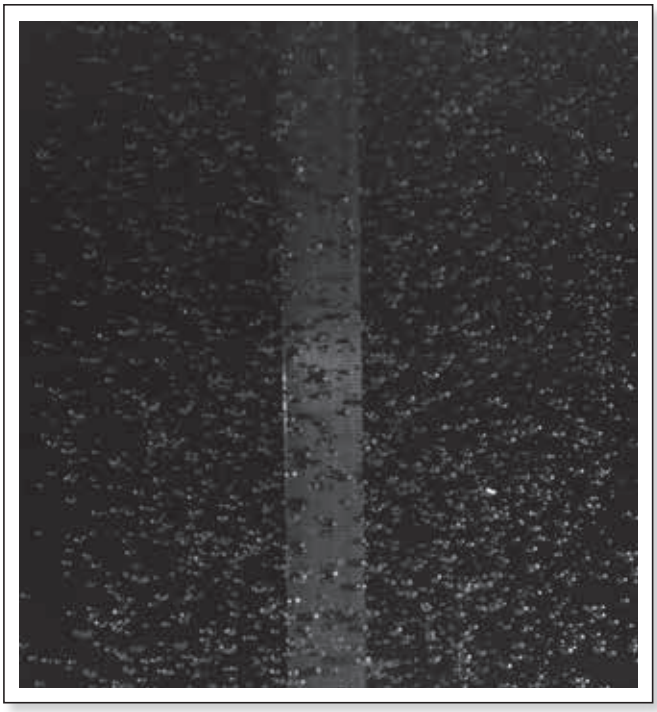

Figure 4. *High speed photography frame of bubbles generated by a hybrid plug at a flow rate of 5 l/min. The bubble size can be estimated by the measuring rod.*

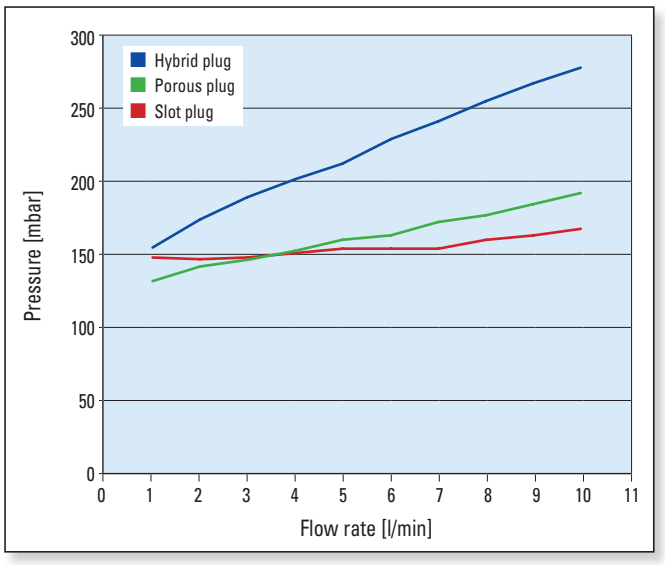

Figure 5. *Flow characteristics of a hybrid, porous, and slot plug operated under a low flow regime.*

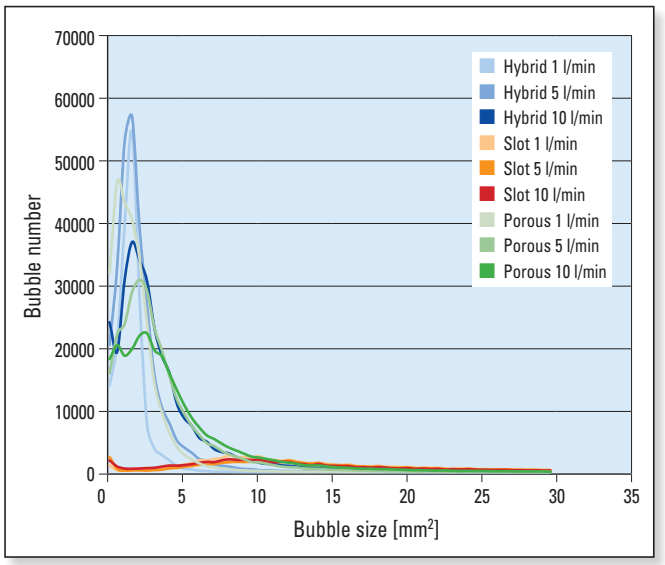

Figure 6. *Relationship between the flow rate and bubble size distribution generated by a hybrid, porous, and slot plug. Individual bubbles were determined in all 500 frames.*

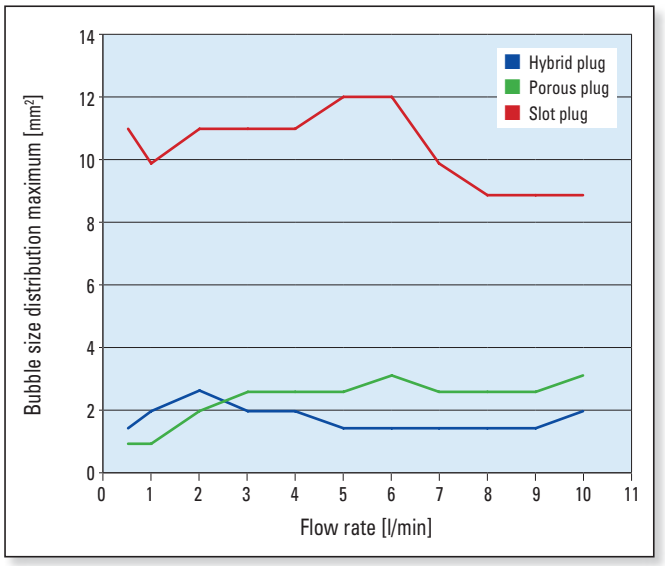

Figure 7. *Predominant bubble size generated from a hybrid, porous, and slot plug versus the flow rate.*

Porous Plug

The bubble size distributions determined for the porous plug are given in Figure 6. The distribution curves for the porous plug are quite similar to those of the hybrid plug. This is not surprising as both plugs are based on porous ceramics generating randomly distributed gas passage ways. The actual bubble size was rather constant, with the majority of bubbles having a cross-sectional area in the range of 1.5–3.0 mm^2, irrespective of the flow rate (Figure 7). This corresponds to a bubble diameter of 1.4–2.0 mm. With increasing flow rates, the relative number of larger bubbles increased. However, even at 10 l/min the area of hardly any bubbles reached 10 mm^2 or more, which was equivalent to a bubble diameter of ~ 3.6 mm.

Slot Plug

The bubble size distributions determined for the slot plug are given in Figure 6. The distribution curves for the slot plug differ significantly from the hybrid and the porous plug, resp. Not only was the bubble number significantly smaller, but the distribution itself was rather broad. The bubble sizes generated by a slot plug were larger, with a maximum area of about 8–12 mm^2. This was equivalent to a bubble diameter of ~3.2–4 mm. Figure 7 shows the predominant bubble size generated at a specific flow rate compared to hybrid and porous plug.

Summary and Verification

The water modelling results clearly demonstrated that both hybrid and porous plug were quite similar in their purging characteristics at low flow rates whereas the slot plug showed a different behaviour. The predominant bubble cross-sectional areas were determined to be 2 mm^2 for the hybrid plug, 2.5 mm^2 for the porous plug and 8.5 mm^2 for the slot plug resulting in mean bubble volumes of 2.05 mm^3 for the hybrid, 2.97 mm^3 for the porous and 18.45 mm^3 for the slot plug. Therefore, for a given low flow rate hybrid plug and porous plug have to generate about 10 times more bubbles than the slot plug. The average surface areas of individual bubbles generated by the hybrid, porous and slot plug were 8 mm^2, 10 mm^2, and 34 mm^2, respectively.

As hybrid plug and porous plug generate 10 times more bubbles than the slot plug the equivalent surface ratio is 80:34 (hybrid to slot) and 100:34 (porous to slot), which is approximately 2.3 to 2.9. This is in good agreement with the water modelling observations (Table II).

Discussion

There is a long history of using water modelling to investigate bubble flows in various liquids [7]. More than two decades ago, RHI focused on examining purging plug behaviour in water models. A previous water modelling comparison of hybrid, porous, and slot plugs on a very general, qualitative level showed clear differences between the different plug types regarding their purging behaviour [5, 6]. The comprehensive approach performed to examine and characterize bubble formation in this investigation was an attempt to differentiate between the hybrid, porous, and slot plug on a more quantitative basis.

Considering all the difficulties and challenges related to counting and quantifying bubbles by automated image processing, especially at higher flow rates, it is necessary to be very cautious regarding the conclusions. However, the results indicate that slot plugs are a rather poor solution for low gas flow rates. Their flow rate was difficult to control and precise adjustment to a specific rate was only possible when using flow control equipment with mass flow controllers [3, 4, 8]. The bubble number generated by this plug was comparatively low and remained almost constant with increasing flow rates. The bubble size distribution was broad with a maximum rather large bubble size. The total extrapolated bubble surface also remained relatively constant with increasing flow rates.

In contrast, hybrid, and porous plug were easy to control and a specific flow rate could be easily achieved. The bubble number was controlled by the flow rate. The bubble size was very small for both plug designs and stayed almost constant with increasing flow rates. At higher gas flow rates the total extrapolated bubble surface area increased considerably compared to the slot plug and could be easily increased or reduced by adjusting the flow rate.

Flow rate [l/min]	Hybrid plug total bubble surface area [mm^2]	Slot plug total bubble surface area [mm^2]	Ratio of hybrid/slot plug total bubble surface areas
0.5	7035	9508	0.7
1	8358	11016	0.8
2	15005	12644	1.2
3	21228	8932	2.4
4	20768	13156	1.6
5	19319	11008	1.8
6	22861	11368	2.0
7	25303	13936	1.8
8	28909	13652	2.1
9	29407	10204	2.9
10	33491	9496	3.5

Table II. *Ratio of the extrapolated spherical bubble surface areas generated by a hybrid and slot plug in the defined field at different flow rates.*

Conclusion

Inert gas purging in ladle secondary metallurgy comprises in general the following main process steps: homogenization, desulphurization and alloying at high gas flow rates and soft bubbling, inclusion shape control [9] and cleanliness stirring at very low gas flow rates at the end of the ladle treatment [2, 3]. These opposing purging objectives have to be met by purging plugs working perfectly at high as well as at low flow rates.

Prior investigations [5, 6] have shown that slot plugs operate perfectly at high flow rates normally used for standard metallurgical procedures (e.g., homogenizing the steel melt) [2, 3, 4]. At low flow rates slot plugs were difficult to control. This is in good agreement with our work where flow control equipment with mass flow controllers was necessary to control slot plugs at flow rates usually applied for soft purging. This behaviour in combination with a relatively small number of bubbles generated by the slot plug indicates that slot plugs are a rather poor solution for operating reliably at soft bubbling conditions.

Contrary to this behaviour porous plugs operate perfectly at low flow rates and their flow rate can be easily controlled. They generate a large number of small bubbles making them ideal for soft bubbling purposes. However, when operated at higher flow rates porous plugs tend to have excessive wear rates resulting in considerably lower average life times compared to slot plugs. Consequently higher plug consumption and more frequent plug exchanges with all the related extra efforts are necessary. Hybrid plugs with their combination of random and directed porosity show top performance at low as well as at high gas flow rates and have an excellent initial opening rate.

At very low flow rates the purging gas mainly passes through the porous element as the slots are blocked by infiltrated steel. Optimum soft bubbling conditions are achieved. With increasing flow rates the gas is able to open the blocked slots and purging takes place mainly through the slots. Optimum conditions for homogenization are achieved. This two-way purging characteristics considerably reduces wear on the porous insert and leads to plug life times on state-of-the-art level in modern ladle purging. The hybrid plug combines optimum purging results with economic efficiency. The results from all this studies will be used to develop an improved generation of purging plugs as RHI is committed to being a solution provider for holistic purging with tailor-made products for customers worldwide.

References

[1] Neifer, M., Rödl, S., Bannenberg, N. and Lachmund, H. Research into the Movement and Removal of Inclusions in Gas-stirred Steel Melts. *Stahl und Eisen*. 1997, No. 5, 55—63.

[2] Lachmund, H., Metallurgie der Pfannenstandentgasungsanlage (VD- Metallurgy) presented at VDEh Stahlakademie Secondary Metallurgy, Krefeld, March 25th, 2014.

[3] Gantner, A. Metallurgurgie des Pfannenofens (LF- metallurgy) presented at VDEh Stahlakademie Secondary Metallurgy, Krefeld, March 25th 2014.

[4] Viertauer, A. Pfannenmetallurgische Verfahren und Beanspruchung des Feuerfest (Ladle Metallurgical Processes and Implication on Refractories) presented at VDEh Stahlakademie Feuerfest Technologie, Bad Neuenahr, April 26—29, 2015.

[5] Hammerer, W., Raidl, G. and Barthel, H. Gas Purging for Steel Ladles. *Radex-Rundschau*. 1992, Heft 4, 217—226.

[6] Kneis L., Trummer B. and Knabl, B. The Hybrid Plug – An Innovative Purging Plug for Steel Ladles. *RHI Bulletin*. 2004, No. 1, 34—38.

[7] Höfele, E.O. and Brimacombe, J.K. Blasenströmungen in verschiedenen Flüssigkeiten (Bubble Flow in Various Liquids). *Metallurgical and Materials Transactions B*. 1979, 10B, 631—648.

[8] Kirschen, M., Ehrengruber, R., Spiess, B. and Rotsch, J. Process Improvements in EAF, Ladle, and AOD for High Alloyed and Stainless Steel Grades by Gas Purging Excellence, Proceedings of the 8th European Stainless Steel & Duplex Stainless Steel Conference, Graz, Austria. April 28—30, 2015.

[9] Abraham, S., Bodnar, R. and Raines, J. Inclusion Engineering and the Metallurgy of Calcium Treatment. *Iron & Steel Technology*, 2014, July, 57—68.

Reprinted with permission from ACerS and the UNITECR Proceedings.
Originally presented at the 14th Biennial Worldwide Congress, UNITECR 2015.

Authors

Bernd Trummer, RHI AG, Steel Division, Vienna, Austria
Wolfgang Fellner, RHI AG, Technology Center, Leoben, Austria
Andreas Viertauer, RHI AG, Steel Division, Vienna, Austria
Leopold Kneis, RHI AG, Steel Division, Vienna, Austria
Gernot Hackl, RHI AG, Technology Center, Leoben, Austria
Corresponding author: Bernd Trummer, bernd.trummer@rhi-ag.com

Return to Content

RHI Bulletin > 1 > 2016, pp. 39–44

Gregor Arth, Andreas Viertauer, Gernot Hackl, Georg Krumpel, Bernd Petritz and Daniel Meurer

Tundish Technology and Processes: Ladle to Mould Systems and Solutions (Part I)

Non metallic inclusions (NMI) are known to affect the material properties of cast steel products significantly. In times of continuously increasing demands on so called "clean steels", in general a reduction of NMI's in the liquid steel and cast product, the tundish is one of the locations to raise the steel cleanliness to an enhanced purity level. Several systems have been developed to protect the steel from contact with the surrounding atmosphere and to avoid the chemical and mechanical interaction with the refractory material. The latter to reduce the formation of so called exogenous NMI's, but additionally to prevent the steel from increased oxygen, nitrogen, and hydrogen pickup. The aim of this article is to provide the initial overview of RHI's customer tailor-made sized solutions to ensure the production of high quality steel grades, minimizing the risk of gas pick-up during ladle to mould transfers and a reduction in NMI's in the final product.

Introduction

Steel cleanness modification begins during secondary metallurgy and can be enhanced by several tasks such as deoxidation, alloying, slag chemistry, additives, stirring, vacuum treatment, if required Ca-metallurgy, and more [1–4]. Flow control of the liquid steel from the ladle to the tundish is the first of several sections in tundish metallurgy, where the casting process must pay attention not to decrease the steel cleanliness, mainly controlling:

>> Refractory material,
>> Low pressure inside the casting channel,
>> Ladle shroud position,
>> Shroud submerging depth [5],
>> Impact pot selection,
>> Slag carry over from ladle to tundish, e.g., using an appropriate slag detection system,
>> Chemically stable tundish cover material.

This article focuses on especially this first section in tundish metallurgy, to keep the cleanliness level of the steel elevated (equal to cleanliness in the ladle or probable to improve) by using optimized refractory solutions regarding design and material selection.

The influence of different casting parameters on the impact pot performance will be the topic of part II of this publication series. The interaction of tundish cover powder/slag with the wear lining and tundish furniture as well as the influence on the steel cleanliness also will be content of further publications in the RHI Bulletin.

Ladle to Mould Systems and Solutions (Part I)

Part I of this publication series focuses on the casting channel and the impact pot (Figure 1). Detailed information about the new ladle gate type S system (slide gate) has been previously published.

Negative pressure in the casting channels of shrouds can occur during ladle to tundish transfer of the steel, leading to air ingress into the casting stream [7]. In addition to material developments to reduce and/or avoid clogging, an improvement of the casting channel design can lead to lower air ingress during steel transfer from ladle to tundish, furthermore from tundish to mould.

Casting Channel

Details of the simulations for an optimized design of the casting channel of the inner nozzle in the slide gate system have been published previously [8]. The simulation predicts significant differences in the pressure distribution inside the

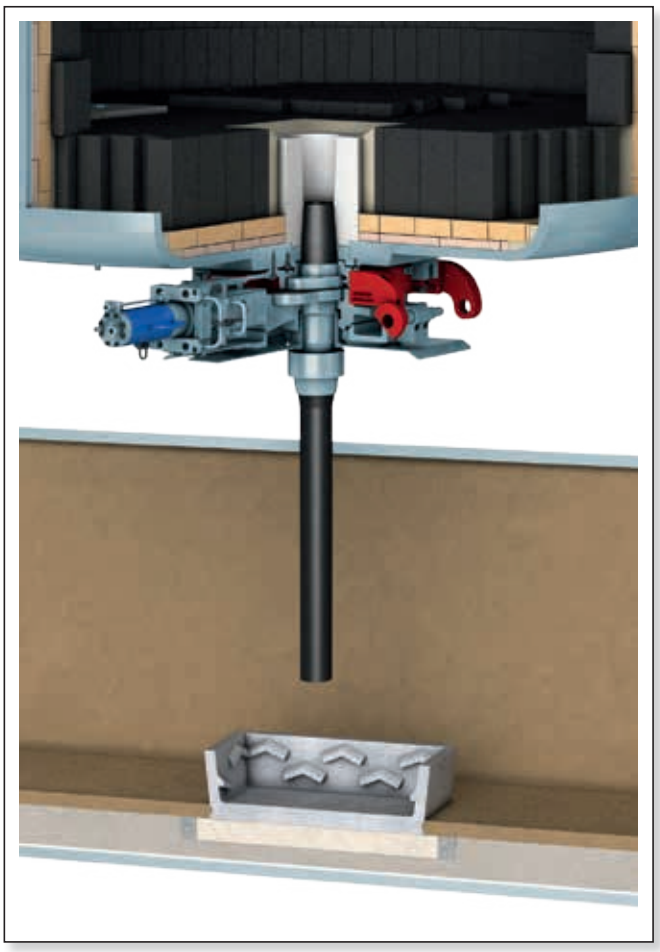

Figure 1. *RHI ladle to mould systems and solutions.*

casting channel between the two investigated designs (Figure 2). The standard nozzle design leads to a severe contraction of the fluid at the top of the inner nozzle. High turbulences and under-pressure along the entire casting channel downstream occurs. In contrast, an optimised channel design avoids areas of under-pressure, reducing the risk for air ingress and all the negative effects associated, namely deterioration of the refractory due to elevated temperature as well as refractory decarburisation, and moreover the re-oxidation of steel.

In-house CFD-simulations and water modelling are appropriate tools to assist the selection of customer specific flow control arrangement solutions. Most modelling studies concerning the ladle to tundish casting channel assume a perfectly vertically aligned and centred ladle shroud. However, in steel plant operations this is frequently not the case and quite a large inclination angle may occur [8], and any slight misalignment of a ladle shroud affects the unstable turbulent flow within the tundish and thus the steel quality [5]. The impact of shroud alignment on the total oxygen content can be seen in Figure 3, where a misaligned shroud leads to a significant increase of oxygen due to this unstable flow [9].

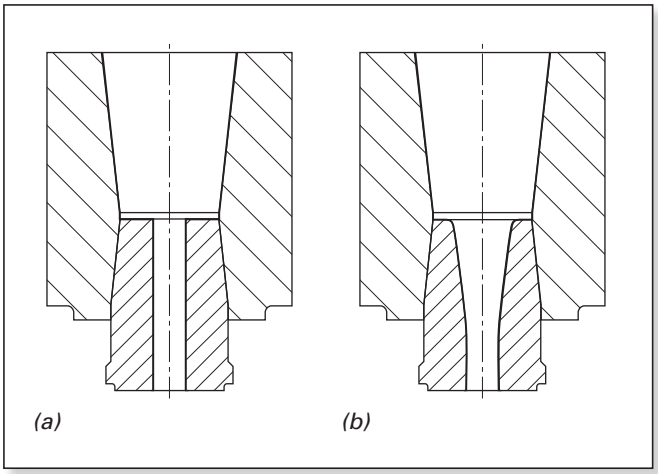

Figure 2. *Schematic of casting channel, showing (a) the standard design and (b) the optimized design [8].*

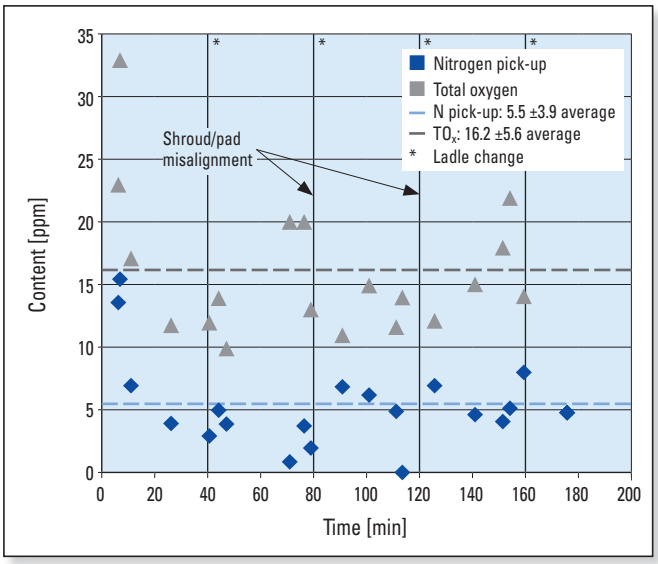

Figure 3. *Oxygen and nitrogen contents during a casting sequence, increased oxygen content due to shroud misalignment [9].*

While areas of under pressure inside the casting channel can be minimized or avoided, misaligned ladle shrouds can lower the benefits of a well designed casting channel by offering new gaps for air entrainment, thus leading to increased N, O, and H pickup and most likely faster clogging. Well designed ladle shrouds geometries that consider for example, immersion depths and the intersection of the ladle shroud and collector nozzle, are recommended for every caster type to ensure a protected and optimized steel flow from the ladle to the tundish. Essential key parameters are therefore an optimum connection of the ladle shroud to the ladle collector nozzle, a controlled liquid steel flow over the whole casting operation, a maximum protection against reoxidation, prevention of steel splashing during casting and excellent cold start performance without preheating prior to use.

Of fundamental importance is the connection between ladle shroud and the collector nozzle. The appropriate design of shroud and nozzle can be enhanced by using a suitable gasket at the connecting interface. Current technology uses fibre gaskets to avoid air entrainment and to improve the seal between the nozzle and the ladle shroud. Fibre gaskets are characterized by a high temperature stability, low heat capacity, flexibility and long service life. An alternative to standard fibre gaskets are expandable gaskets shown in Figure 4, to further reduce the N pick up from ladle shrouds during standard casting conditions.

(a)

(b)

Figure 4. *Expandable gasket solutions. Showing (a) the gasket components and (b) in installation.*

These gaskets are comprised of an expandable graphite sealing material, refractory material, and a binder and can either be fixed on a collector nozzle or directly inside the ladle shroud. When this gasket type is subjected to high temperatures, an intercalate expandable material pushes adjacent layers of graphite apart, resulting in an irreversible and mechanically strong form of graphite with a changed molecular structure. The randomly oriented layers of expandable graphite promote an even expansion in all directions and therefore create an excellent seal.

In the frame of a comparative field trial at a large european slab caster 70 ladle shrouds containing an expandable gasket and 65 ladle shrouds containing a standard fibre gasket were used and the N pick-up was measured accordingly. As can be seen in Figure 5, using an expandable gasket clearly helps to reduce the N pick up during standard casting conditions.

The previously published results of Ehrengruber [6,10] show that the additional inert gas purging between slide gates helps to generate a 100% oxygen-free atmosphere around the throttling position. Nevertheless, to avoid air ingress a combination with the shielded shroud connection (SCC) application will provide the best solution to reduce N pick up, which is a measure of the reoxidation potential of steel. The SCC application, shown in Figure 6, provides reliable prevention of air aspiration at the joint between the ladle nozzle and ladle shroud, controlling supply and maintenance of a positive argon pressure over the entire nozzle/shroud sealing interface surface [11].

The degree of NMI formation is also influenced by the volume of ladle slag entrained into the tundish. Even if slag carryover cannot be completely avoided, several applications with electromagnetic or optical detection methods, the use of vibration or weight monitoring techniques as well as

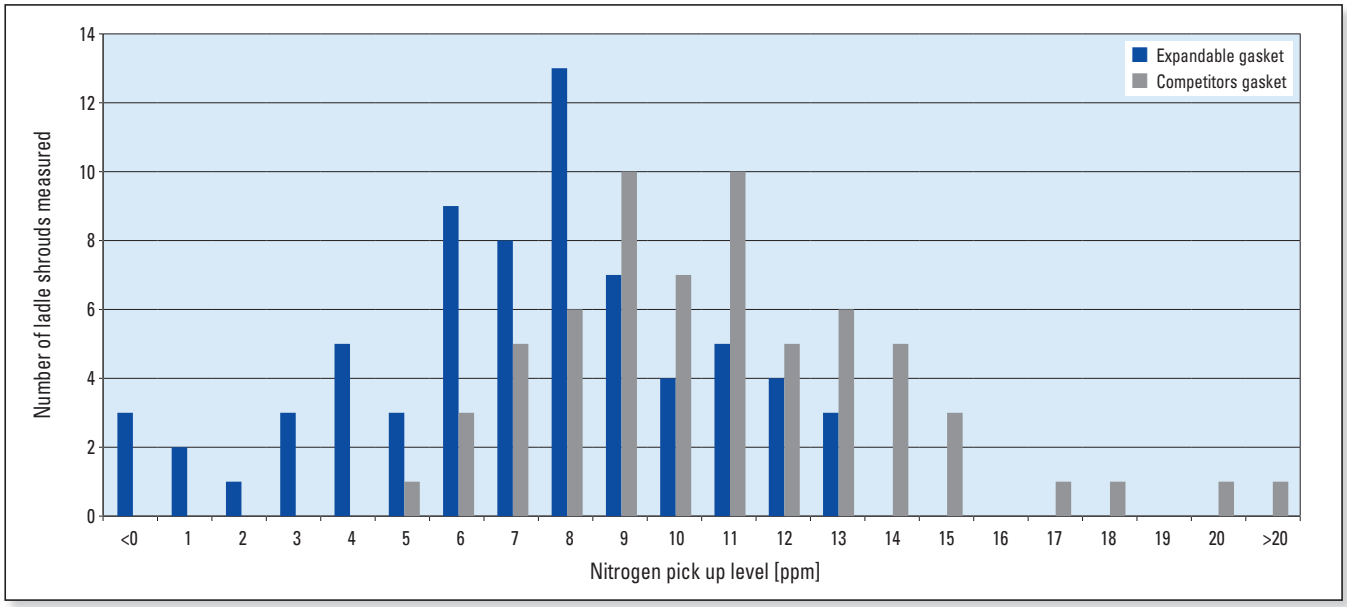

Figure 5. *Nitrogen pick-up at a slab caster, expandable gasket vs. conventional gasket.*

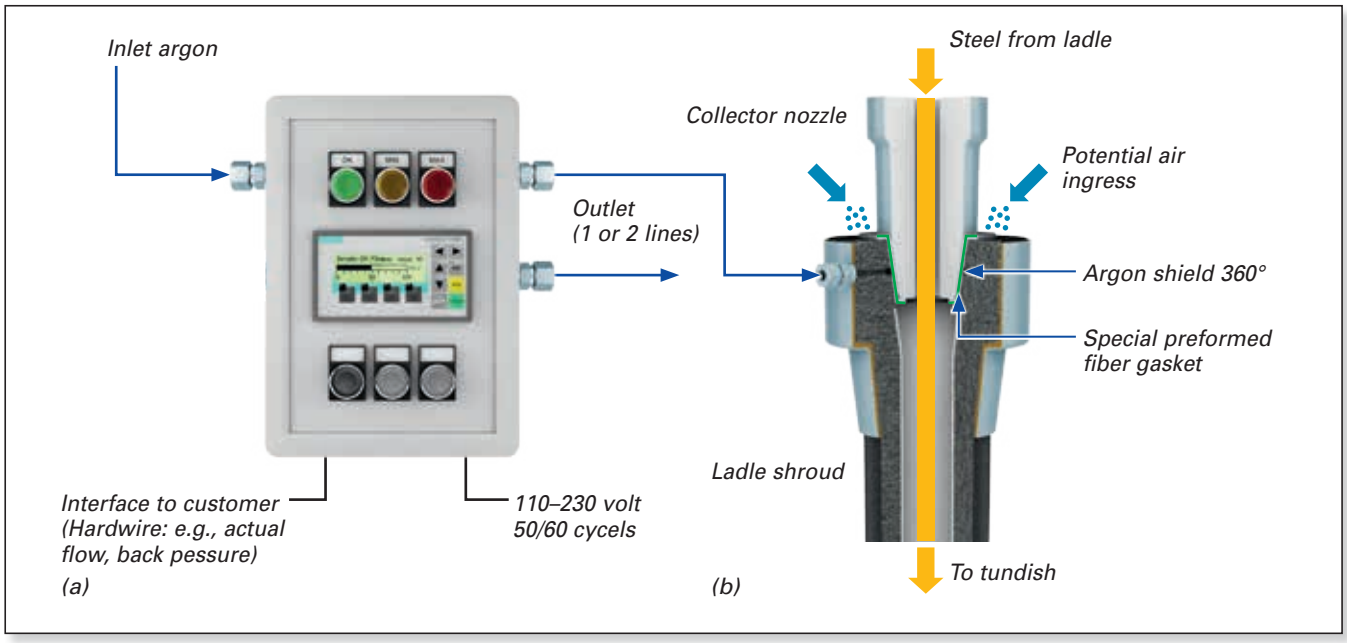

Figure 6. *Shielded Shroud Connection (SCC) showing (a) the controlling unit and (b) the connection of the collector nozzle with the ladle shroud.*

slag float valves can help to reduce this amount, compared to the approach of visual observation by the operator [12] as shown in Figure 7.

The influence of the amount of entrained ladle slag on the steel cleanliness and the tundish lining performance, and the importance to reduce slag entrainment into the tundish, will also be topic of further parts of this publication series.

TUNFLOW™ Impact Pots

Tundish tasks have changed from a distribution and buffer vessel to a multifunctional refining unit over the past years [13], aiming for homogeneous temperature distribution, steel plug flow, high residence time to enhance NMI's flotation, and more. A general overview on influencing factors on steel cleanliness and solutions have been published elsewhere [14]. As was mentioned previously, shroud immersion depth [5], ladle slag carry over, and impact pot selection have a significant influence on the metallurgical performance of the tundish and hence the product quality. In addition to minimising splashing during the initiation of casting, the correct selection and installation of the impact pot can reduce open eye formation and high surface turbulences.

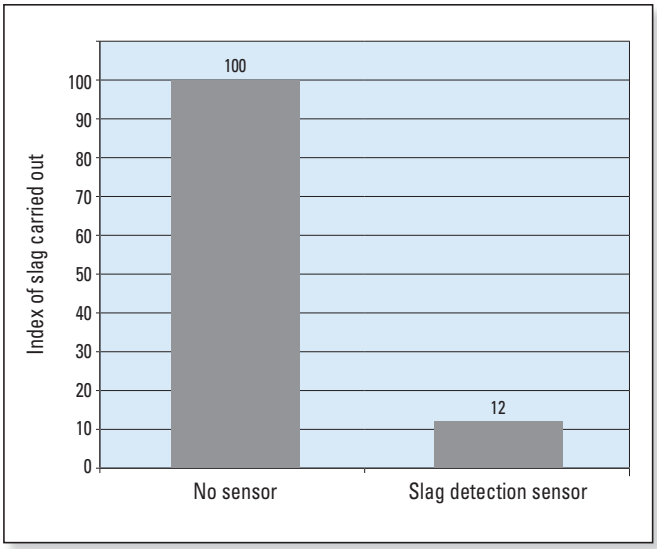

Figure 7. *Reduction of slag index through the use of a slag detection sensor [12].*

Figure 8 shows representative snapshots for the characterisation of surface turbulence and "open eye" formation obtained by a water model benchmark. Three different impact pot designs assuming a perfect vertically aligned shroud were compared. The installation of the RHI Flowerpot leads to a significant decrease of the open eye compared to a conventional lipped design. Using the latest product design family called TUNFLOW™ CHEVRON, the surface turbulence is further reduced and as a consequence the open eye formation under the experimental conditions can almost be completely avoided. Details of similar simulations with misaligned ladle shrouds can be found in the references [8,15].

The next example below depicts typical CFD simulation results, in this case where a conventionally lipped product is compared to the TUNFLOW™ using a vector plot in the central plane of a two strand slab caster tundish (Figure 9). The corresponding residence time distribution (RTD) data provided evidence of the superior TUNFLOW™ performance, as the minimum residence time (t_{min}), the average residence time (t_{mean}), and the plug flow volume (V_p) were increased, whereas the dead volume (V_d) was reduced (Figure 10, Table I). The RTD parameters were calculated according to the model of Sahai and Emi, considering the dispersed plug flow volume [16]. Additional information about RTD curves can be found in [9], details of the simulation setup and procedure is summarized in [15].

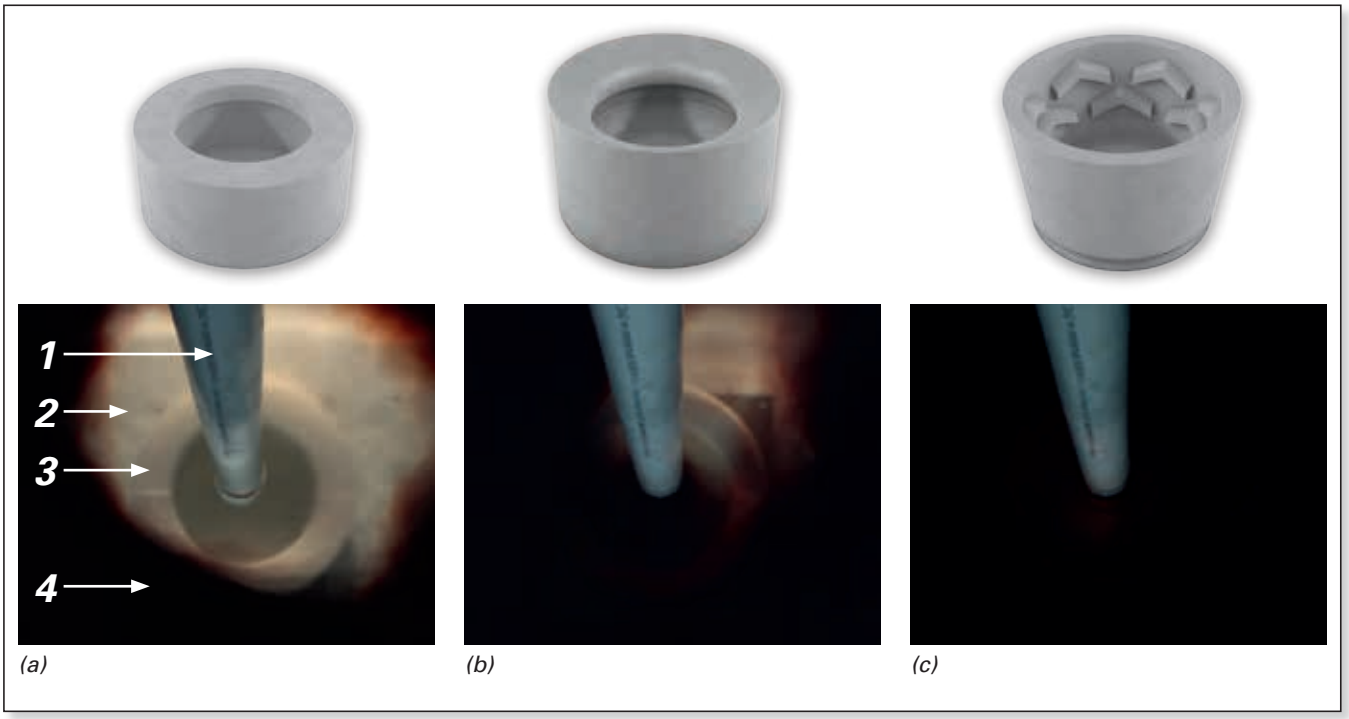

Figure 8. *Impact pot performance respective open eye formation, showing representative snapshots for the characterisation of surface turbulence and "open eye" formation obtained by a water model benchmark of (a) conventional lipped design (1, ladle shroud, 2, tundish bottom, 3, impact pot, and 4 slag) and (b) Flowerpot and (c) TUNFLOW™ CHEVRON.*

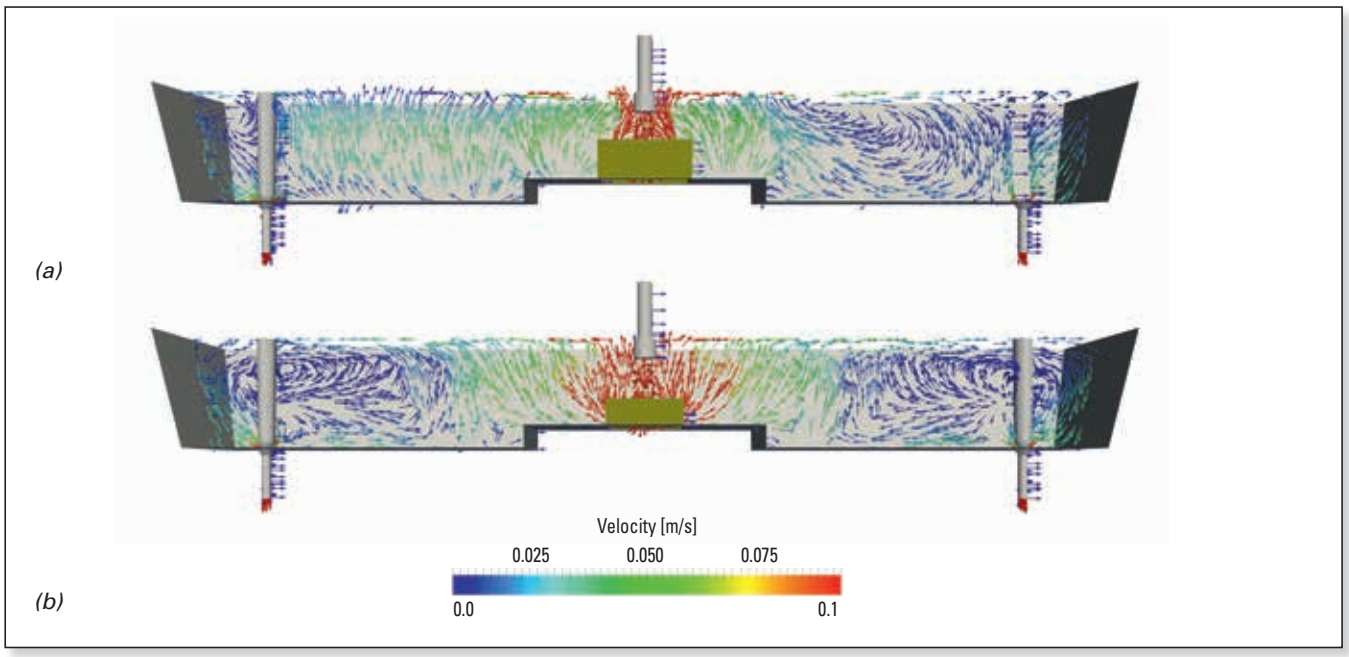

Figure 9. *Vector plot of the center plane of the tundish, showing (a) conventionally lipped design and (b) TUNFLOW™ Slot.*

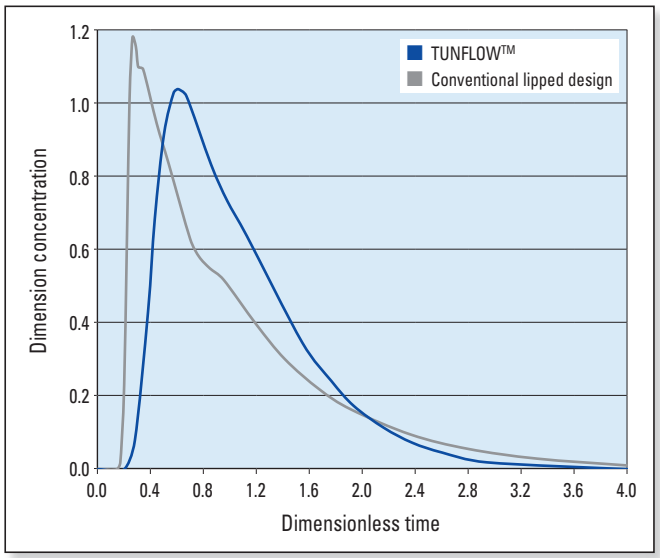

Figure 10. *The residence time distribution curves for both designs.*

Table II provides information about typical and enhanced product designs of the TUNFLOW™ product family. All these in-house CFD simulations have been confirmed at the RHI water modelling laboratory and proven by several customers. For completeness, the benefits of an optional installed purging beam on steel cleanliness regarding NMI separation, thus reduced clogging problems during casting, have to be included here. Details concerning the influence of argon purging and the advantages can be found elsewhere [10,12]. Further investigations on purging beams in tundishes and their influence on steel cleanliness will be presented in upcoming articles of this publication series.

Summary

The enhanced tundish tasks to maintain steel cleanliness on an equal niveau, or even an improved level, offer refractory suppliers and steelmakers new possibilities to realize the demands of the customers for cleaner steels. Using simulation tools like CFD and water modelling to improve refractory design is one of RHI's contributions as refractory

Parameter	Influence on tundish efficiency	TUNFLOW™ Slot	Conventional lipped design – no slot
		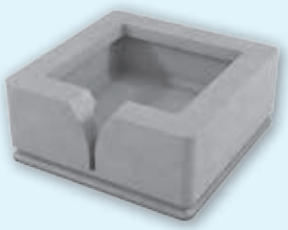	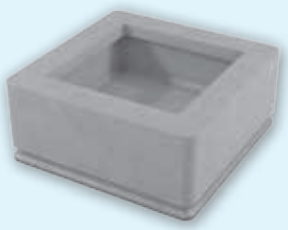
t_{min} [s]	The higher – the better	68.0	56.0
t_{mean} [s]	The higher – the better	380.0	330.0
V_p [%]	The higher – the better	39.3	17.5
V_d [%]	The lower – the better	5.7	22.0

Table I. *RTD data comparison TUNFLOW™ Slot vs. conventional lipped design.*

solution provider, helping to understand and minimize air ingress and clogging tendency.

Nevertheless, beneficial effects of optimized casting channel design can be lowered if one does not pay attention to vertically aligned ladle shrouds. Gaskets as well as the installation of the SCC system can therefore help to maintain a high steel cleanliness level, even if ladle shrouds are fixed with a slight inclination. The correct selection of the impact pot design also helps to reduce open eye formation and avoid N pick up and reoxidation, even if a misalignment of the shroud occurs. Additionally the application of a slag detection system can help to minimise ladle slag carryover, thus reducing the formation of NMI's in the steel.

The influence of different casting parameters on the impact pot performance will be the topic of part II of this publication series. The interaction of tundish cover powder/slag with the wear lining and tundish furniture as well as the influence on the steel cleanliness also will be the content of further publications in RHI's Bulletin.

References

[1] Zhang, L. and Thomas, B.G. State of the Art in Evaluation and Control of Steel Cleanliness. *ISIJ International.* 2003, 43, No. 3, pp. 271–291.

[2] Misra, S., Li, Y. and Sohn, I. Hydrogen and Nitrogen Control in Steelmaking at U.S. Steel. *AISTech Proceeding,* St Louis, USA, 4–7 May, 2009; pp. 829–840.

[3] Deckers, R., Blanpain, B., Plessers, J. and Wollants, P. Steel Cleanliness and Hydrogen in Liquid Steel. Proceedings of the *VII International Conference on Molten Slags Fluxes and Salts,* Cape Town, South Africa, 25–28 Jan., 2004; pp. 753–762.

[4] Millman, S., IISI Study on Clean Steel: Clean steel—Basic Features and Operation Practices. *The International Iron and Steel Institute (IISI);* Brussels, 2004; pp. 8, 39-60.

[5] Chattopadhyay, K., Isac, M. and Guthrie, R.I.L. Physical and Mathematical Modelling to Study the Effect of Ladle Shroud Misalignment on Liquid Metal Quality in a Tundish. *ISIJ International* 2011, 51, No. 5, pp. 759–768.

[6] Ehrengruber, R. and Bühlmann, R. INTERSTOP Ladle Gate Type S— A New Milestone in Ladle Gate Technology. *RHI Bulletin.* 2015, No. 1, pp. 61–66.

[7] Bannenberg, N., Inclusion Modification to Prevent Nozzle Clogging. Proceedings 78th Steelmaking Conference, Iron and Steel Society, Nashville, USA, April 2–5, 1995, pp. 457–463.

[8] Hackl, G., Ehrengruber, G., Tomas, M. and Eglsäer, C. Flow Control Refractory Design Optimisation by Modelling and Simulation. Presented at UNITECR 2015, Vienna, Austria, Sep., 15–18, No. 447.

[9] Wakelin, D. (Ed.), *The Making, Shaping and Treating of Steel. 11th Edition; Casting Volume: Chapter 13, Tundish Operations.* The AISE Steel Foundation; Pittsburg, Pa, 2003.

[10] Ehrengruber, R., Excellence in Inert Gas Control Systems for the Steel Industry, *RHI Bulletin.* 2015, No. 1, pp. 7–15.

[11] Badr, K., Tomas, M., Kirschen, M. and McIlveney, G. Refractory Solutions to Improve Steel Cleanliness. *RHI Bulletin.* 2011, No. 1, pp. 43–50.

[12] Sahai, Y. and Emi, T. *Tundish Technology for Clean Steel Production.* World Scientific Publishing; Singapore, 2007.

[13] Marique, C., IISI Study on Clean Steel: State of the Art and Process Technology. The International Iron and Steel Institute (IISI); Brussels, 2004, pp. 16–17, 165-182.

[14] Secklehner, B.A., Casado, M.T. Viertauer, A., Wappel, D. and Brosz, B. Tundish Technology and Processes: A New Roadmap. *RHI Bulletin.* 2015, No. 1, pp. 68–77.

[15] Hackl, G., Wappel, D. Meurer, D., Tomas, M. and Komanecky, R. Product Development and Flow Optimization in the Tundish by Modelling and Simulation. AISTech Proceedings, Indianapolis, USA, 5–8 May, 2014, pp. 1911–1919.

[16] Sahai, Y. and Emi, T. Melt Flow Characterization in Continuous Casting Tundishes. *ISIJ International.* 1996, 36, No. 6, pp. 667–672.

Authors

Gregor Arth, RHI AG, Steel Division, Leoben, Austria.
Andreas Viertauer, RHI AG, Steel Division, Vienna, Austria.
Gernot Hackl, RHI AG, Technology Center, Leoben, Austria.
Georg Krumpel, RHI AG, Steel Division, Vienna, Austria.
Bernd Petritz, RHI AG, Technology Center, Leoben, Austria.
Daniel Meurer, RHI AG, Technology Center, Leoben, Austria.
Corresponding author: Gregor Arth, gregor.arth@rhi-ag.com

Return to Content

Neha Jain, Florian Barthmann and Ghufran Ansari

RHI Zirconia Nozzles in Tundish Application

This article aims to give an insight into the world of zirconia nozzles for tundish applications at RHI. Tundish nozzle changer systems offer a considerable cost benefit versus simple metering nozzle practice. With production sites in Germany and India, RHI offers a broad portfolio of zirconia nozzles for nozzle changer systems as well as metering nozzles. Different combinations of zirconia and carrier material together with the correct production techniques enable RHI to supply nozzles for the popular nozzle exchanger systems worldwide. State of the art research facilities available at the RHI Technology Center in Leoben drive product developments and improvements in this field.

Introduction

The tundish nozzle changer system is of extreme importance in the open casting of steel. Maximum service life and flexibility with regards to the casting speed are vital. RHI offers well-block-nozzle sets as well as refractory components for the tundish nozzle changer systems. Under the trade name INTERSTOP, RHI also offers the well proven MNC nozzle changer systems. A selection of some of the nozzles available is shown in Figure 1. With two production sites and production of millions of nozzles per year RHI is equipped to supply a wide range of zirconia nozzles worldwide.

Simple Metering Nozzle practice: Casting sequences approx 1–15 heats on average due to the increased diameter of the metering nozzle and increased casting speed, shown in Figure 2.

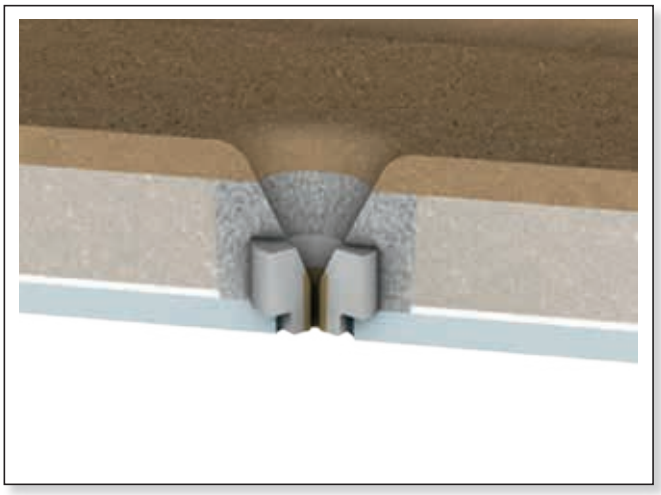

Figure 2. *Simple metering nozzle design.*

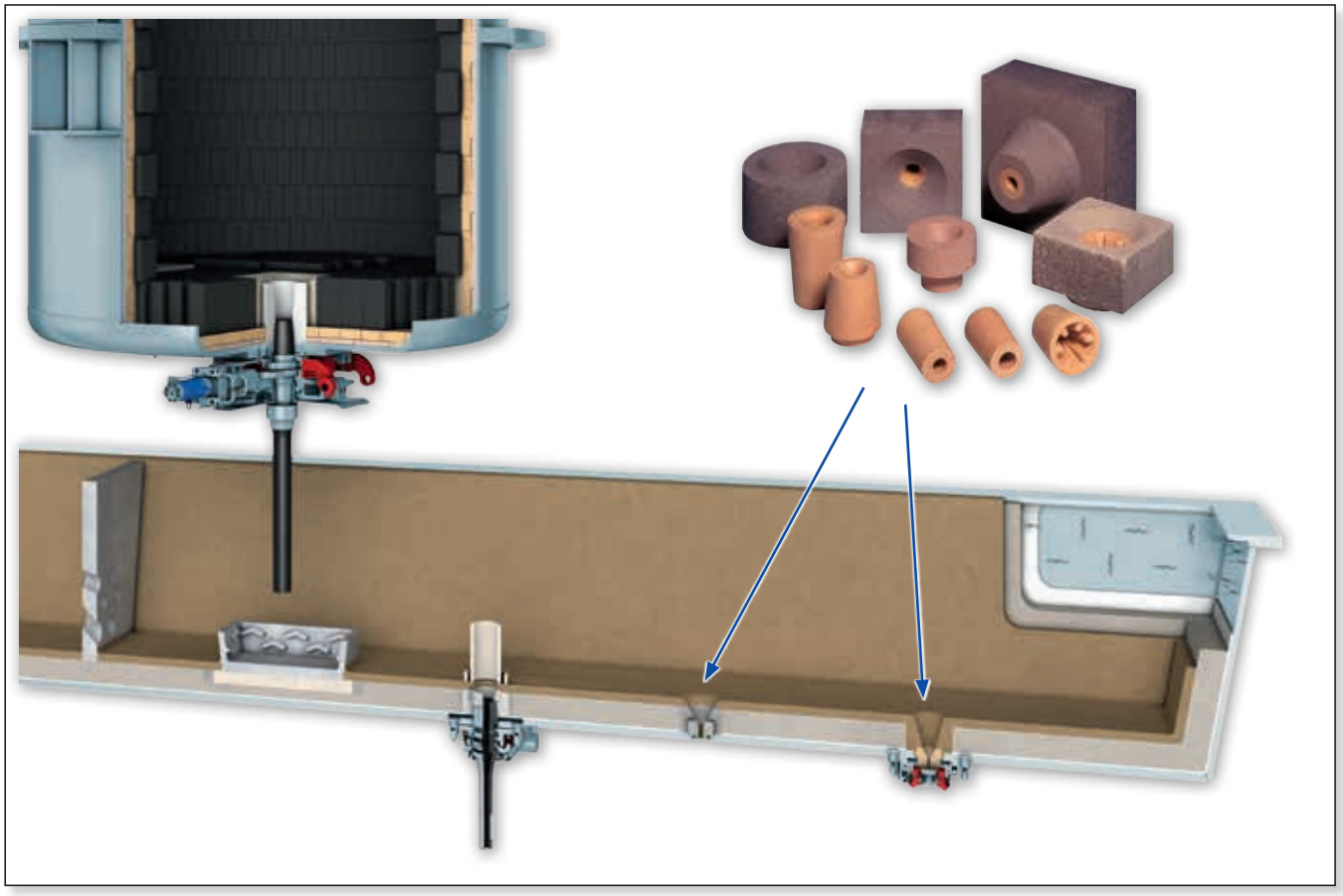

Figure 1. *Tundish nozzles as a part of tundish furniture [1].*

Nozzle Changer System practice, shown in Figure 3, provides the following benefits:

>> Longer casting sequences, approx. 15–100 heats.
>> Increased safety.
>> Flexibility with regards to the casting performance by changing diameter during operation or shutdown and re-start of casting.
>> Cost saving.

Nozzle exchanger systems offer a significant cost advantage in tundish operation over a period of time. With increased safety measures and definite cost saving the benefits of MNC nozzle exchanger systems over simple metering nozzles are considerable.

During the last few years RHI has more than doubled the zirconia nozzles production capacity, delivering millions of units worldwide and it is established as the most widely used manufacturer for zirconia nozzles. Currently there are more than 200 different insert and exchangeable nozzle shapes available. Tundish flying nozzles and well-block-nozzle sets are mainly manufactured in the following two locations:

Marktredwitz Production Plant

The production plant in Marktredwitz is located in the heart of Europe, in Bavaria, Germany (Figure 5). The plant has a long and impressive history, going back to the year 1899 when it was established as Chamottewerk by Didier. In 1967, the production was changed to high temperature materials, zirconium oxide being a part thereof. There are currently approximately 340 employees including 30 apprentices working in the plant. Currently 90% of products go in the steel industry, more specifically in the area of flow control for steering and dosing of liquid steel, mainly in the field of continuous casting plants. The products include, among others, slide plates, inner and collector nozzles, top-hats, zirconia nozzles, and inserts, based on diverse raw materials. The products are supplied to all the major steel producing companies worldwide. Overseas customers are supplied via sea containers from the Hamburg port.

ORL Bhiwadi Production Plant

The RHI production plant ORL is located in the industrial area of Bhiwadi, in the state of Rajasthan, India, around 70 kilometers away from the national capital New Delhi (Figure 6).

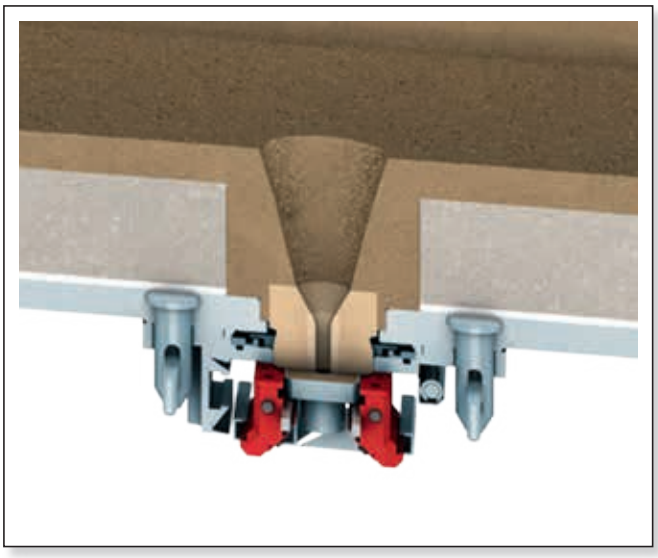

Figure 3. *Schematic of the nozzle changer system.*

Figure 5. *RHI production facility in Marktredwitz, Germany.*

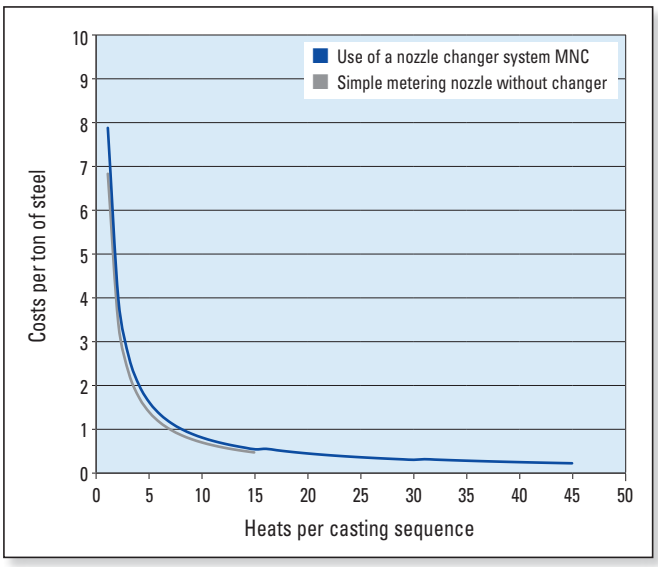

Figure 4. *Example of cost saving by using MNC nozzle exchangeable system versus simple metering nozzle [2].*

Figure 6. *RHI production facility in Bhiwadi, India.*

ORL was founded in 1980 and began commercial production in 1986. There are currently 480 people employed at ORL. A wide variety of products for steel flow control applications are produced in ORL, namely slide gate plates, isostatically pressed continuous casting refractories, zirconia nozzles, and inserts, pre-fabricated products, high-, low-, ultra low- cement castables, self flow castables, and mortars with 50–80% alumina. The products are supplied domestically all over India, and exported to countries such as Egypt, Germany, Indonesia, Iran, Thailand, and Turkey.

Raw Materials

A range of carefully selected raw materials is used for the production of the zirconia nozzles, the critical raw material being zirconium oxide. Natural, as well as synthetic raw materials are used, for example baddeleyite from Russia, synthetic monoclinic zirconia from China, South Africa, and Australia etc. Stringent quality checks start from the incoming materials until the packing of final product to ensure consistent quality.

Manufacturing Process

Depending on the raw material and the product application the following are the major production steps involved in the production of the nozzles (Figure 7).

Pressures of up to 250 MPa are used to ensure the high density of the zirconia nozzles. Based on the zirconia grade and product application, high temperature treatments over 1600 °C are required with different temperature profiles to achieve the desired strength, phase transformation, and product characteristics. Co-pressing, casting, and fixing using mortar are the three process routes through which the zirconia inserts are fit to form the nozzles.

Important Factors in the Production of Zirconia Nozzles [3]

Degree of Stabilization of Zirconia

The high temperature behaviour of zirconium oxide is critical because of the phase transformation and the linear expansion hysteresis curve. This necessitates a specific heat-up process for these materials before use to reduce thermal shock when the first strand is cast and to prevent cracking. The optimum heat-up process requires a slow heating of the zirconia nozzles up to 200 °C to eliminate the residual moisture. This step is then followed by a one hour heat-up to approximately 800 °C. During the heat-up of zirconia it is important not to exceed 1000 °C as the cooling down of the nozzle could lead to crack formation once the burners are switched off. The heating of zirconia from between 1100 °C to 1300 °C leads to a conversion from monoclinic to tetragonal resulting in volume decrease. On the other hand, the cooling of zirconia from above 1300 °C to temperatures below the conversion point cause an expansion of the material and leads to tensile stresses.

The degree of stabilization of zirconia directly influences the thermal expansion of the product and can be measured from the intensity peaks using X-ray diffraction. The more stabilized the zirconia, the smaller the volume expansion during cooling at the tetragonal ZrO_2 to monoclinic ZrO_2 transformation temperature.

Correct Grain Size Distribution

The grain size and reactivity of fine particles influences the shrinkage of zirconia. The D50 and D90 values (the diameter where respectively 50% and 90% of the particles have smaller particle size) help in adjusting the milling time to reach the correct grain size distribution.

Surface Flatness and Tolerances

The precise computer numeric control (CNC) finishing methods and quality controls ensure the surface finish is within the narrow tolerances. This is vital in ensuring correct steel flow and preventing problems such as building of steel tongues on the nozzles.

Advanced Techniques for Analysis and Further Developments [3], [4]

In addition to the wide range of popular refractory test methods such as density, porosity, cold crushing strength, chemical analysis using x-ray fluorescence, hot and cold modulus of rupture, refractoriness under load, and creep, etc., the Technology Center in Leoben has state-of-the-art

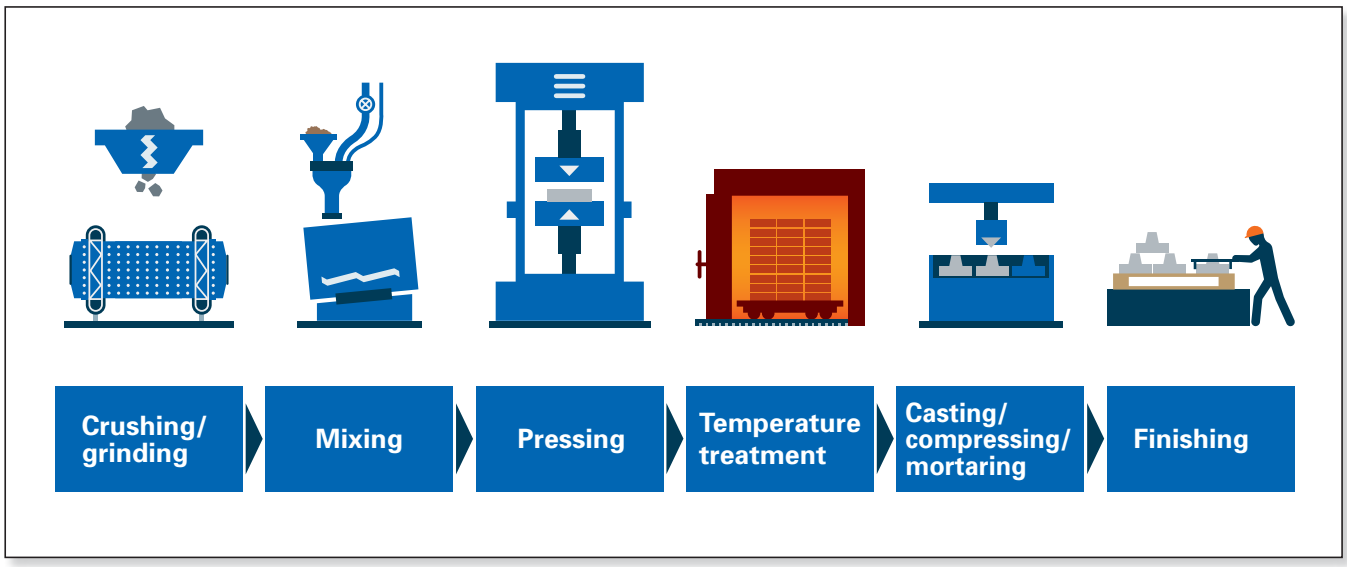

Figure 7. *Production steps for the nozzle manufacturing process.*

testing and research facilities, which offer further testing possibilities for quality control, product development, and customer support. Innovative ideas in the field of pre- and post-mortem sample analysis drive product developments and improvements.

Thermo Mechanical Finite Element Analysis

Through the simulation of operational conditions, for example, molten steel at 1600 °C, the finite element analysis may help to understand the temperature distribution, principal stresses, and deformation of the nozzles under steady state conditions (Figure 8).

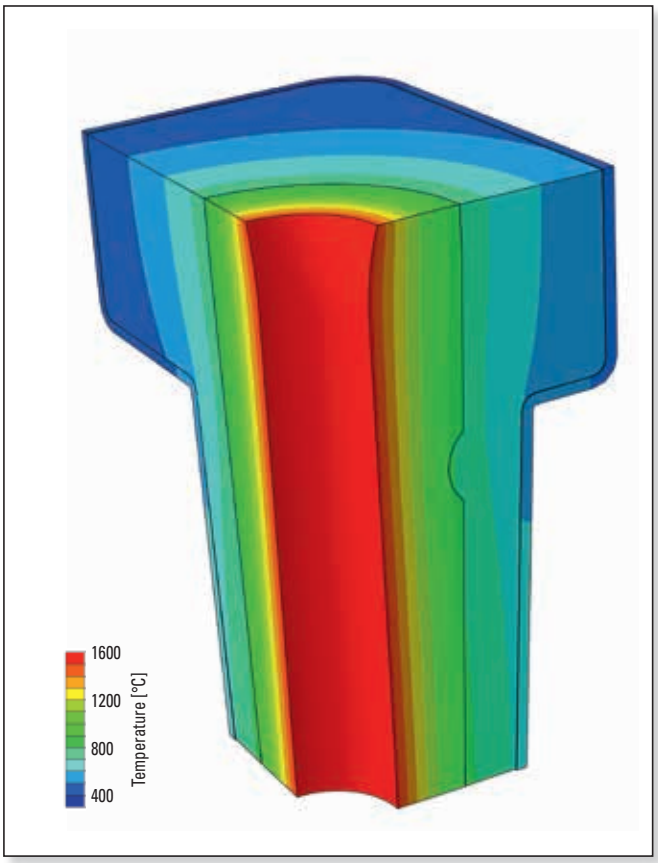

Figure 8. *Example of temperature distribution after one hour of casting.*

Simulation of Oxygen Lancing

The corrosion of the zirconia insert caused by oxygen lancing at the start or end of a casting strand may oxidize the steel and cause the iron oxide to react with the zirconia nozzle. The corrosion can be simulated by pouring molten steel through the nozzle or using molten iron oxide in an induction furnace, as seen in Figures 9 (a) and 9 (b) respectively. The solubility of iron oxide in zirconium oxide at 1600 °C is approximately 5.5 mol. % or ~3.3 wt. %. Above that, zirconia and a melting phase are expected to be present, which may lead to excessive wear as seen in the phase diagram (Figure 10).

High Temperature Abrasion Test

This test, a modification of the usual refractory abrasion test, uses high velocity abrasive SiC particles to determine the material wear under abrasive conditions. The sample is pre-heated at high temperatures and bombarded with SiC particles. The loss in weight and the depth of wear are indicators of the extent of abrasion.

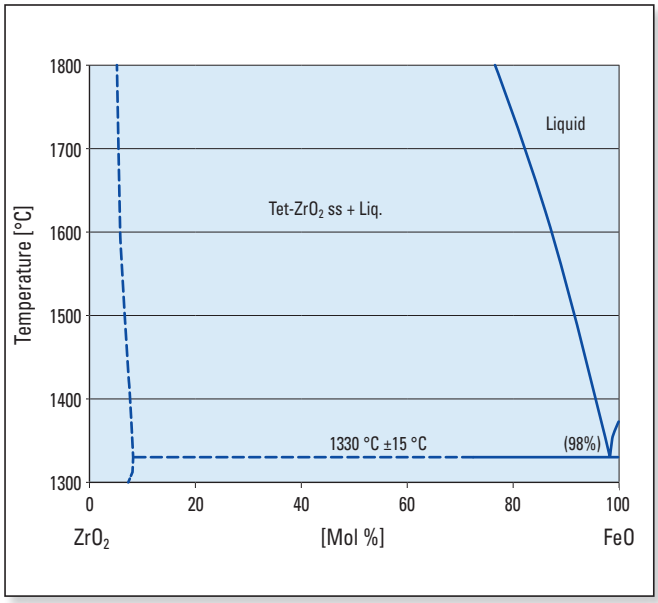

Figure 10. *Phase diagram of system ZrO_2-FeO_2 above 1300 °C (Tet = tetragonal) [6].*

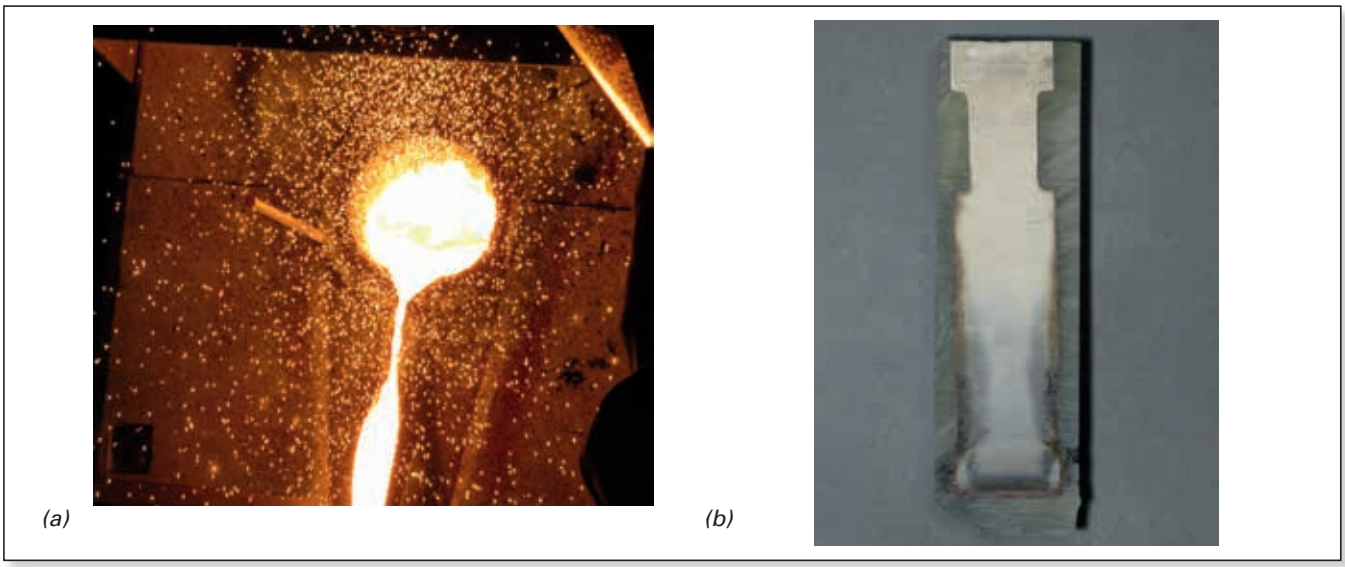

Figure 9. *Showing a) Simulation of oxygen lancing and b) macroscopic appearance of the cut samples after the iron oxide corrosion test.*

RHI Brands for Zirconium Oxide and Zirconium Silicate Based Nozzles

RHI offers a wide range of zirconium oxide grades (Table I), together with different carrier materials for tundish nozzle applications (Table II). Based on application conditions, steel quality, and nozzle geometry; a combination of suitable grades tailored for the customer can be selected (Figure 12).

Normally zirconium oxide nozzles are preferred over the zirconium silicate based nozzles because they offer better casting time. However, in few cases nozzles with zirconium silicate inserts may be used based on the application.

Figure 11. *Sample after high temperature abrasion test.*

Figure 12. *Showing different views on upper and exchangeable nozzles.*

	RHI Grade	Bulk density [g/cm³]	Porosity [%]	ZrO_2 [%]	MgO [%]	SiO_2 [%]	Fe_2O_3 [%]
Zirconium oxide nozzle grades	ZETTRAL 9515B	5.2	4.5	95.5	2.5		
	ZETTRAL 9515C	5.0	8.8	95.5	2.5		
	ZETTRAL 95HD	5.1	9.5	95.6	2.2	1.0	0.7
	ZETTRAL 95SA	4.9	13.2	95.5	2.6	1.0	0.7
Zirconium silicate nozzle grades	ZETTRAL 6512	3.8	17.2	66.5		28.5	0.3
	ZETTRAL 65SA	3.7	21.3	66.5		28.5	

Table I. *Showing RHI portfolio zirconia and zircon grades for nozzles [5].*

RHI Grade	Bonding	Main component	ρ_{bulk} [g/cm³]	P_{open} [%]	Al_2O_3 [%]	SiO_2 [%]	Application
SANIT 065-4 T3	Ceramic	Tabular alumina	3.1	8.0	88.5	10.0	Upper nozzle
RESISTAL 052LO T3	Ceramic	Tabular alumina, white fused alumina, mullite	2.9	9.0	82.0	16.5	Upper nozzle
DIDURITAL V013 0-3	Hydraulic	White fused alumina	3.1	16.5	97.5	0.3	Flying nozzle / upper nozzle
DIDURITAL V013 0-1	Hydraulic	White fused alumina	3.1	16.0	97.0	0.1	Flying nozzle
DIDURITAL SFC-3	Hydraulic	Tabular alumina	3.0	13.0	97.0	0.1	Flying nozzle
RESISTAL TWB-2	Phosphate	Brown fused alumina	3.0	16.2	90.0	4.5	Metering nozzle / upper nozzle
RESISTAL IN-6	Phosphate	Bauxite, tabular alumina	2.9	18.0	87.0	8.1	Metering nozzle / upper nozzle
RESISTAL A87PCW	Phosphate	Tabular alumina, white fused alumina, mullite	2.8	17.5	87.0	10.0	Metering nozzle / upper nozzle
RESISTAL B80PCWLO	Phosphate	Bauxite	2.7	20.5	78.0	14.0	Metering nozzle / upper nozzle

Table II. *Showing different of nozzle set carrier materials and characteristics [1, 5].*

System	Remarks	Supplier	No. of refractory components
MNC	Metering Nozzle Changer	Stopinc / Switzerland	2
CNM	Concast Nozzle Manipulator	Concast / Switzerland	3
FNC	Flying Nozzle Changer	Danieli / Italy	3
CNC/SYS120	Calibrated Nozzle Changer	Vesuvius / United Kingdom	3

Table III. *A summary of some nozzle exchanger systems and suppliers the various systems and suppliers.*

RHI Portfolio: Nozzle Changer Systems [1]

Using the different zirconia and zircon grades in combination with the wide range of carrier materials RHI is equipped to supply nozzles for all the prominent nozzle exchanger systems worldwide, Table III shows a summary of the various nozzle exchanger systems. With the MNC Systems RHI offers high performance nozzle exchanger systems coupled with increased safety, simplified handling, higher reliability and yield in casting sequence (Figure 13).

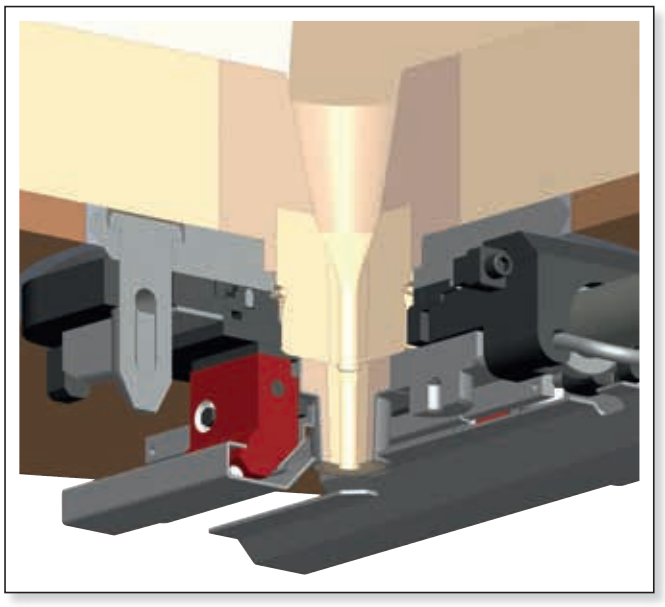

Figure 13. *RHI Metering Nozzle Changer AS.*

Conclusion

With a broad portfolio of zirconia grades and carrier materials RHI meets the requirements of the different nozzle changer system in tundish applications. This, coupled with years of in-house technical knowledge and production expertise of its employees, state of the art research facilities and worldwide presence establish RHI as a suitable partner for refractory solutions and will continue to strengthen this position in future.

References

[1] RHI Product Information: Flow Control Tundish. May 2015, Vienna, Austria.
[2] Sorger R. Projects Steel, Personal Communication 2016.
[3] Grasset-Bourdel, R. Billet Nozzles Project Testing of RHI and ORL Standard Zirconia Grades. RHI Internal Report. Leoben, Austria, unpublished results 2015.
[4] Marschall, H, U. FEA Report Thermo-Mechanical Investigation of different Nozzle Configurations. RHI Internal Report, Leoben, Austria, unpublished results, 2015.
[5] Grasset-Bourdel, R. RHI Internal Report, Leoben, Austria, unpublished results 2015.
[6] Fischer, W.A. and Hoffmann, A. Equilibrium Studies in the System Iron (II)-Oxide-Zirconium Oxide. Arch. Eisenhuettenwes. 1957, Vol 28, No. 11, pp. 739–743.

Authors

Neha Jain, RHI AG, Steel Division, Leoben, Austria.
Florian Barthmann, RHI AG, Steel Division, Marktredwitz, Germany.
Ghufran Ansari, ORL, Bhiwadi, India.
Corresponding author: Neha Jain, neha.jain@rhi-ag.com

Return to Content

RHI Bulletin > 1 > 2016, pp. 51–56

Christoph Bauer, Barbara Rollinger, Georg Krumpel, Oliver Hoad, Javier Pascual, Norman Rogers and Helmut Dösinger

Characterization Methods to Investigate Zirconia Phase Transformations in Slag Bands

Isostatically pressed products used for flow control in the continuous casting of steel commonly combine the thermal shock resistance of an alumina-graphite main body material with the enhanced chemical resistance of a zirconia-graphite slag band. In order to optimize both the thermomechanical properties as well as chemical corrosion resistance, it is important to characterize the raw materials. Detailed insights into the microstructure in combination with an understanding of the crystallographic phase transformations of zirconia enable the material performance to be predicted. In this paper characterization methods for CaO-partially stabilized zirconia are presented and the physical properties of zirconia-bearing materials were determined. Zirconia grains that had recrystallized during operation were examined by elemental distribution mapping because the associated crystallographic and exsolution phenomena are fundamental and limiting factors regarding thermal shock resistance. In addition, the chemical wear resistance changes with ongoing recrystallization. Since these wear patterns are potentially linked to the varying specific casting conditions, understanding chemical and structural processes within the material are central to the continuous optimization of refractory performance.

Introduction

Chemical-resistant zirconia exists in three known phases: Monoclinic (< 1170 °C), tetragonal (1170–2370 °C), and cubic (> 2370 °C) [1]. The reversible volume expansion caused by the tetragonal to monoclinic transformation induces large stresses and leads to crack formation. However, when zirconia is doped with certain oxides (e.g., CaO, MgO, or Y_2O_3) the cubic phases are stabilized keeping the high-temperature modification metastable upon cooling. Depending on the amount of stabilizer added, the zirconia is either partially or fully stabilized. The physical characteristics of partially stabilized zirconia, including transformation toughening and chemical stability, make it appropriate for refractory applications.

Isostatically pressed products for shrouded steel transfer during continuous casting frequently have a chemically resistant slag band of zirconia-graphite incorporated into the alumina-graphite main body material (Figure 1). This band, which is either the entire thickness of the tube wall (through wall) or the partial wall thickness (duplex slag band), is in contact with corrosive mould slag. In this area highest refractory wear rates are observed resulting from two principal acting mechanisms that alternate [2]: (1) the oxidic part of the refractory is wetted by slag and

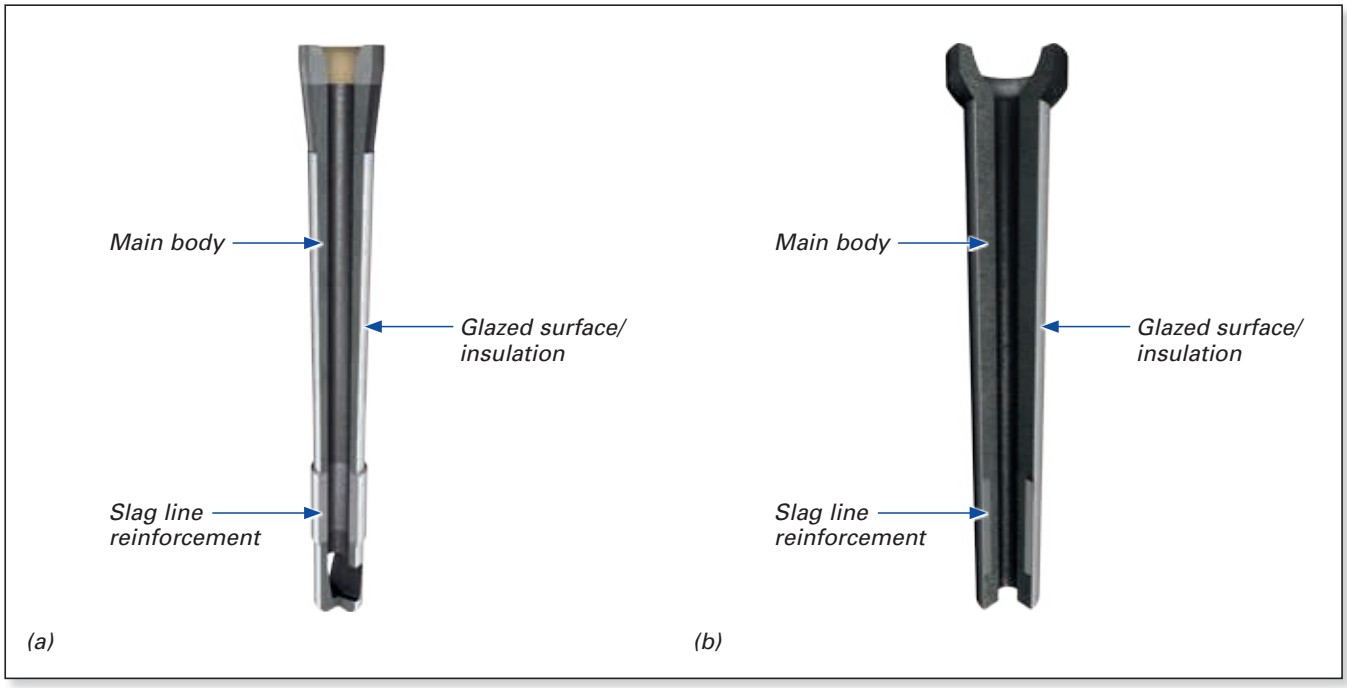

Figure 1. *(a) submerged entry nozzle with a through wall slag band and (b) submerged entry shroud with a duplex slag band.*

chemically corroded and (2) as a consequence graphite is concentrated in this reaction area and is preferentially dissolved by steel [2]. Disintegration of CaO-partially stabilized zirconia (CaO-PSZ) grains and recrystallization are also frequently observed [3] and considered a result of removing a proportion of stabilizing dopant and assumed to be a prominent lifetime limiting factor.

Besides destabilization and subsequent disintegration of the zirconia grains, which is assumed to be associated with the change from a cubic to monoclinic crystal lattice system [3], the loss of carbon binder additionally increases slag penetration into the refractory material. A detailed study of CaO-PSZ dissolution reported that Ca depletion from zirconia is accompanied by the formation of a $CaO\text{-}Al_2O_3\text{-}SiO_2$-rich melt phase and recrystallization of CaO-free zirconia, assumed to be in the monoclinic form, was described [3]. In addition, the impact of Si sources, namely from graphite impurities, antioxidants, or slag, were found to be crucial for destabilization. Chemical corrosion was also determined to be highly dependent on the graphite content, which influences the thermal shock resistance. Therefore, it is crucial to follow the change in physical and chemical properties of materials containing CaO-PSZ once they are partly eroded and destabilized.

It has been established from the investigation of unused zirconia that electron backscatter diffraction (EBSD) is a powerful tool to characterize the crystal structure [4]. Raman spectroscopy is another useful and nondestructive in-situ method to examine zirconia, where the excited specimen area is restricted to ~ 1 µm, according to the laser beam focus [5]. As is common for fingerprint methods, the unknown specimen is compared with a standard material on the basis that varying atomic bonding lengths—caused by chemical variations—may shift a Raman spectrum in a similar manner to X-ray diffraction peaks, while retaining the relative peak positions.

The aim of this study was to investigate zirconia alteration during hot operation in various zirconia-graphite slag band materials containing carbon-bonded CaO-PSZ and Si antioxidants. The melt phase that formed together with Ca-depletion of the zirconia was characterized in detail. Due to the significant impact of the zirconia crystal structure on the physical properties, namely the thermomechanical characteristics in the range of 800–1100 °C, crystallographic studies of the zirconia reaction products were performed.

Microstructural Investigation

Postmortem analyses were performed on submerged entry nozzles with a duplex slag band, which had been used under varying casting conditions. According to the observed microstructure, different mechanisms of zirconia deterioration had occurred. Following contact with mould slag, disintegrated zirconia grains were easily eroded (Figure 2), as described in the literature [3]. In deeper matrix areas, some samples revealed disintegrated zirconia grains throughout the entire slag band despite the absence of any slag phases in the altered area (Figure 3). CaO-PSZ grains located at the boundary to the alumina-graphite material showed disintegration mainly on one side, namely towards the body material (Figure 4), in addition to interstitial melt phases containing Al_2O_3. In certain samples this was the only ZrO_2 alteration detected.

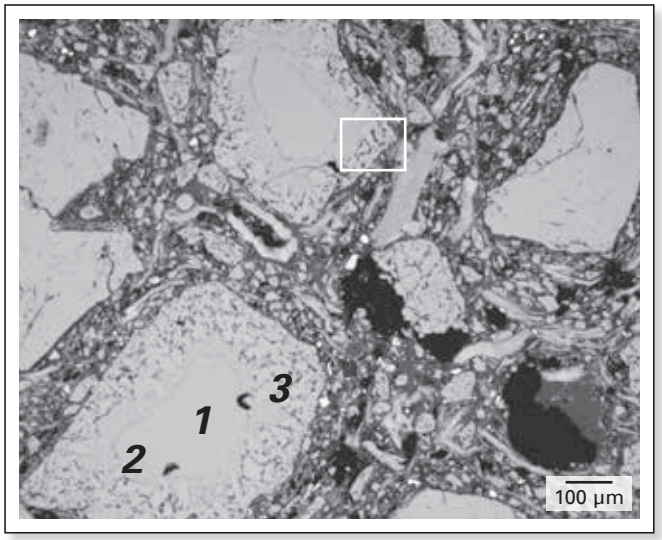

Figure 3. *Disintegrated CaO-PSZ grains from the centre of a slag band comprising original core areas (1), fine-grained intermediate seams (2), and CaO-free, coarser recrystallized outer rims (3). No slag is present.*

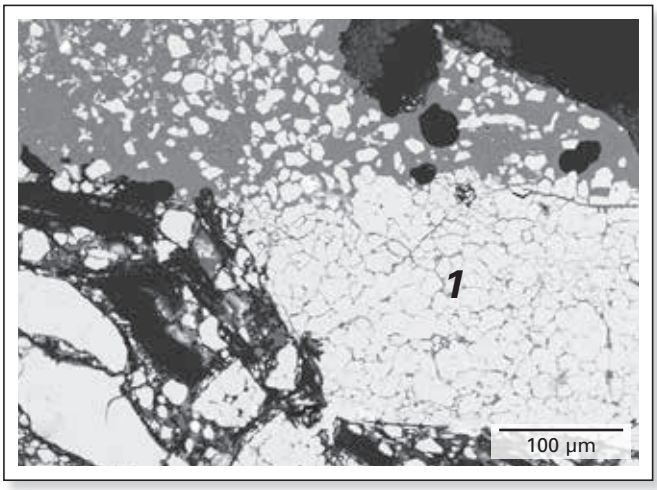

Figure 2. *Totally disintegrated ZrO_2 grain (1) eroded by mould slag.*

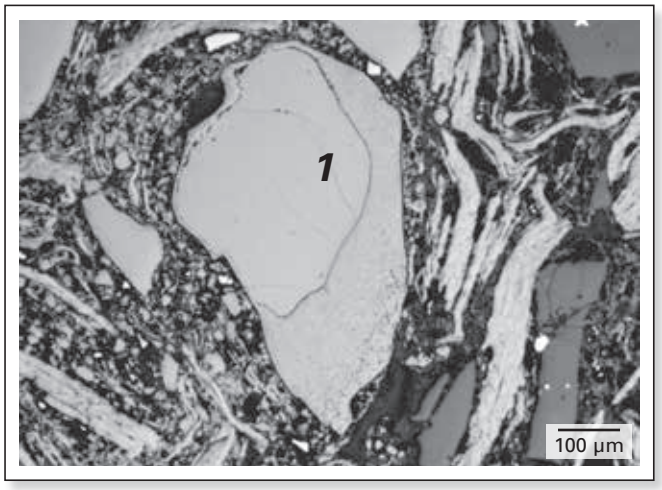

Figure 4. *CaO-PSZ grains (1) located at the transition to the alumina-graphite body (towards the bore) show a fine-grained altered rim. The grains are mainly affected from one direction.*

The Ca-content decreased towards the outer recrystallized rim (Figure 5); typical calcium oxide concentrations in single grain regions are detailed in Table I. In interstitial regions between the disintegrated zirconia grains, a CaO-Al_2O_3-SiO_2-rich melt phase (with lower MgO and ZrO_2 contents) had formed. Such phases have been reported to be close to pseudowollastonite ($CaSiO_3$) consisting mainly of CaO (~ 40 wt.%) and SiO_2 (~ 50 wt.%), with Al_2O_3 restricted to approximately 20 wt.% [3]. Low ZrO_2 levels were also detected, but interpreted to be semiquantitative due to analytical reasons.

	CaO (wt.%)	ZrO_2 (wt.%)	HfO_2 (wt.%)
Core areas	4.9	94.1	1.0
Fine-grained seam	3.2	96.5	0.3
Coarse outer rim	bdl	99.1	0.9

Table I. *Typical chemical composition of the different areas within disintegrated zirconia grains. Abbreviations include below detection limit (bdl). The grain regions are indicated in Figure 3.*

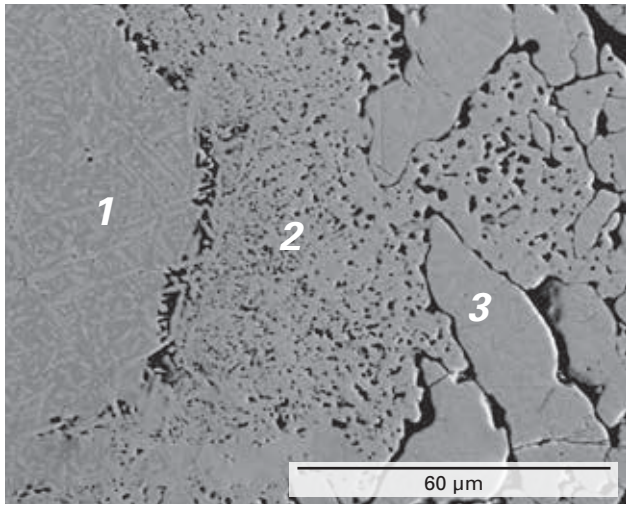

(a)

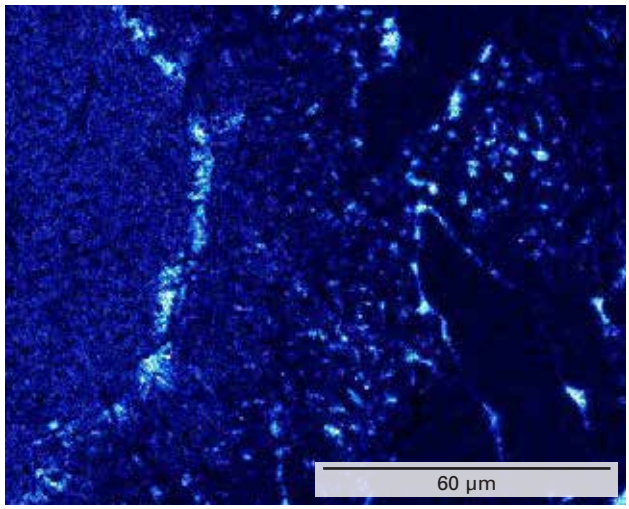

(b)

Figure 5. *Region indicated by the rectangle in Figure 3 (a) BSE image and (b) Ca element mapping (blue). High Ca concentrations are bright and there is distinct Ca accumulation on the transition edges to the next area. Core area (1), fine-grained intermediate seam (2), and coarser recrystallized outer rim (3).*

Interstitial melt phase analyses from the current study are plotted in the CaO-SiO_2-Al_2O_3 ternary system (Figure 6). The location of these interstitial phases was subdivided into (1) hot face close to the mould slag (orange dots), (2) central part of the slag band (green dots), and (3) near the duplex wall (blue dots). No slag phases or other infiltrating phases were observed in the central part of the slag band or close to the duplex wall. For comparison, a published data range of the glassy phase compositions that formed in zirconia-graphite refractories dipped in various synthetic slags [3] is indicated by the ellipse.

The interstitial phases within the disintegrating zirconia grains contained an average ZrO_2 concentration of 11 wt.% (± 3.9 wt.% 1σ; restricted to a dataset of 25 spot analyses where the influence of grain size matrix effects could be excluded). When the three regions are compared, the compositions near the hot face and in the central part of the slag band were close to the literature data examining zirconia-graphite samples. The composition of the interstitial phases near the duplex wall showed increased Al_2O_3 concentrations.

Crystallography

Within CaO-PSZ, precipitation of tetragonal lenses with rectangular orientation—according to the crystal orientation of the cubic matrix—has been well described [6]. In this study due to the textural variations of altered CaO-PSZ grains in the different slag band locations, a crystallographic characterization was performed. In the central slag band region (no slag phases), the transitions from the core to outermost recrystallized rim (Figure 7) were mapped with EBSD. The lamellae in the core were a mixture of monoclinic and tetragonal ZrO_2, embedded in a cubic matrix. In the fine-grained intermediate seam, all three ZrO_2 modifications were detected (Figure 7c). In the outermost rim, the grains were mainly cubic with an orientation close to the 001 plane (reddish colour in the crystal orientation map). In contrast, EBSD analysis of a CaO-PSZ grain from the transition region near to the alumina-graphite body liner (Figure 8), which showed more fine-grained alteration from one side

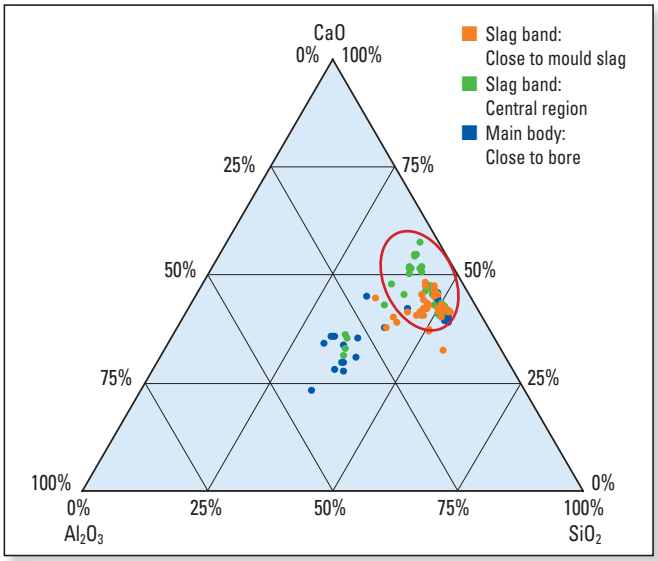

Figure 6. *CaO-SiO_2-Al_2O_3 ternary system showing the composition of measured interstitial phases in the zirconia-graphite material close to the hot face, in the central part of the slag band, and near the duplex wall compared to reported values [3] (ellipse).*

(slag phases were absent) (see Figures 7 and 8) revealed that the unaltered matrix was cubic, although traces of monoclinic ZrO_2 were present. The recrystallized corroded area was also mainly cubic but was built up from a patchwork of differently orientated subgrains, indicated by the different colours. The green colour in the phase identification mappings indicated ~ 50% cubic ZrO_2; tetragonal and monoclinic ZrO_2 were also present in the matrix. CaO-free cubic zirconia was detected in corroded CaO-PSZ grains located at the hot face.

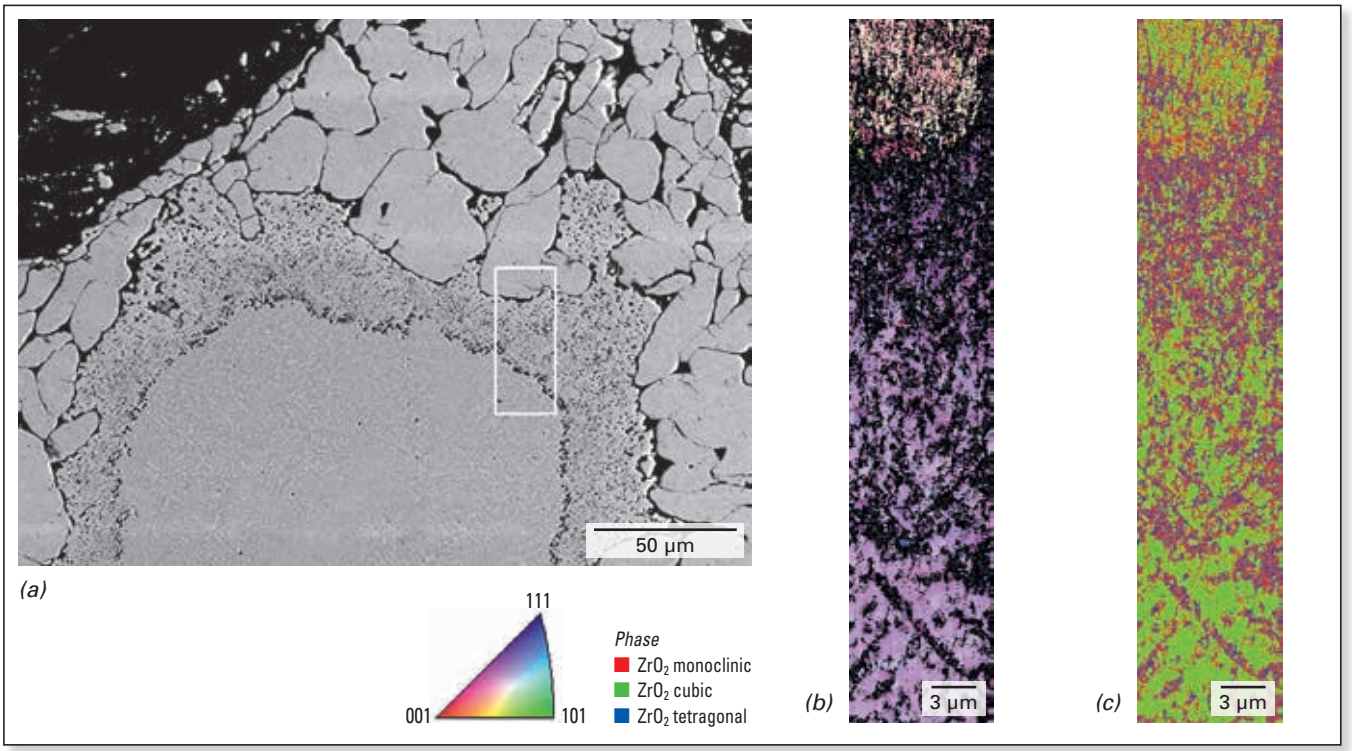

Figure 7. *(a) BSE image of Figure 3 showing the transition zones within a zirconia grain from the central slag band region. The rectangle indicates the area of EBSD analysis that spans the original core, fine grained intermediate seam, and coarser recrystallized outermost rim. (b) crystal orientation mapping for cubic ZrO_2. The orientation of the surface plane is given by the colours in the stereographic triangle. (c) phase identification map of the same area; amounts and distribution of the three modifications are indicated according to the colour key: Mainly cubic ZrO_2 was detected.*

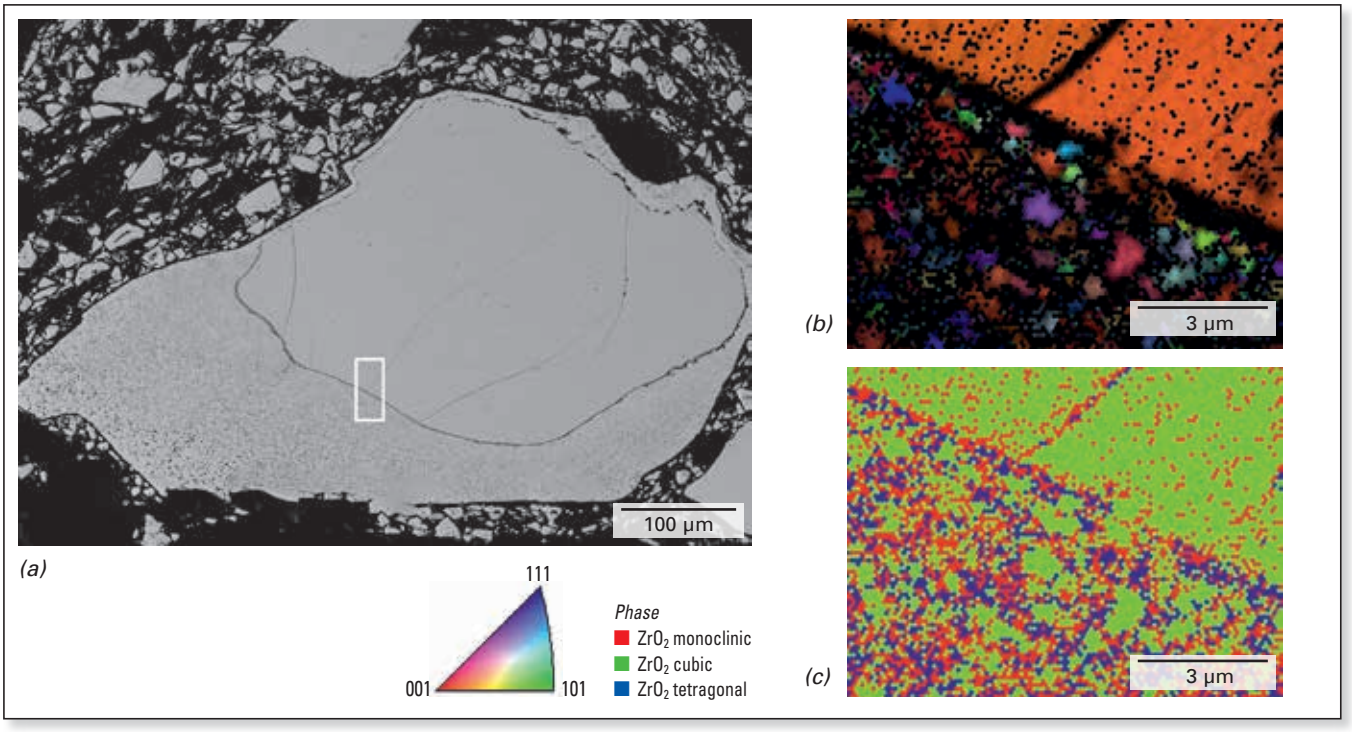

Figure 8. *(a) BSE image of a CaO-PSZ grain located at the transition region to the alumina-graphite body layer (see Figure 4). The rectangle indicates the EBSD mapping area. (b) crystal orientation mapping for cubic ZrO_2. (c) phase identification map of the same area: Mainly cubic ZrO_2 was detected.*

Spectroscopy

In order to confirm the EBSD data with another analytical method, Raman spectroscopy was applied on the same microtextures. Although as a reference Y_2O_3-stabilized cubic zirconia generated a Raman band identical to the literature [7] (single mode at approximately 610 cm^{-1}), an application problem was encountered because (1) the Raman intensity of monoclinic ZrO_2 was much higher and the cubic ZrO_2 fingerprint disappeared below the monoclinic ZrO_2 bands and (2) the CaO-PSZ raw material was not pure cubic ZrO_2 and had, according to XRD analyses as well as to supplier information, a stabilization degree of 60–80%, depending on the CaO concentration. Therefore, CaO-free monoclinic zirconia was used as a reference, which showed good correlation with literature data [8] as well as original CaO-PSZ raw material (core areas), which (according to XRD and the supplier) was mainly cubic but also contained monoclinic and tetragonal regions for comparison.

Raman spectroscopy was used to examine the phases in a sample from the CaO-depleted recrystallized rim. Initially the comparison was made to a monoclinic ZrO_2 standard (Figure 9). The spectra indicated that the recrystallized rim contained a mixture of tetragonal and monoclinic ZrO_2, but differed significantly from the standard monoclinic ZrO_2 spectrum particularly in the 100–500 cm^{-1} range. The low intensity cubic band at 610 cm^{-1} was hidden below a higher intensity monoclinic peak. When the CaO-depleted recrystallized rim was compared with the original matrix of CaO-PSZ grain some tetragonal peaks were clearly visible in addition to monoclinic ZrO_2 bands (Figure 10). The recrystallized rim only showed good peak correspondence in the 450–650 cm^{-1} range.

Discussion and Conclusions

Based on microstructural observations and the interstitial melt phase compositions in corroded CaO-PSZ grains, it was shown that besides mould slag and internal Si carriers, an addition destabilizing gaseous source exists, since there was a trend to Al_2O_3-enrichment in interstitial phases near the duplex wall. The two potential sources of aluminium-rich gas phase are outgassing from the alumina-graphite body material and aluminium-containing steel. The importance of internal Si gas supply was previously described in the literature [3] to explain zirconia deterioration in matrix areas where mould slag was absent in zirconia-graphite samples dipped in various slags.

Normally the microtextural appearance of CaO-free recrystallized ZrO_2 together with increasing XRD peak intensities of monoclinic ZrO_2 has led to the conclusion that CaO-free ZrO_2 is monoclinic—which is concordant with phase diagram information. However, to characterize the crystallographic structure in greater detail, alternative methods were employed in this study. It was demonstrated that EBSD is a powerful tool for postmortem investigations of zirconia-graphite slag bands. Furthermore, Raman spectroscopy proved to be another useful approach to describe different zirconia polymorphs in refractory materials. Despite the difficulties of fingerprint interpretations, it was possible to confirm the crystallographic information gained by EBSD with this nondestructive microanalysis method.

Contrary to the literature, it was found that not all the recrystallized CaO-free zirconia had a monoclinic crystal structure; the main part was cubic. Despite severe recrystallization, it appears to be a gas phase induced loss of integrity that influences slag band lifetime rather than the transition to another crystallographic modification.

To address the highly complex alteration processes in CaO-PSZ bearing slag bands, the aim of future investigations will be to obtain further knowledge about the deterioration reactions and recrystallization processes. Aside from this, the elevated chemical corrosion resistance of pure monoclinic zirconia should be exploited for slag band applications. When the thermal expansion of zirconia is compensated by the matrix, susceptibility to chemical corrosion can be reduced to a minimum and the product properties can be better adapted to specific casting conditions.

This work is dedicated to the memory of Dr. Oliver J. Hoad.

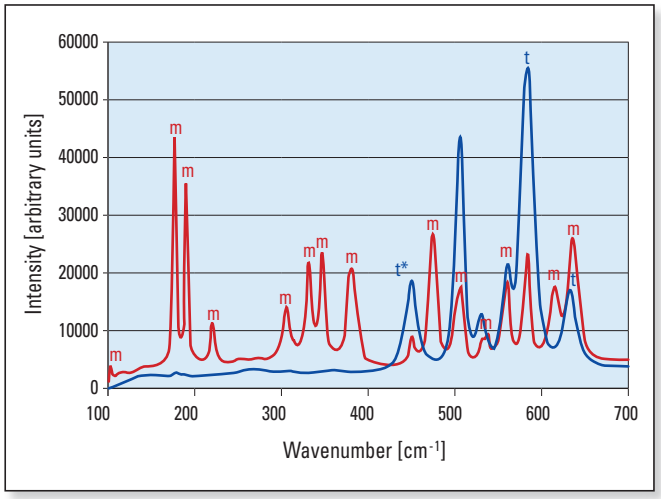

Figure 9. *Raman spectrum of a CaO-depleted recrystallized rim (blue) compared with a monoclinic ZrO_2 standard (red). The recrystallized rim shows a mixture of tetragonal ZrO_2 (t) (one slightly shifted*) and monoclinic ZrO_2 (m) bands but significantly differs from a pure monoclinic ZrO_2 spectrum (see missing bands from 100–500 cm^{-1}). The low-intensity cubic band disappears in the background.*

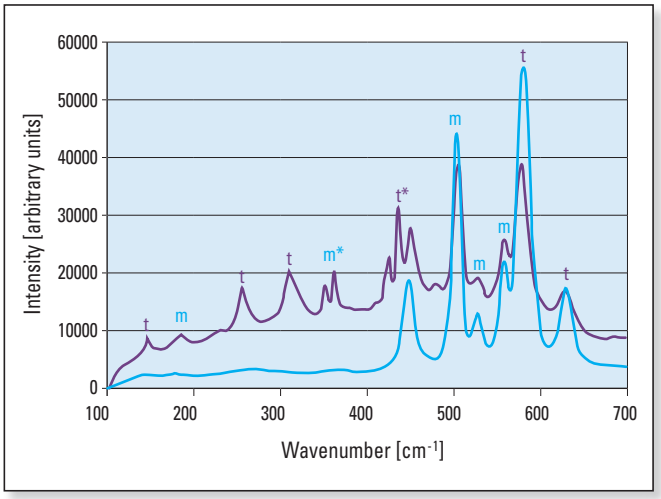

Figure 10. *Raman spectrum of a CaO-depleted recrystallized rim (light blue) compared with the original matrix of a CaO-PSZ grain (purple), where some tetragonal (t) ZrO_2 peaks are clearly visible (one shifted*); monoclinic (m) ZrO_2 bands additionally occur. The recrystallized rim shows good accordance with the original CaO-PSZ grain spectrum from 450–650 cm^{-1}.*

Acknowledgements

The authors would like to express their gratitude to Mr Sartory at the MCL Leoben, Austria, for assistance with the EBSD and Mr Krenn from the Institute of Earth Sciences, Karl Franzens University, Graz, Austria, for support with the Raman analyses.

References

[1] http://en.wikipedia.org/wiki/Zirconium_dioxide

[2] Mukai, K., Toguir, J.M., Stubina, N.M. and Yoshitomi, J. A Mechanism for the Local Corrosion of Immersion Nozzles. *ISIJ International*. 1989, 29, No. 6, 469–476.

[3] Aiba, Y., Oki, K., Sugie, M., Kurihara, K. and Oya, S. Study of Corrosion and Penetration of Zirconia Refractories by Molten Steel and Slag. *Taikabutsu Overseas*. 1985, 5, No. 1, 3–11.

[4] Sibil, A., Douillard, T., Cayron, C., Godin, N., R'mili, M. and Fantozzi, G. Microcracking of High Zirconia Refractories After t → m Phase Transition During Cooling: An EBSD Study. *Journal of the European Ceramic Society*. 2011, 31, 1525–1531.

[5] Beran, A. and Libowitzky, E. (Eds) Spectroscopic Methods in Mineralogy. *European Mineralogical Union*. 2004, 6, 281–329.

[6] Stevens, R. Zirconia and Zirconia Ceramics. Magnesium Elektron Ltd. 1986, 56, No. 5, 8–51.

[7] Cai, J., Raptis Y.S. and Anastassakis, E. Stabilized Cubic Zirconia: A Raman Study Under Uniaxial Stress. *Applied Physics Letters*. 1993, 62, No. 22, 2781–2783.

[8] Quintard, P.E., Barbéris, P., Mirgorodsky, A.P. and Merle-Méjean, T. Comparative Lattice-Dynamical Study of the Raman Spectra of Monoclinic and Tetragonal Phases of Zirconia and Hafnia. *Journal of the American Ceramic Society*. 2002, 85, No. 7, 1745–1749.

Reprinted with permission from ACerS and the UNITECR Proceedings. http://www.wiley.com/WileyCDA/WileyTitle/productCd-1118837037.html

Authors

Christoph Bauer, RHI AG, Technology Center, Leoben, Austria.
Barbara Rollinger, Semperit Technische Produkte GesmbH, Material Development Sempertrans, Wimpassing, Austria.
Georg Krumpel, RHI AG, Steel Division, Vienna, Austria.
Oliver Hoad, RHI AG, Technology Center, Leoben, Austria.
Javier Pascual, RHI AG, Technology Center, Leoben, Austria.
Norman Rogers, RHI AG, Technology Center, Leoben, Austria.
Helmut Dösinger, RHI AG, Technology Center, Leoben, Austria.
Corresponding author: Christoph Bauer, christoph.bauer@rhi-ag.com

Return to Content

Dean Gregurek, Stefanie Redik, Christine Wenzl and Alfred Spanring

Zinc and Refractories

Zinc is a component of many input materials used in various pyrometallurgical processes, for example primary lead and zinc production from Pb/Zn ores and recycling processes dealing with zinc-containing residues (e.g., copper recycling, WAELZ process). As a result, zinc and its compounds are present in the respective metallurgical vessels and interact with the refractory lining. In the present work the zinc attack on the refractory from various primary and secondary furnaces is briefly introduced and discussed. At the prevailing processing temperatures in the metallurgical vessels, zinc oxide is highly corrosive to the brick components. The knowledge of the wear behaviour is based on a detailed chemical and mineralogical characterization carried out on post mortem samples, but also on FactSage™ calculations. This together with results obtained from practical testing in the RHI pilot plant represents an important prerequisite for product development and brick selection for the individual customer application.

Introduction

Zinc is normally found and mined together with other metals, especially Pb, but also Ag and Cu [1, 2]. Zinc enters other metal production processes via:

>> Copper: ores, (brass) scrap, residue recycling.
>> Lead: ores, residue recycling.
>> Silver: ores, residue recycling.
>> Steel–EAF route: recycling of galvanized steel.

Hence, zinc is an important by-product of many metallurgical processes, e.g., flue dusts from copper, lead, and steel production (evaporation during "normal" process or separate Zn slag fuming stage). Pyrometallurgical zinc production is predominantly done using the WAELZ process, the most important input material being EAF dust (Zn coming from galvanization layers on recycled steel scrap) and Zn containing residues from hydrometallurgical Zn production.

Zn is a relatively ignoble metal (standard electrode potential of -0.76 V) and also has a relatively low melting and evaporation point (T_m = 420 °C; T_v = 907 °C) [3]. This leads to the following behaviour:

>> Reductive effect for oxides of more noble elements.
>> Easy evaporation of metallic Zn in reduction processes.

While these effects can be exploited in the metallurgical processes, they also have to be considered when choosing refractory materials for the respective applications.

Evaporation

Metallic zinc is easily evaporated under the prevailing process temperatures in nonferrous metals production and depending on the process conditions, namely available oxygen in the furnace atmosphere, either stays in the metallic form as Zn vapour or is reoxidized. The later formation of solid ZnO is an exothermic reaction and must therefore be considered in the thermal balance of the furnace, especially if larger amounts of Zn are present. Depending on the off-gas flow conditions, the Zn or ZnO in the gas phase will come into contact the furnace refractory lining in a certain region and will show the according interactions with the refractories.

Reductive Effect

Due to the position of zinc in the Ellingham diagram, it is apparent that zinc has a tendency to act as reductant for oxides of more noble metals. In the case of refractories, this is especially important for iron oxides, as present in varying amounts in most refractory materials, but also for chromites.

The presence of Fe facilitates the reduction of Cr oxide, as the activity of Cr is reduced by alloy formation. In case of reduction of Fe oxide (to metallic Fe) from a mixed Fe-Cr oxide, active centres are formed at the Cr oxide where the reduction reaction can proceed. This effect, which is exploited in FeCr production, also occurs in the case of Zn contacting Fe-Cr oxides in the refractory materials, as the Cr oxides used in refractory production also contain a certain amount of Fe oxides [3, 4].

Similarity of ZnO and MgO

As zinc is less noble than the metals with which it is co-produced, a certain residual amount of ZnO is found in the slag. Due to the similar valence and size of Mg and Zn cations, ZnO is incorporated within the magnesia of basic bricks and reacts with the alumina in nonbasic bricks [5, 6].

Hence, the main reaction mechanisms are:

>> ZnO: incorporation in MgO of basic materials and spinel formation with alumina in nonbasic materials.
>> Zn: reductive effect on certain refractory oxides.

These two effects are the basis for refractory attack by Zn.

Post Mortem Studies

The wear mechanisms described in the following sections are representative case studies of investigations carried out at the laboratories in the RHI Technology Center Leoben and aim to highlight the complexity of in service wear processes.

In the Figure 1a, a massive (22 tonne) build-up had formed in a WAELZ kiln processing EAF dust and residues from Zn leaching, namely in the area where the magnesia-chromite bricks were installed. The build-up formation however was not a Zn-related wear effect, but due to the prevailing process conditions, namely co-reduction of Fe oxides to metallic iron and reoxidation to magnetite [7].

The initial stage of a post mortem study starts with the visual inspection the brick cross section followed by selection of samples for chemical analysis and mineralogical investigation.

The investigated sample shown in Figure 1b represents a broken section which was partly covered with a thin metal coating on the immediate brick hot face. In the cross section, cracks parallel to the brick hot face are visible. These cracks were partly filled with metal. Slag and metal also penetrated the brick joints. The brick has been completely infiltrated with complex metallic sulphides.

ZnO Attack on Basic and Nonbasic Refractories

The attack on the refractories is twofold, the SiO_2 attack on the magnesia leads to the formation of various silicates, such as monticellite ($CaMgSiO_4$), forsterite (Mg_2SiO_4), merwinite ($Ca_3MgSi_2O_8$) etc. and a high ZnO supply to the basic brick also results in corrosion through the incorporation of ZnO within the magnesia [8]. The latter can frequently be observed in the roof lining of various furnaces in nonferrous metallurgy where process conditions favour Zn evaporation and reoxidation in the furnace atmosphere.

The ZnO reacts with the magnesia mainly through diffusion processes. This was confirmed by scanning electron microscope investigations which showed an increased ZnO content in the magnesia. The second brick component chromite was also enriched with ZnO but in comparison to magnesia less corroded (Figure 2a).

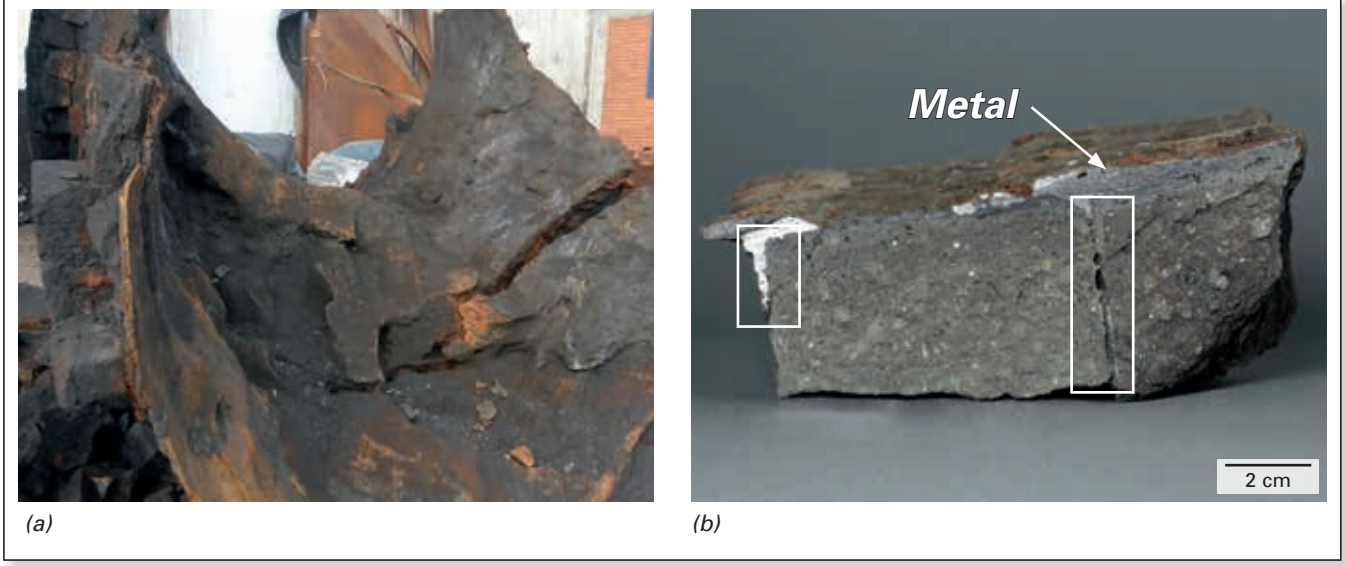

Figure 1. *Massive build-up formed in a WAELZ kiln in the installation area of the magnesia chromite brick (a) and metal penetration between the brick joints (rectangles) (b) showing the metal coating on the immediate brick hot face.*

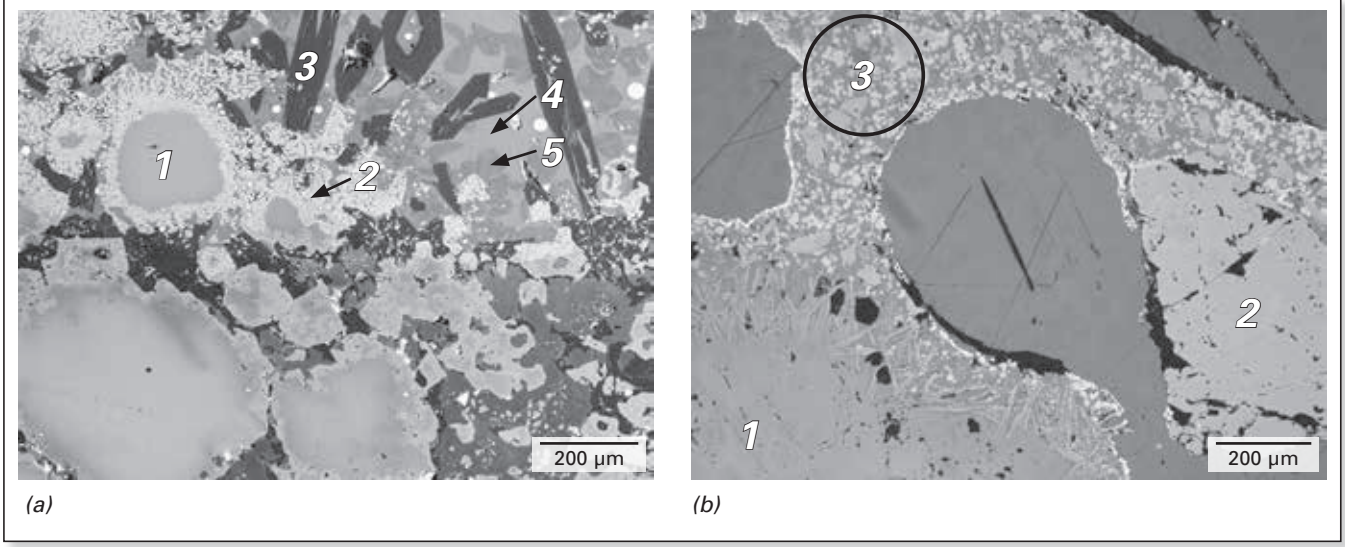

Figure 2. *Mineralogical investigation by reflected light microscopy and scanning electron microscope. Magnesia-chromite brick from the roof of copper production furnace (a). Completely corroded magnesia. Chromite relics (1) highly enriched with ZnO. Zn-Sn-(Cu)-Ni-Mg-Fe-Al-Cr-oxide of spinel type (2). Forsterite (3) enriched with NiO and ZnO. (Sn)-(P)-(Zn)-(Cu)-Na-Ca-Mg-Fe-Al-silicates (4 and 5). Alumina-silica brick from the same furnace (b). The main brick component andalusite (1) is more corroded than the fused alumina (2). Reaction zone (3).*

	MgO [wt.%]	Al_2O_3 [wt.%]	SiO_2 [wt.%]	P_2O_5 [wt.%]	K_2O [wt.%]	CaO [wt.%]	TiO_2 [wt.%]	Cr_2O_3 [wt.%]	Fe_2O_3 [wt.%]	NiO [wt.%]	CuO [wt.%]	PbO [wt.%]	ZnO [wt.%]
Hot face	0.2	32.0	23.0	1.0	1.0	0.5	0.4	2.0	10.0	1.6	9.4	5.1	11.0
Cold face		69.0	27.1	2.3	0.3	0.1	0.2		0.7				

Table I. *Chemical analysis of a alumina-silica brick from a copper production furnace.*

The severest degradation of the basic refractory in industrial furnaces was observed in a furnace for silver production. In this particular case the magnesia showed numerous newly formed (Zn)-Mg-oxide precipitations in the matrix. At the brick hot face an additional corrosion of chromite from the formation of Zn-Mg-(Mn)-Fe-Al-Cr-spinel could be observed.

Also in the case of the nonbasic refractories (alumina-silica brick), a strong chemical attack due to ZnO supply was observed. The refractory hot face was is enriched with up to 11 wt% of ZnO (Table I).

The microstructure of the refractory hot face was changed, it showed a thermochemically changed microstructure with a high prewear of the matrix fines. The coarse grains of andalusite (Al_2SiO_5) and fused alumina (Al_2O_3) were "swimming" without bonds in the reaction product. In this particular case the main brick component andalusite was more corroded than the fused alumina (Figure 2b).

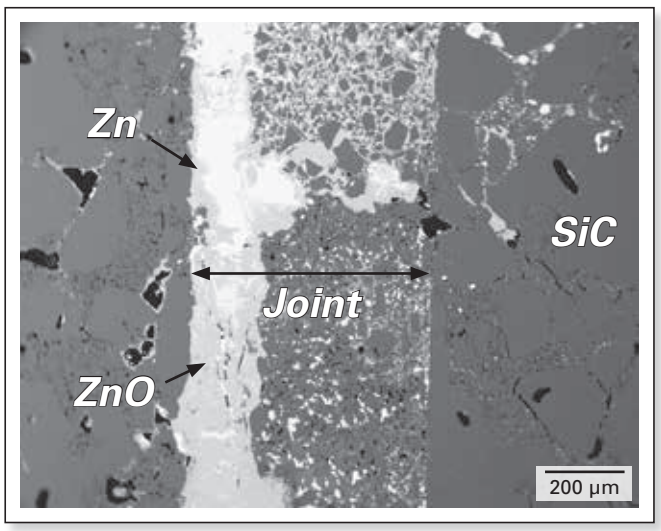

Figure 3. *Mineralogical investigation by scanning electron microscope. Showing metallic zinc penetration of the brick joints. The ZnO was formed through a reaction with the bonding component of the SiC-bearing mortar and subsequently formed Zn-silicate.*

Zinc Metal and Sulphide Infiltration

As macroscopically observed in Figure 1b, there was a pore-filling infiltration of the brick microstructure with complex metallic sulphides (FeS, PbS, Fe-Cu-sulphide, Zn-Fe-Mn-sulphide, Ba-Cu-Fe-Pb-sulphide).

Infiltration was generally combined with filling of the pore space within the refractory, without corrosion of the individual refractory components. Nevertheless, such a deeply infiltrated brick microstructure has an increased thermal conductivity and is therefore more susceptible to crack formation and spalling especially in batch-wise processes. The metal or sulphide infiltration is dependent on several parameters such as porosity of the brick, bath density, temperature, surface tension of bath, and the wetting angle [9].

An example of metallic zinc penetration in a non basic brick (SiC) through to the cold face is shown in Figure 3. Not only metallic zinc was detected within the brick joints, but also ZnO. The latter was formed through a reaction with the bonding component of the SiC-bearing mortar (phosphate bonded) and subsequently formed Zn silicates.

Laboratory Experiments

To better understand the wear phenomena in the industrial furnaces, a static cup test was performed in the pilot plant of the RHI Technology Center Leoben. For that purpose sample cups with dimension 80x80x70 mm were prepared from the selected brick types. The dimensions of the inner cylindrical hole were 40 mm diameter and 45 mm height (Figure 4a).

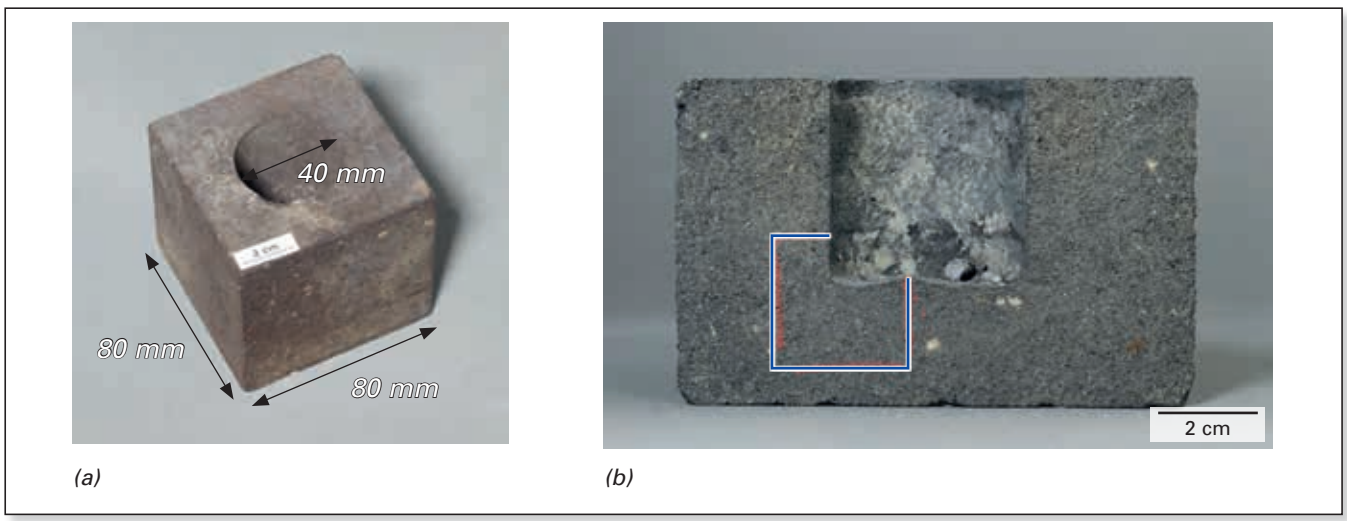

Figure 4. *Cup sample before testing (a) and after testing (cross sectional view, b). Sample for mineralogical investigation (rectangle).*

For the tests, which were performed in a laboratory electric furnace, 250 grams of customer-provided zinc were used. The filled crucible was sealed at the top with the refractory material. Testing was performed on basic (magnesia-chromite) and nonbasic (alumina-chrome and alumina-silica) bricks at a temperature of 1100 °C for 10 hours. The cross-section of a magnesia-chromite brick is shown in Figure 4b.

The initial results revealed that almost all tested magnesia-chromite bricks showed a severe reduction of Fe-oxides, chromite, and chromite precipitations to metallic Fe(Cr) (Figure 5a). Only one tested magnesia-chromite brick (4.1 wt% Fe_2O_3 content) was not affected by the reduction of chromite. The highest reduction was observed for the bricks with a high Fe_2O_3 and Cr_2O_3 content (14 wt% and 19 wt%, respectively). This confirms the theoretical considerations regarding Fe-Cr co-reduction.

Based on the practical results and FactSage™ calculations, the possible explanation for the above phenomena in basic bricks is as follows:

>> Infiltration of molten metallic zinc into the brick microstructure.
>> Co-reduction of Fe oxides and chromite by metallic zinc and simultaneous oxidation of zinc to ZnO.
>> ZnO enrichment of the magnesia/chromite by diffusion.

In the alumina-chrome brick no reduction of the brick components was visible. In the first few mm of the cup bottom (i.e., metal contact zone) the ZnO reacted with fused alumina, more specifically Cr alumina.

The alumina-silica brick showed an enrichment of the brick microstructure with ZnO over the whole polished section (0–25 mm). The andalusite and the brick bonding phase (phosphate bonded brick) reacted with ZnO, resulting in formation of Zn-Ca-Al-phosphate (Figure 5b).

These findings agree with the results of the FactSage™ calculations: Figure 6 shows the general formation of spinel phase and inclusion in MgO phase in non-basic and basic bricks.

Conclusions

Zinc in the form of Zn metal, oxide or sulphide affects both basic and non basic refractory materials. The main mechanisms are redox reactions with refractory oxides, dissolution/incorporation in brick components, and infiltration.

To better understand the wear phenomena in the industrial furnaces cup tests were performed in the pilot plant of the RHI Technology Center Leoben. Based on the first results it can be concluded, that in case of basic bricks (magnesia-chromite) the reduction potential is obviously related to

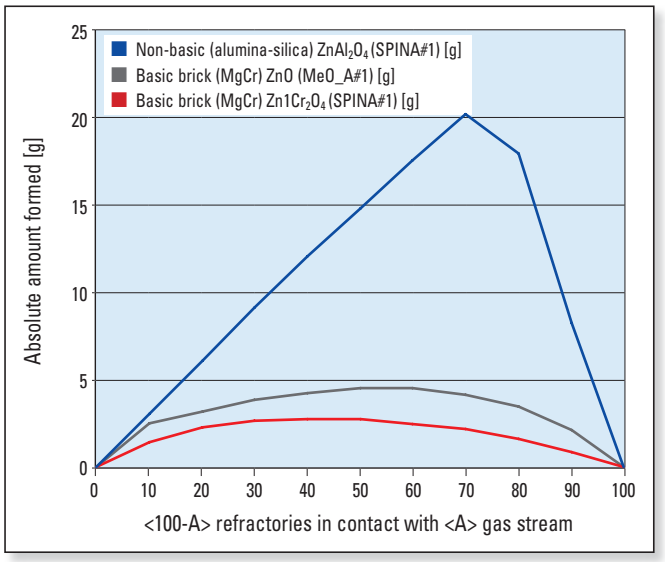

Figure 6. *Effect of Zn in non-basic and basic refractories–formation of spinel phase and inclusion in MgO phase (x-axis: 100% refractories at <A> = 0, 100% gas phase at <A> = 100).*

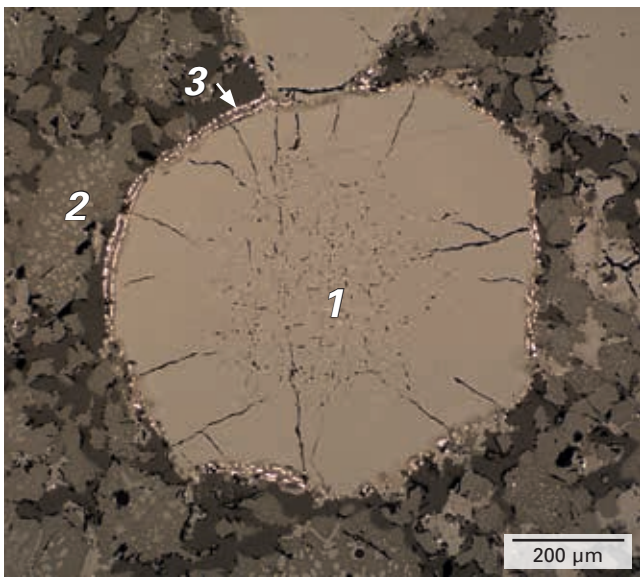

(a)

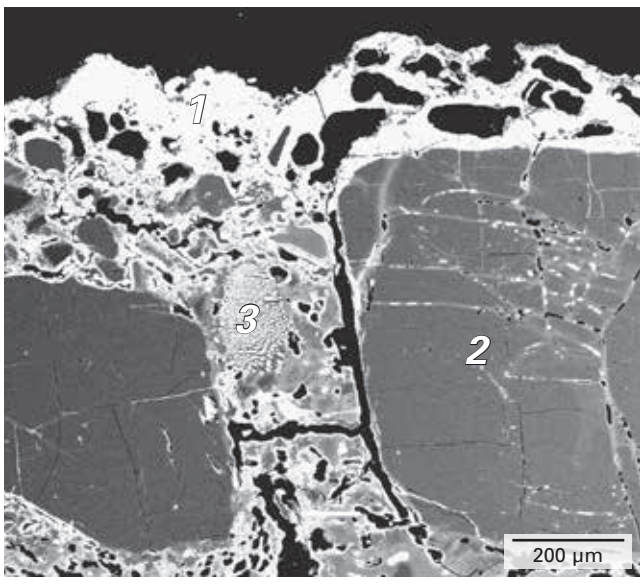

(b)

Figure 5. *Mineralogical investigation by reflected light microscopy and scanning electron microscope. Magnesia-chromite brick (a). Severe reduction of chromite (1) to metallic Fe(Cr) (3). Magnesia (2). Alumina-silica brick (b). Zn-Ca-Al-phosphate (1) formed after corrosion of andalusite (2). Zircon mullite (3).*

Fe_2O_3 content of the brick, as well as to content of chromium ore which has a high Fe_2O_3 content. Unlike basic bricks, the non basic bricks (i.e., alumina-chrome and alumina-silica) do not show reduction of single brick components, nevertheless reactions of the main refractory components with ZnO were detected. Further trials and comparison with FactSage™ calculations are currently ongoing.

References

[1] Hassall, C. and Roberts, H. Changing Dynamics of Long-Term Zinc and Lead Supplies. *Erzmetall*, Vol 68, No. 4, 2015, pp. 218—224.

[2] Elvers, B., Hawkins, S. and Russey, W. (Eds). *Ullmann´s Encyclopedia of Industrial Chemistry, 5th Edition;* Wiley-VCH Verlag: Weinheim, 1990, pp. 632.

[3] Gasik, M. (Ed) *Handbook of Ferroalloys*. Butterworth Heinemann: Kidlington, UK, 2013, pp. 509.

[4] Routschka, G. and Wuthnow, H. (Eds). *Handbook of Refractory Materials, 4th Edition*, Vulkan-Verlag: Essen, 2012; pp. 86—92.

[5] Chen, L., Guo, M., Shi, H., Scheunis, L., Jones, P. T., Blanpain, B. And Malfliet, A. The influence of ZnO in fayalite slag on the degradation of magnesia-chromite refractories during secondary Cu smelting, *Journal of European Ceramic Society*, Vol. 35, Issue 9, 2015, pp. 2641—2650.

[6] Riedel, E. and Janiak, C. *Anorganische Chemie*, Walter de Gruyter GmbH & Co. KG: Berlin, 2004, pp. 75.

[7] Kozlov, P.A. *The Waelz Process*, Ore and metals Publishing House, Moscow, 2003.

[8] Gregurek, D., Ressler, A., Reiter, V., Franzkowiak, A., Spanring, A. and Prietl, T. Refractory Wear Mechanisms in the Non-Ferrous Metal Industry: Testing and Modeling Results. *Journal of Metals*, Vol. 65, Issue 11, 2013, pp. 1622—1630.

[9] Gregurek, D., Reinharter, K., Majcenovic, C., Wenzl, C. and Spanring, A. Overview of Wear Phenomena in Lead Processing Furnaces", *Journal of European Ceramic Society*, Vol. 35, Issue 6, 2015, pp. 1683—1698.

The final version of this paper was published in 7th International Symposium on High-Temperature Metallurgical Processing, J-Y. Hwang, T. Jiang, P.C. Pistorius, G.R.F. Alvear F., O. Yücel, L. Cai, B. Zhao, D. Gregurek, and V. Seshadri, Eds., 2016, pp. 149-156, DOI: 10.1002/9781119274643.ch19.
Copyright 2016 by The Minerals, Metals & Materials Society.

Authors

Dean Gregurek, RHI AG, Technology Center Leoben, Austria.
Stefanie Redik, RHI AG, Technology Center Leoben, Austria.
Christine Wenzl, RHI AG, Industrial Division, Vienna, Austria
Alfred Spanring, RHI AG, Industrial Division, Vienna, Austria.
Corresponding author: Dean Gregurek, dean.gregurek@rhi-ag.com

Return to Content

RHI Bulletin > 1 > 2016, pp. 62–67

Christoph Wagner, Christine Wenzl, Dean Gregurek, Daniel Kreuzer, Stefan Luidold and Holger Schnideritsch

Experimental Study of Refractory Wear Mechanisms Caused by Molten Slags

Refractory linings in pyrometallurgical vessels are often attacked by molten metal and /or slag. The corrosion of these refractory materials results in reduced production efficiency, furnace shut-downs and a reduced refractory lifetime. To understand the reactions involved in refractory corrosion, it is very important to have an understanding of the thermodynamics and chemical equilibria behind. The present work studies high temperature interaction between refractories and molten slag comprising experimental work and theoretical thermodynamic analysis by also taking into consideration additional slag compounds.With the results, future implications for improving the refractory lifetime should be drawn by a better understanding of corrosion processes.

Introduction

Refractory performance is an important factor in furnace operations and hence requires continuous improvement to ensure process efficiency and safety. The critical question to overcome is to choose adequate lining materials under the consideration of minimizing chemical corrosion and maximizing furnace lifetimes. Refractory corrosion is caused by a combination of chemical attack, thermal, and mechanical stresses especially in the slag zone, normally the furnace area with highest refractory wear. Hence, numerous studies have been carried out to study slag corrosion phenomena in detail on lab scale [1, 2]. A deeper understanding of refractory/slag interactions is necessary to describe corrosion mechanisms more in detail and draw implications for optimizing furnace linings. The present work investigated a synthetic FeNi slag based on the system "FeO"-SiO_2-MgO [3-7], in contact with MgO refractory substrate, both on a theroretical (thermodynamic calculations using the software FactSage™ [8] and experimental (hot-stage microscopy study) basis. Additionally, the effects of different slag components on the corrosion mechanisms were analyzed.

Methodology

High temperature interactions between refractory materials and molten slags were investigated by combining the results of the hot-stage microscopy investigations with thermodynamic analysis using FactSage™ as described in the next section.

Experimental Setup and Conditions

The interaction of a molten slag in contact with a refractory substrate was investigated by using a hot stage microscope. The hot stage microscope (EMI-201; Hesse Instruments Germany) is a complete testing system designed to determine high-temperature characteristics with a measuring method based on thermo-optical analysis. Evaluation of the silhouette of a cylinder-shaped specimen is used to determine characteristic temperatures according to DIN 51730, ISO 540 and CEN/TS 15404 and 15370-1. Figure 1 shows the experimental apparatus.

The experiments were conducted by preparation of a cylindrical slag specimen of 3 mm diameter and 3 mm in height.

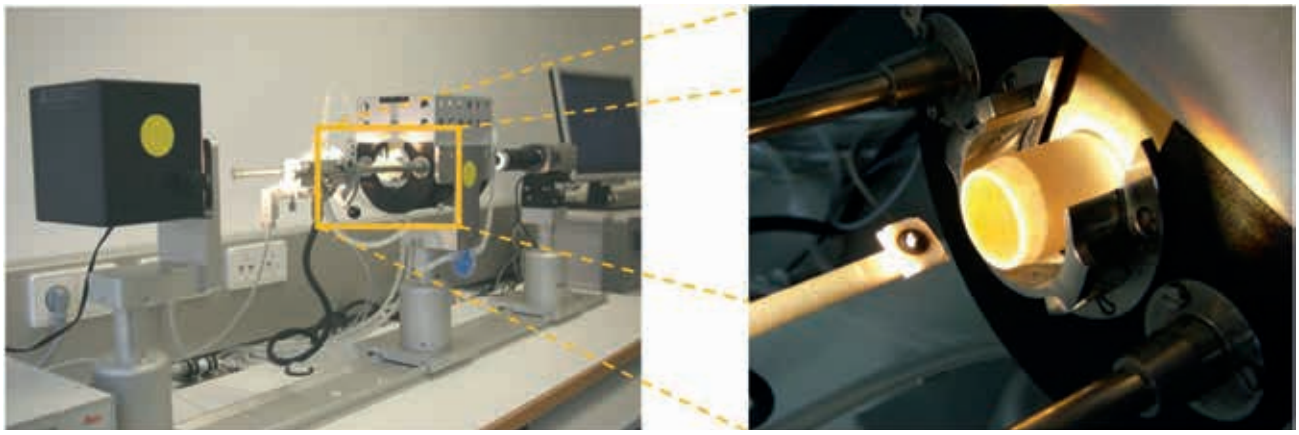

(a) (b)

Figure 1. *Configuration of hot stage microscope for high-temperature interactions, showing a) the complete device and b) the measuring chamber.*

The specimen was placed at the top centre of a refractory substrate (14x14x2 mm). The test conditions are summarized in table I.

After the investigation with the hot stage microscope the specimens were immersed in resin with hardener and then prepared to metallographic specimens. The cross sections were were examined using a scanning electron microscope (JEOL JSM-IT300 LV) equipped with an energy X-ray analyzer.

Thermodynamic Analysis

The thermodynamic calculations of the refractory/slag interface were conducted using FactSage™ (Version 6.4) with the aim to compare and simulate refractory attack caused by slag. A thermodynamic analysis of a simplified case (reduced number of oxides) and an observation of the impact of additional oxides was carried out.

Materials

Synthetically Produced Slag

In the study a synthetically produced SiO_2-Fe_2O_3-MgO slag that contained 50 wt.% SiO_2, 30 wt.% Fe_2O_3 and 20 wt.% MgO was used. The ternary system forms the basis for the slags produced during smelting of FeNi [7]. The slag was prepared by mixing and melting the pure oxides of silicon, iron, and magnesium The composition of the prepared slag is shown in the ternary SiO_2-MgO-FeO_x phase diagram in Figure 2.

Refractory Substrate

As refractory substrate a magnesium oxide plate (14x14x2 mm) was used. The chemical analysis is shown in Table II.

Corrosion Test – SEM/EDS Analysis

Polished cross sections of the slag/refractory interface after hot-stage microscopy were characterized by scanning electron microscopy (JEOL JSM-IT300 LV) with EDS. It should be noted that the following EDS analysis were not obtained from a single spot but from an interaction volume with a dimension in the µm range and offer a good qualitative statement of the chemical differences in the studied areas. The EDS mappings provide an overview of the elemental distributions in the investigated areas.

SiO_2-MgO-FeO_x System (Synthetic Slag on Refractory Substrate)

The interface between refractory material and molten slag (Figure 3) showed slag infiltration (infiltration depth of about 0.30 mm).

Heating program	RT → 1650 °C, 10 K/min
Holding period	60 min at 1650 °C
Gas flow	200 ml/min, 1 bar
Gas	CO/CO_2 mixture (60:40) – reducing conditions (p_{O_2} at 1650 °C – 1.94 x 10^{-7} atm)
Imaging	CCD camera + analysis software Starting at 600 °C every 60 seconds
RT room temperature;	

Table I. *Testing conditions of the heating microscope.*

Chemical analysis and physical properties	
MgO (wt.%)	> 99.3
CaO (wt.%)	< 0.35
SiO_2 (wt.%)	< 0.35
Fe_2O_3 (wt.%)	< 0.12
Al_2O_3 (wt.%)	< 0.25

Table II. *Chemical composition of refractory substrate.*

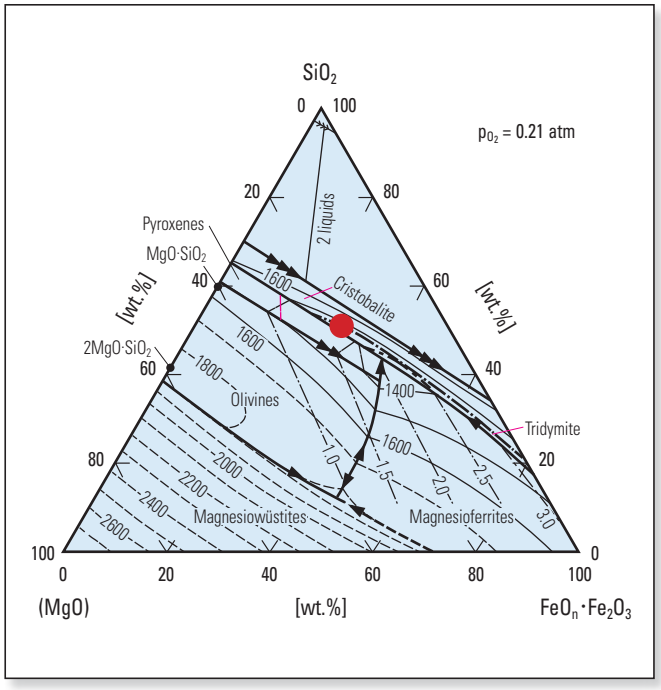

Figure 2. *Liquidus surfaces in the system FeO_x-MgO-SiO_2 in air projected on the FeO·Fe_2O_3-MgO-SiO_2 plane after Muan, Osborn. The light dash-dot lines show the Fe_2O_3/FeO ratio in the liquid at liquidus temperatures [9].*

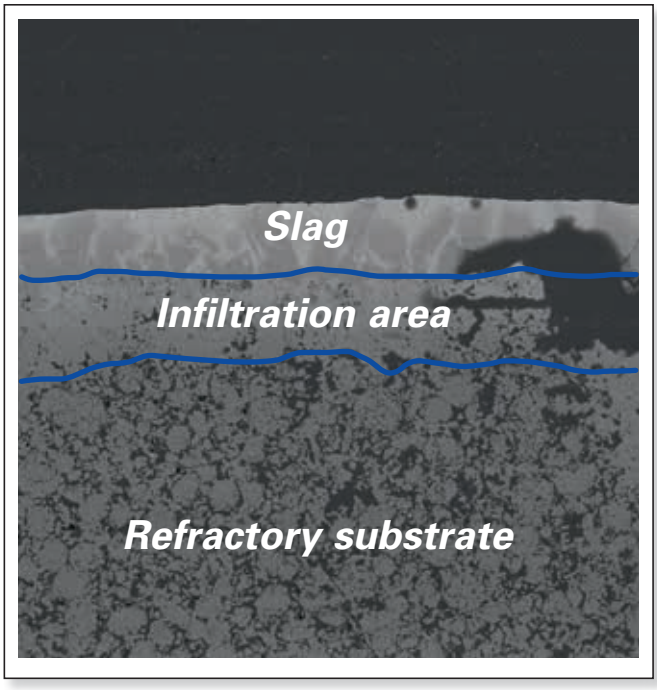

Figure 3. *SEM image of interface between refractory material and molten slag.*

In order to identify the elements present within the refractory interface area, EDS mappings of the main elements of the interface (Figure 4) and analysis of a series of spots distributed in the interface were performed (Figure 5).

In the infiltrated area, the refractory matrix fines consist of Mg, Si, and O. In contrast, all of the coarse grains surrounded by slag, are composed of Mg, Fe, and O. Si was not detected in the modified coarse grains. The MgO grains are highly enriched with Fe oxide.

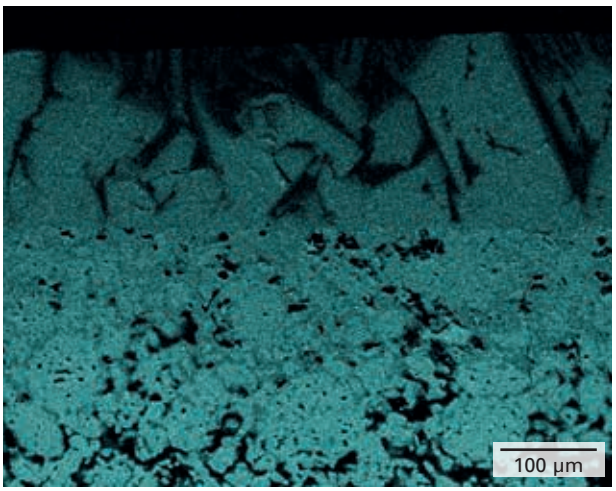

(a) Mg

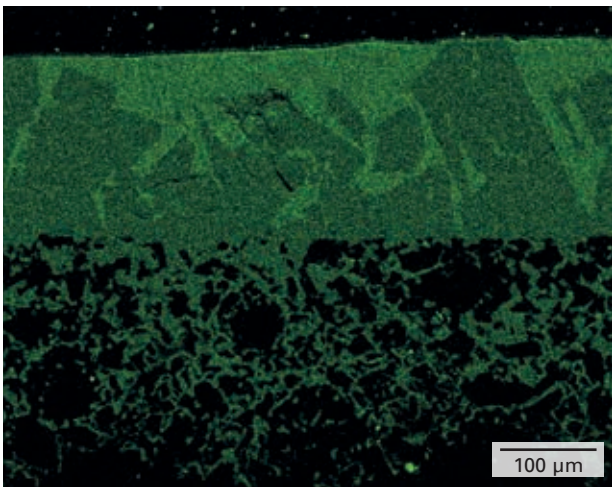

(b) Si

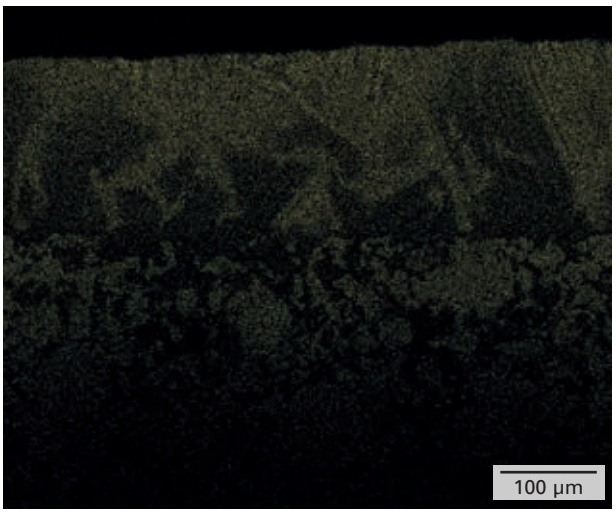

(c) Fe

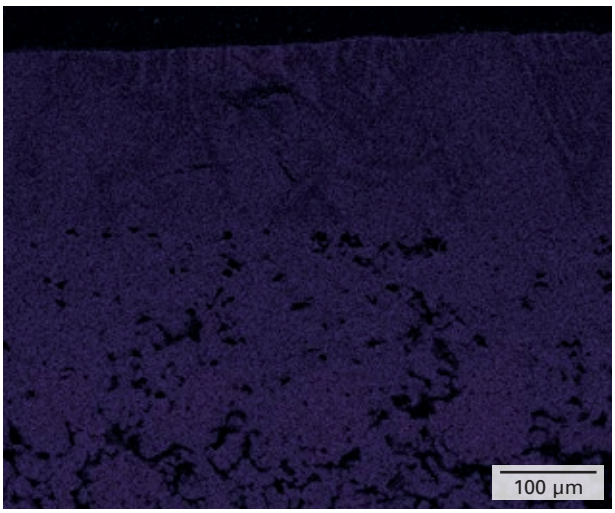

(d) Al

(e) Ca

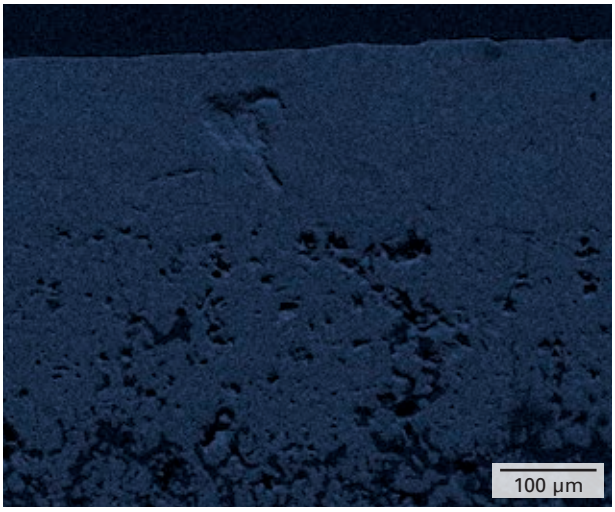

(f) O

Figure 4. *EDS mapping of interface area, Mg (a), Si (b), Fe (c), Al (d), Ca (e), and O (f).*

The ratios of the main elements analyzed are shown in Table III.

Spots 1–3 represent the compositions at different depths in "the slag".

Mg, Fe, and O dominate the spot 4 inside the MgO coarse grain, while besides Mg and O, Fe and Si are found in low concentrations in spot 5. Spot 6 shows the original composition of the coarse refractory grain. The investigation showed that primarily the Si component of the slag penetrated into the brick pores and play a crucial role in refractory corrosion reactions of the matrix fines. The amount of the SiO_2 slag component decreases at the rims of the MgO grains. The coarse grains were also slightly corroded at rims. The main reactions products include Mg silicates of type forsterite (Mg_2SiO_4). Additionally due to a high iron oxide supply the MgO was highly enriched with Fe oxide which results in a formation of low melting magnesia wuestite ((Mg,Fe)O).

Thermodynamic Calculations

Different thermodynamic calculation procedures have been applied and described to investigate refractory/slag interactions, which all have certain limitations. [10, 11] The present study proposes a new representation of results, considering phase formation as a function of temperature and the ratio between refractory and slag.The aim of additional thermodynamic calculations was to observe the role of additional oxides. All calculations were performed for a constant oxygen partial pressure with FactSage™ software.

Element	EDX spot					
	1	2	3	4	5	6
Mg (wt.%)	1.3	19.0	27.5	46.5	50.9	56.3
Si (wt.%)	26.5	16.1	16.7	-	2.6	-
Fe (wt.%)	18.3	18.7	7.5	12.1	3.0	-
O (wt.%)	53.9	46.2	48.4	41.4	43.6	43.7

Table III. *Ratios of elements at different spots analyzed by EDS.*

SiO_2-MgO-FeO_x System (Synthetic Slag on Refractory Substrate)

The system studied was a simplified case in the ternary system SiO_2-MgO-FeO_x. The refractory was composed of approximately 99 wt.% MgO and the synthetically produced SiO_2-Fe_2O_3-MgO slag contained 50 wt.% SiO_2, 30 wt.% Fe_2O_3, and 20 wt.% MgO.

In Figure 6 the resulting mineral and slag phases from FactSage™ calculations, simulating the contact zone between slag and refractory material, are displayed as a function of [MgO/(Fe_2O_3 + SiO_2)] ratio, which represents varying portions of refractory/slag and temperature. As the slag reacts with the refractory substrate, the composition of the liquid slag changes until saturation. Where the thermodynamic results show that the refractory substrate should not be further chemically attacked by the slag. The newly formed phases between slag and refractory are due to the dissolution of the refractory and precipitation of new solid phases indicates corrosion.

Considering the synthetic slag in contact with the refractory substrate the following phase assemblage at a temperature of 1650 °C can be observed:

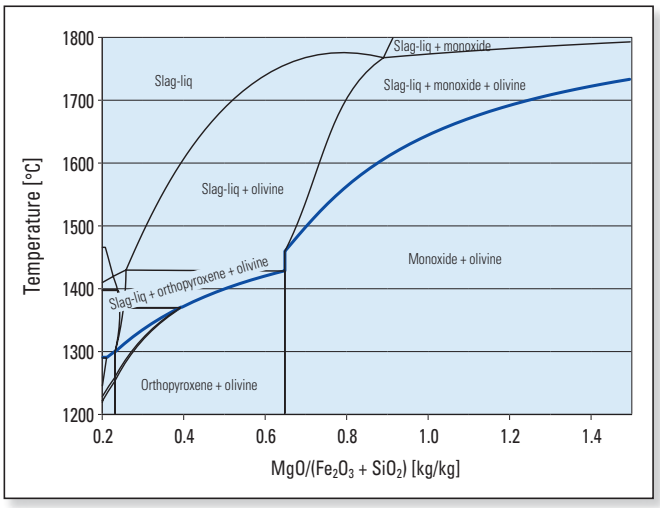

Figure 6. *Phase assemblage predicted by thermodynamic simulations for the corroded refractory substrate as a function of [MgO/(Fe_2O_3 + SiO_2)] ratio and temperature.*

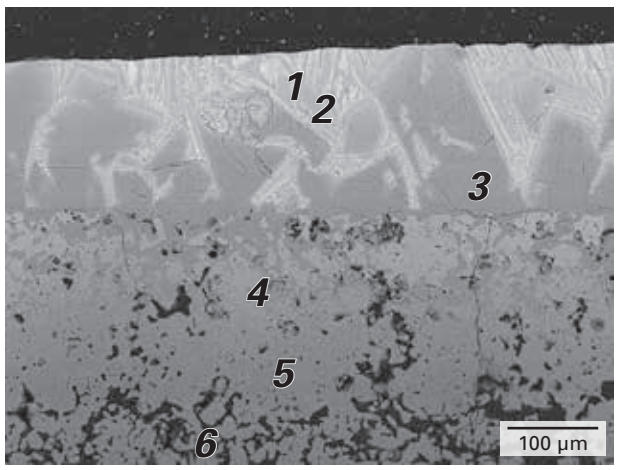

(a)

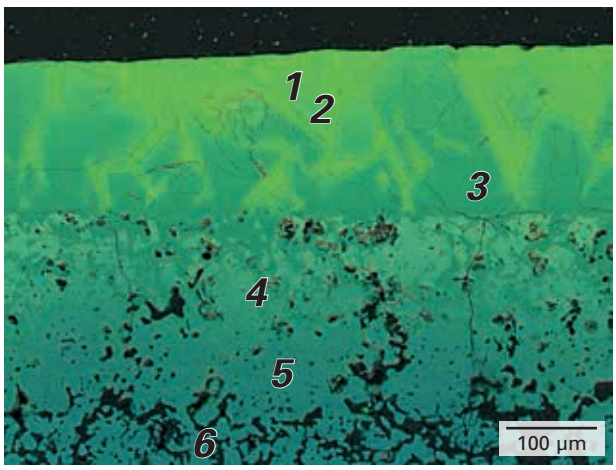

(b)

Figure 5. *Analyzed spots of interface area: (a) SEM-image of interface area and (b) superposed corresponding illustration of areas of constant element concentration based on EDS.*

For the highest ratio [MgO/(Fe_2O_3 + SiO_2)] = ∞ one phase is observed – monoxide (MgO refractory substrate).

For 1.02 < [MgO/(Fe_2O_3 + SiO_2)] < ∞ the system is composed of two phases, monoxide and olivine. The amount of monoxide decreases as [MgO/(Fe_2O_3 + SiO_2)] decreases and the amount of olivine increases.

For 0.76 < [MgO/(Fe_2O_3 + SiO_2)] < 1.02 three phases are observed (monoxide, olivine, and slag). The slag phase is in contact with two solid phases: monoxide and olivine. The weight proportion of monoxide and olivine decrease as [MgO/(Fe_2O_3 + SiO_2)] decreases and the amount of slag increases.

For 0.45 < [MgO/(Fe_2O_3 + SiO_2)] < 0.76 the system is composed of two phases, olivine and slag. Monoxide is no longer present and MgO is completely dissolved into the slag phase.

For 0 < [MgO/(Fe_2O_3 + SiO_2)] < 0.45, slag is the only phase formed.

The thermodynamic calculation shows the species monoxide, olivine, and slag which could be formed in the SiO_2-MgO-FeO_x system at a temperature of 1650 °C. It is interesting to correlate the reaction rate of the system with the evolution of the slag (the amount and composition).

When the system is composed of two solid phases and the slag, the amount of slag increases with decreasing [MgO/(Fe_2O_3 + SiO_2)] ratio and the composition of the slag becomes steady in agreement with the phase rule of Gibbs. When the system comprises one solid and the slag, the composition varies. The liquid phase could be considered as the driving force behind the corrosion phenomenon.

SiO_2-MgO-FeO_x-X System (X = CaO, Al_2O_3, Cr_2O_3, MnO or TiO_2, each 5 wt.%)

Different sub-systems (SiO_2-MgO-FeO_x-X with X = CaO, Al_2O_3, Cr_2O_3, MnO or TiO_2) were investigated:

>> SiO_2-MgO-FeO_x-CaO
>> SiO_2-MgO-FeO_x-Al_2O_3
>> SiO_2-MgO-FeO_x-Cr_2O_3
>> SiO_2-MgO-FeO_x-MnO
>> SiO_2-MgO-FeO_x-TiO_2

For the calculations a quantity of 5 wt.% of an additional slag component such as CaO, Al_2O_3 etc. was added to the slag in contact with refractory substrate.

SiO_2-MgO-FeO_x-CaO System

As an example, the resulting mineral and slag phases of the subsystem SiO_2-MgO-FeO_x-CaO (with 5 wt.% CaO addition) are shown in Figure 7 as a function of [MgO/(Fe_2O_3 + SiO_2)] ratio and temperature.

The result for 1650 °C can be divided into different zones, as shown in Figure 7, and discussed below:

For the highest ratio [MgO/(Fe_2O_3 + SiO_2)] = ∞ one phase is observed – monoxide (MgO refractory substrate).

For 0.74 < [MgO/(Fe_2O_3 + SiO_2)] < ∞ three phases are observed (monoxide, olivine and slag); the slag phase is in contact with two solid phases: monoxide and olivine. The amounts of monoxide and olivine decrease as [MgO/(Fe_2O_3 + SiO_2)] decreases and the amount of slag increases.

For 0.46 < [MgO/(Fe_2O_3 + SiO_2)] < 0.74 the system is composed of two phases, olivine and slag. Monoxide is no longer present and MgO is completely dissolved into the ≤slag and olivine phase.

For 0 < [MgO/(Fe_2O_3 + SiO_2)] < 0.46 slag is the only phase formed.

Results and Discussion

The calculations with synthethic slag in contact with refractory material show the formation of slag and two solid phases: monoxide and olivine; which could coexist in varying amounts in a system. When the system is composed of two solid phases and the slag, the amount of slag increases with decreasing [MgO/(Fe_2O_3 + SiO_2] ratio and the composition of the slag becomes steady. When the system is composed of one solid and the slag, the composition varies. The liquid phase is the driving force behind the corrosion phenomenon.

CaO additions to the slag (5 wt.%) were found to increase the phase distribution areas to lower temperatures. Liquidus temperature decreases with addition of CaO. At a constant temperature of 1650 °C, the amounts and the range of formation of the solid phases decreased with increase of CaO quantity.

Al_2O_3 additions to the slag (5 wt.%) were found to increase the phase distribution areas to lower temperatures. Liquidus temperature decreases with addition of Al_2O_3.

Cr_2O_3 additions to the slag (5 wt.%) were found to broaden the phase areas to higher temperatures. Liquidus temperature increases with addition of Cr_2O_3. At a constant temperature of 1650 °C, the amounts and the range of formation of the solid phases increased with addition of Cr_2O_3. Spinel results from the reaction of the refractory material with slag.

MnO additions to the slag (5 wt.%) did not have a significant impact on the phase distribution and liquidus formation.

TiO_2 additions to the slag (5 wt.%) were found to broaden the phase areas to lower temperatures. Liquidus temperature

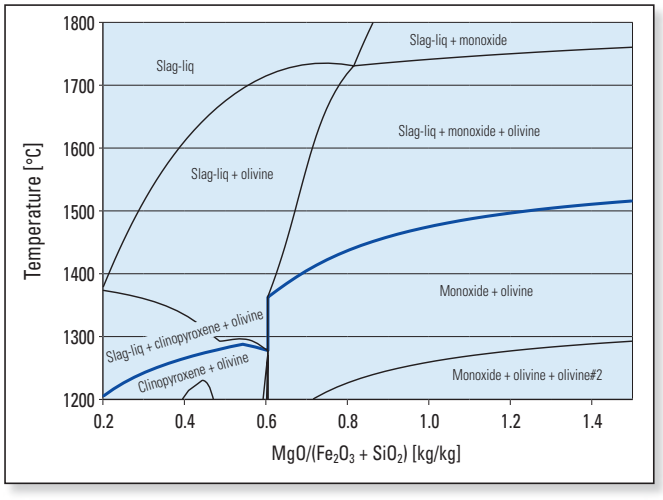

Figure 7. *Phase assemblage predicted by thermodynamic simulations for the corroded refractory substrate as a function of [MgO/(Fe_2O_3 + SiO_2)] ratio and temperature.*

decreases with addition of TiO_2. At a constant temperature of 1650 °C, the amounts and the range of formation of the solid phases decreased with increase of TiO_2 quantity.

Furthermore, the comparison of the presented subsystems indicated that the existence of different additional slag components (CaO, Al_2O_3, Cr_2O_3, MnO or TiO_2, each 5 wt.%) did not significantly shift the ratio refractory/slag given by [MgO/(Fe_2O_3 + SiO2)] for the first occurrence of a solid phase besides liquid slag (about 0.42 to 0.52) and for the first appearance of monoxide (0.73 to 0.81). Within these individual supplemented oxides, Al_2O_3 and TiO_2 show the greatest effects towards increasing attack of the refractory. Furthermore, these ratios are further shifted to 0.58 and 0.9 for the real slag. Consequently, the latter can dissolve higher portions of refractory (MgO) prior the formation of solid phases at the contact zone between liquid slag and solid refractory (monoxide phase) and also before the monoxide becomes thermodynamically stable.
The stability of the refractory (monoxide phase) and of the liquid slag without formation of solid phases as described above as a function of slag composition and temperature gives a first indication about possible chemical attack of the slag to the refractory, which will be influenced by many other parameters (wettability, viscosity, kinetics, etc.).

Conclusions

For analyzing the corrosion mechanisms of refractories, an understanding of the individual phases present in their microstructures is required. Combined investigation concepts, hot stage microscopy coupled with thermodynamic analysis, were applied to investigate these corrosion mechanisms between magnesia refractory materials and synthetic slag.

Thermodynamic calculations were carried out from simplified cases with only few oxides (synthetic slag in contact with refractory material) to systems (containing SiO_2, MgO, Fe_2O_3, CaO, Al_2O_3, Cr_2O_3, MnO, and TiO_2) as a function of reaction rate and temperature.

The characteristic of the phases predicted by the thermodynamic calculations correspond with the assumptions and results of the hot stage microscopy.

Although physical parameters such as the granulometric differences between the aggregates and the matrix, the location of these phases in the refractory microstructure, and the open porosity and permeability of the refractory material were neglected, the thermodynamic calculations directly reflect the results from the hot stage microscopy and vice versa.

However, the thermodynamic calculations are suitable for predicting the sequence of phase transformations in equilibrium and therefore are a valuable for experimental work. By combining the results of the hot stage microscopy study and the thermodynamic analysis using FactSage™, it is possible to understand refractory corrosion mechanisms in a better way and draw implication for improving the refractory performance and lifetime. Ongoing studies focus on applying the described methodology to different slag systems and refractory substrates.

Acknowledgements

The financial support by the Austrian Federal Ministry of Science, Research and Economy and the National Foundation for Research, Technology and Development is gratefully acknowledged.

References

[1] Lee, W. and Zhang, S. Melt Corrosion of Oxide and Oxide-Carbon Refractories. *Int Mater Rev* Vol. 44 (3), 1999, pp. 77–104.
[2] Gregurek, D., Ressler, A., Reiter, V., Franzkowiak, A., Spanring. A. and Prietl, T. Refractory Wear Mechanisms in the Nonferrous Metal Industry: Testing and Modelling Results. *J Miner Metals Mater Soc*, Vol. 65 (11), 2013, pp. 1622–1630.
[3] Bowen, N.L. and Schairer, J.F. The System MgO-FeO-SiO_2. *Am. J. Sci.*, Vol 29, 1935, pp. 151–217.
[4] Chen, S., Jak, E. and Hayes, P.C. Phase Equilibria in the Cristobalite, Tridymite and Pyroxene Primary Phase Fields in the MgO-"FeO"-SiO_2 System in Equilibrium with Metallic Iron. *ISIJ International*, Vol. 45, 2005, pp. 791–797.
[5] Chen, S., Jak, E. and Hayes, P.C. Phase Equilibria in the Olivine Primary Phase Field of the System MgO-"FeO"-SiO_2 in Equilibrium with Metallic Iron. *ISIJ International*, Vol. 45, 2005, pp. 1095–1100.
[6] Jak, E. and Hayes, P.C. Slag Phase Euqilibria and Viscosities in Ferronickel Smelting Slags. *The Twelfth International Ferroalloys Congress*, Helsinki, Finland, June 6–9, 2010; pp. 631–639.
[7] Diaz, C. M., Landolt, C.A., Vahed, A., Warner, A.E.M. and Taylor, J.C. A Review of Nickel Pyrometallurgical Operation. J. Met.,Vol. 40, 1988, pp. 28–33.
[8] Bale, C.W., Chartrand, P., Degterov, S.A., Eriksson, G., Hack, K., Ben Mahfoud, R., Melancon, J., Peltron, A.D. and Petersen, S., FactSage™ Thermochemical Software and Databases. *Calphad*, Vol. 26 (2), 2002, pp. 189–228.
[9] Slag Atlas 2nd edition, Edited by VDEh, Verein Deutscher Eisenhüttenleute, Düsseldorf, 1995.
[10] Berjonneau, J., Pringent, P. and Poirier, J. The Development of a Thermodynamic Model for Al_2O_3-MgO Refractory Castable Corrosion by Secondary Metallurgy Steel Ladle Slags. *Ceram. Int.*, Vol. 35 (2), 2009, pp. 623–635.
[11] Luz, A.P., Tomba Martinez, A.G., Braulio, M.A.L. and Pandolfelli, V.C. Thermodynamic Evaluation of Spinel Containing Refractory Castables Corrosion by Secondary Metallurgy Slag. *Ceram. Int.*, Vol. 37, 2011, pp. 1191–1201.

Authors

Christoph Wagner, RHI AG, Industrial Division, Vienna, Austria.
Christine Wenzl, RHI AG, Industrial Division, Vienna, Austria.
Dean Gregurek, RHI AG, Technology Center Leoben, Austria.
Daniel Kreuzer, RHI AG, Industrial Division, Vienna, Austria.
Stefan Luidold, University of Leoben, Austria.
Holger Schnideritsch, University of Leoben, Austria.
Corresponding author: Christoph Wagner, christoph.wagner@rhi-ag.com

Return to Content

RHI Bulletin > 1 > 2016, pp. 68–73

Christian Manhart, Ulrich Marschall, Gerhard Urbanek and Bernd Lorenzoni

Young's Modulus Determination of CCS Cylinders by the Resonant Frequency Method as a Basis Investigation for Round Robin Tests

A round robin test (RRT) is conducted to compare measured results of methods between different laboratories. A RRT involves significant time and money, especially in the sample preparation procedure. In this paper cylindrical cold compressive strength (CCS) samples for a round robin test which was part of the ReStaR Project [1] were investigated by nondestructive testing methods. The aim was to obtain a consistent Young's Modulus distribution for every sample batch for each participating laboratory. The application of the ultrasonic transmission measurement is time consuming to reduce the measurement uncertainty. An alternative method is the resonant frequency measurement by impulse excitation technique (IET). But the IET method has a disadvantage which is caused by the CCS sample geometry. This problem was solved by the investigations shown in this paper. A resonant frequency relation search procedure was developed and verified by different investigation methods. The resonant frequency method was successfully applied to determine the Young's Modulus of the CCS cylinders and to select the RRT samples for the ReStaR-project.

Introduction

Round robin tests (RRT) are a common tool to verify laboratories [2]. The preparation of samples for round robin test requires significant time and money. Within this study nondestructive testing methods were used to homogenize the material parameter variation of RRT samples for each laboratory to increase the efficiency of the round robin tests. The inclusion of faulty or damaged samples could result in incorrect results from the round robin test.

In this paper the cylindrical sample geometry of the tests method "cold compressive strength [3], density and porosity determination" [4] was the focus. For RRT's a large number of test-specimens are required. Refractory bricks are composed mainly of coarse ceramic components which results in a heterogeneity in the product properties. For a RRT this material property variation is not an advantage. Therefore nondestructive testing methods were selected to obtain more information about the material properties and their distribution within the samples before they were delivered to the participating laboratories. In the past the ultrasonic transmission method was applied to determine the transmission time and calculate the Young's Modulus of a cylindrical sample. The ultrasonic method has a systematic uncertainty which increases the determination time to obtain a statistically certain result. The resonant frequency method applied by the impulse excitation technique (IET) is commonly used for nondestructive material property determination. The IET method has two advantages, the low systematic error and the whole sample volume is investigated. However there is a geometric disadvantage with a CCS cylinder, the diameter to length ratio is one. Therefore, it is not possible to obtain the Young's modulus directly by the standardized IET investigation procedure.

The aim of this part of the study was to obtain the information of if, and how it is possible to determine the Young's Modulus through the resonant frequency method of CCS cylinders which have an incongruous geometry.

It was is also important to verify the applied nondestructive testing methods that have been previously published in [5].

Specimen Geometry

The CCS cylinder geometry is defined by ISO 10059 [3]. The diameter and height are both 50 mm.

Impulse Excitation Technique

With the impulse excitation technique (IET) it is possible to measure the frequency spectrum of a specimen [5]. The mechanical excitation was induced by a standardized hammer which causes a vibration of the specimen. The vibration is measured by a microphone as a time dependent signal. The signal is analyzed by fast Fourier transform (FFT), the result is a frequency spectrum shown in Figure 4 from which the resonant frequency is determined. The experimental set-up is shown in Figure 1.

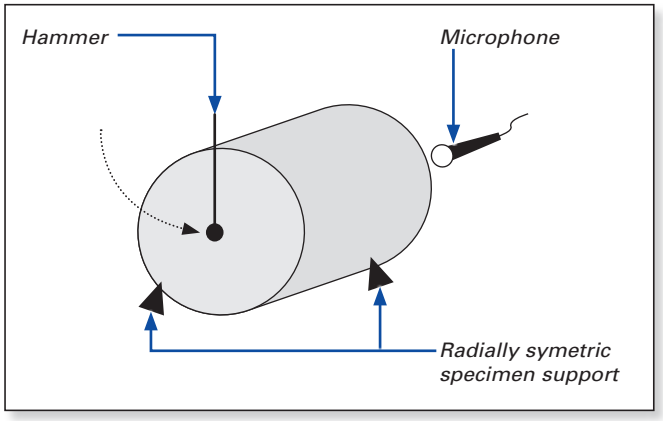

Figure 1. *Sketch of the impulse excitation testing configuration for the cylindrical specimen.*

Young's Modulus Calculation

The following Young's Modulus formulas are applicable for cylindrical shaped specimens. The calculation of the Young's Modulus E_l of the longitudinal frequency f_l [6] is described by equation (1):

$$E_l = \frac{8L^3 m {f_l}^2}{\pi r^2} \cdot T \tag{1}$$

with

$$T = \frac{1}{2L^2 - (\pi\mu r)^2} \tag{2}$$

L is the length and r is the radius of the cylindrical specimen. m is the mass and μ the Poisson ratio.

For nondestructive testing equation 3 is commonly used to calculate the Poisson's ratio μ. This definition of μ assumes an isotropic material. With the resonant frequency method the Young's modulus E and the shear modulus G can be determined for prismatic shaped specimens.

$$\mu = \frac{E}{2G} - 1 \tag{3}$$

The flexural elastic modulus E_f is calculated with equation (4) and described in [7]:

$$E_f = \frac{8\pi L^3 {f_f}^2 m}{\lambda^4 r^4} \cdot C \tag{4}$$

f_f is the flexural frequency and $\lambda = 3\pi/2$ a wavelength factor for the first order vibration and C is described by equation (5).

$$C = \frac{1}{2} + \frac{\lambda^2}{2} \cdot \frac{{i_z}^2}{L^2} \cdot \left(1 + \frac{2}{\chi}(\mu + 1)\right) + \tag{5}$$

$$+ \sqrt{\frac{1}{4} + \frac{\lambda^2}{2} \cdot \frac{{i_z}^2}{L^2} \cdot \left(1 + \frac{2}{\chi}(\mu + 1)\right) + \left(\frac{\lambda^2}{2} \cdot \frac{{i_z}^2}{L^2} \cdot \left(1 + \frac{2}{\chi}(\mu + 1)\right)\right)^2}$$

For a circular cross-section the radius of gyration is $i_z = r/2$ and the geometry dependent constant X has a value of 27/32 .

The calculated values for the factors T and C (equations 2 and 5) depend on the specimen's geometry (length L and radius r) and the Poisson's ratio μ. The CCS cylinder geometry has the length L has a dependency of two on the radius r.

Frequency and Frequency Ratio Calculations

It is also necessary to calculate the resonant frequencies from formula (1) and (4) for the following investigation steps.

The longitudinal resonant frequency f_l is solved for equation (1)

$$f_l = \frac{r}{2} \cdot \sqrt{\frac{\pi E}{2L^3 m T}} \tag{6}$$

and the flexural resonant frequency f_f is solved for equation (4).

$$f_f = \frac{\lambda^2 r^2}{2} \cdot \sqrt{\frac{E}{2\pi m L^3 C}} \tag{7}$$

Now the resonant frequency ratio f_l/f_f can be calculated with (6) and (7).

$$\frac{f_l}{f_f} = \frac{\pi}{\lambda^2 r} \sqrt{\frac{C}{T}} \tag{8}$$

T and C depend on L, r, μ. In the case of the CCS cylinders the dimension of L and $2r$ is 50 mm and it is nearly constant for each sample. In the case of these investigations the ratio f_l/f_f depends on the Poisson's ratio μ only.

For example when the sample geometry is changed through an increased length to diameter ratio the dependency of the ratio f_l/f_f from Poisson's ratio μ decreases.

Ultrasonic Transmission Measurement

The ultrasonic transmission technique [8] was used to determine the Young's modulus from the measured transmission time. In Figure 2, a schematic sketch of the measurement configuration is shown. The ultrasonic pulse signal is emitted from a transducer on one side of the sample and a second transducer, positioned on the opposite side, detects the transmitted signal. In this investigation, dry contact transducers were used. The transmission time t determined by the ultrasonic device provides information about the material properties along the ultrasonic signal path length L. The velocity v is calculated by equation 9.

$$v = \frac{L}{t} \tag{9}$$

In formula (10) the calculation of the Young's modulus is shown.

$$E = v^2 \cdot \rho \cdot \frac{(1 + \mu)(1 - 2\mu)}{1 - \mu} \tag{10}$$

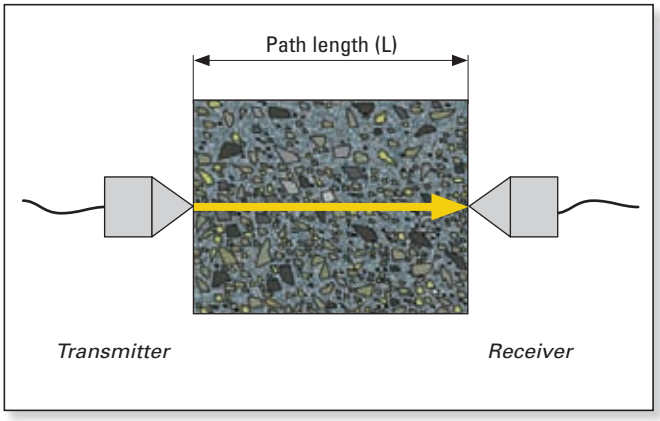

Figure 2. *Dry contact ultrasonic transmission measurement.*

Finite Element Method

The software Abaqus [9] was used to apply the finite element method for the simulation of the vibration modes of the CCS-cylinders. The vibration mode analysis and the eigenfrequency analysis were carried out. The results are shown both numerically and graphically, as a three dimensional deformation plot of the specimen.

Why is the Ultrasonic Transmission Measurement of CCS Cylinders Time Consuming?

The manual ultrasonic transmission measurement contains a systematic influence on the determined transmission time t. This influence is caused by the dry contacted point transducers, by human influence (force and position of the probes) and by the roughness of the specimen surface.

In the following example a theoretical uncertainty of the transmission time Δt (±0.05 µs, ±0.1 µs and ±0.2 µs) was used for model calculations of E [GPa] from the ultrasonic Young's modulus formula shown in equation 10. For each combination of an uncertainty value Δt and ultrasonic transmission time t the coefficient of variation of the Young's modulus value was calculated. The results are shown in Figure 3.

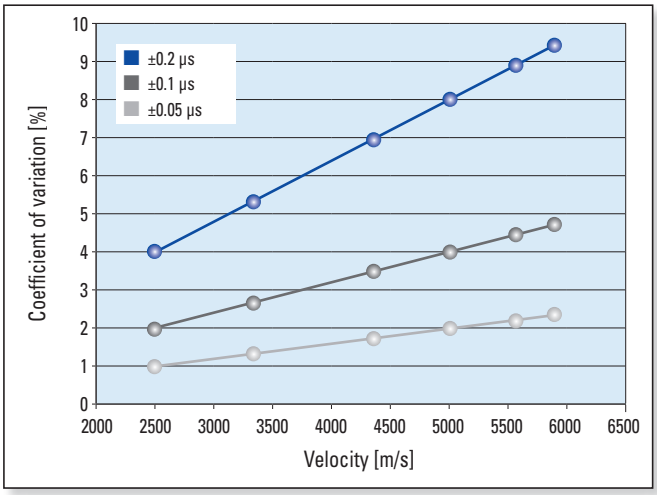

Figure 3. *Coefficient of variation of the Young's Modulus value of ultrasonic transmission measurements of CCS cylinders for an uncertainty of the transmission time of ±0.05 µs, ±0.1 µs and ±0.2 µs in dependency of the ultrasonic velocity v.*

For an ultrasonic measurement uncertainty of ±0.05 µs the coefficient of variation of the Young's modulus value increases from 1% at 2500 m/s to 9.4% at 5882 m/s and an ultrasonic measurement uncertainty of ±0.2 µs. The coefficient of variation of the Young's modulus value increases at this example at 8.4%. This analysis clearly shows strong dependency of the coefficient of variation of the Young's modulus value from the ultrasonic measurement uncertainty and the ultrasonic velocity.

The reduction of this uncertainty to a 99.7% confidence level, requires the repeated measurement of a sample. To increase the statistical certainty it is also important to keep the uncertainty value Δt of the transmission time as low as possible. This leads to increased total measurement time of a sample. In this example it is shown how the effort for sample production increases when the ultrasonic method is used. Therefore, an alternative nondestructive method was required and found in the impulse excitation method.

What is the Advantage of the IET Method Applied at CCS Cylinders?

The impulse excitation method measures the whole specimen volume in one step and the measurement uncertainty is low [5]. In comparison to this the ultrasonic transmission measurement technique requires several measurement points on the cross sectional area of the cylinder to decrease the uncertainty and obtain an average value.

Why it is Difficult to Determine the Resonant Frequency of a CCS Cylinder?

In a refractory cylinder with a CCS geometry (50x50 mm) a mechanical vibration described in Figure 1 causes a frequency spectrum with a number of high amplitude peaks (Figure 4). Where at every peak between 50 kHz and 70 kHz the Young's modulus formulas (1) and (4) are applied, it is possible to obtain a number of plausible results. But it is not possible to assign the specific vibration mode to a high amplitude peak of the frequency spectrum.

In Figure 5 the frequency spectrum of a steel cylinder is shown. Here a frequency spectrum characteristic was found which is similar to the frequency spectrum of a refractory cylinder (Figure 4).

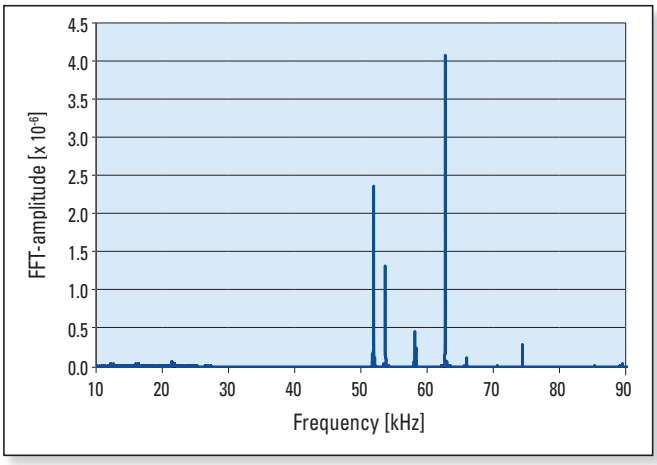

Figure 4. *Frequency spectrum example of a refractory CCS cylinder which shows a number of peaks. Between 50 kHz and 65 kHz four high amplitude peaks were found.*

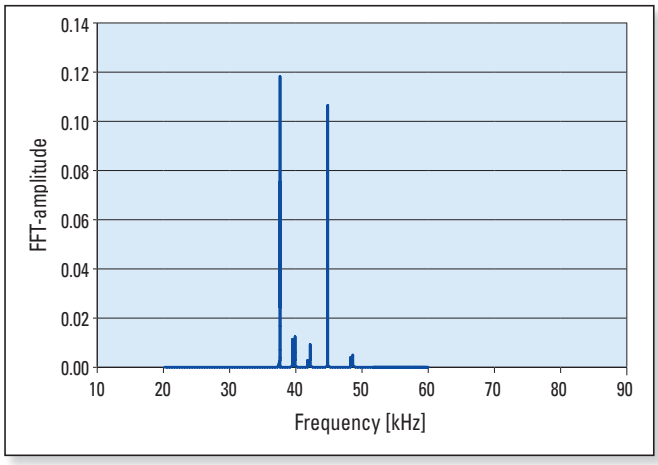

Figure 5. *Frequency spectrum example of a steel CCS cylinder.*

The comparison of Figure 4 and 5 shows that the characteristics of the frequency spectrum are influenced more by the sample geometry than by the material type.

The Investigation Procedure

The following investigation used the impulse excitation method for frequency spectrum and resonant frequency ratio determination. Finite element simulation was used to identify vibration modes and frequencies. Calculation of the frequencies using common formulas, and the dry contact ultrasonic measurement. The results of all investigation methods were correlated with the resonant frequency ratio method for verification.

Finite Element Simulation

The finite element simulation was done for three Young's modulus values of 30, 60, and 90 GPa and a Poisson ratio value of 0.15. At each Young's modulus value a large number of vibration modes were found. The frequencies of the longitudinal and flexural vibration mode were searched manually.

Figure 6a shows the longitudinal mode and Figure 6b and 6c show two variations of the flexural mode.

The numerical results of the finite element simulation show that the ratio values of f_a/f_b are identical (1.194) for 30 and 60 GPa, but at 90 GPa the ratio value is 1.173 (Table I). This was caused by the finite element computation software which stopped the computation procedure too early.

Frequency Calculation and Frequency Ratio f_l/f_f Results

The longitudinal and flexural resonant frequencies were calculated for the cylindrical specimens using the formulas (6) and (7). Table II shows the frequencies for a Young's modulus variation from 30 to 90 GPa and a Poisson's ratio of 0.15.

Figure 7 shows the dependency of the frequency ratio f_l/f_f from the Poisons ratio μ calculated using equation 9.

E [GPa]	f_a [Hz]	f_b [Hz]	f_a/f_b
30	30031	25147	1.194
60	42471	35564	1.194
90	52016	44326	1.173

Table I. *Finite element simulation results (resonant frequency) for Young's modulus values of 30, 60, and 90 GPa and the frequency ratio f_a/f_b.*

E [GPa]	f_l [Hz]	f_f [Hz]	f_l/f_f
30	31405	26010	1.208
60	44403	36755	1.208
90	54408	45031	1.208

Table II. *Frequency calculation results of the longitudinal frequency f_l and the flexural frequency f_f and the frequency ratio f_l/f_f.*

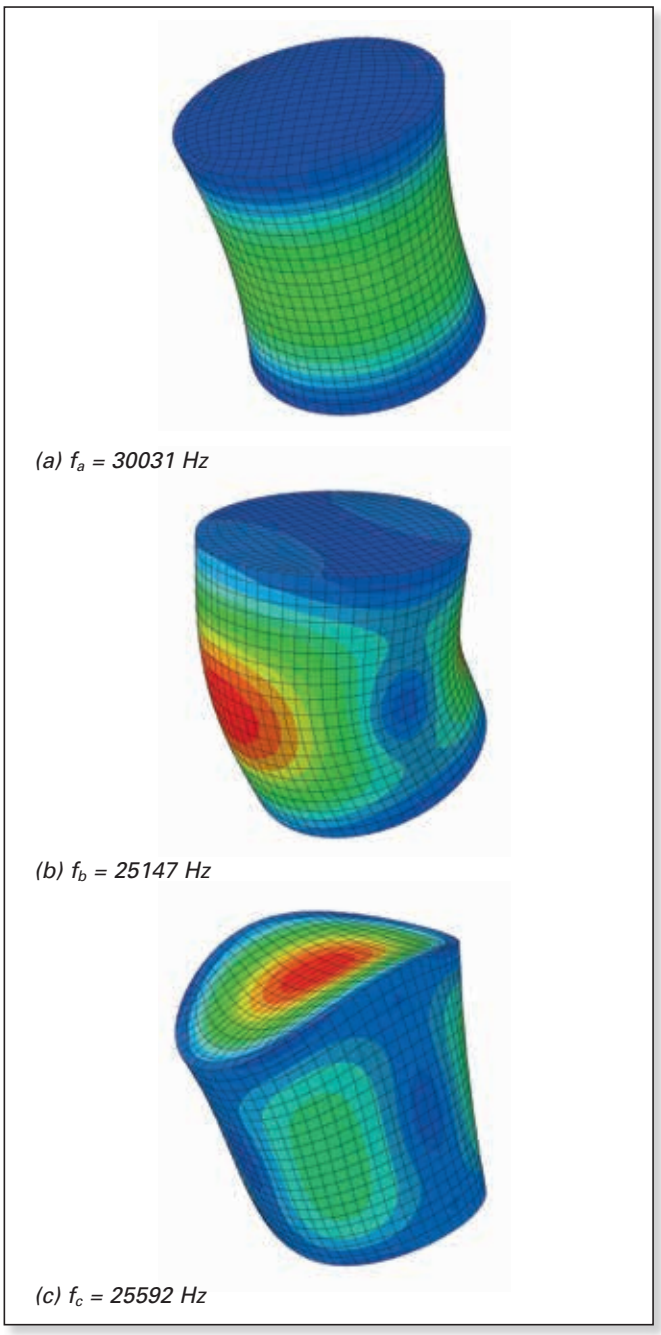

(a) f_a = 30031 Hz

(b) f_b = 25147 Hz

(c) f_c = 25592 Hz

Figure 6. *Finite element simulation example for an elastic modulus of 30 GPa. The longitudinal mode is shown in a) and the flexural modes in b) and c).*

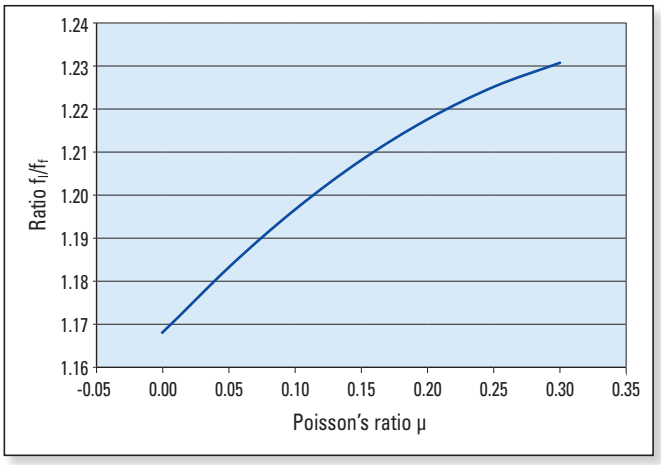

Figure 7. *Dependency of the frequency ratio f_l/f_f on the Poisson's ratio μ.*

Comparison of Frequencies Determined by Simulation, Calculation and IET Measurement

Figure 8 shows the resonant frequency results of the finite element simulation, calculation of the frequency using the Young's modulus formulas and IET measurement of several CCS samples of different refractory types. The IET result was obtained by frequency ratio identification (Table II) to obtain the frequencies with the specific vibration mode. A good correlation between all methods for the frequency was found.

Results of Resonant Frequency Ratios of Different Refractory Types

Figure 9 shows measurement results of frequency ratio f_l/f_f of seven different refractory types with a total number of 178 cylinders.

The statistical analysis of the raw data results showed 75% of all f_l/f_f ratio values were between 1.202 and 1.229. The median and average values are between 1.216 and 1.211. This correlates well with the frequency ratio values calculated in Table I and II and shown in Figure 7. The frequency ratio value can also be used to detect outliers and after a number of repetition measurements to discard a specimen from the sample batch.

Verification of the Young's Modulus Determined by the Frequency Ratio Method with Ultrasonic Measurement

The aim of this part of the investigation was to verify the Young's modulus determined by the IET frequency ratio method with the results of the ultrasonic transmission method. The selected refractory material has a wide Young's modulus variation range (from 15 GPa and 120 GPa). Figure 10 shows the correlation between both methods, the value of the determination coefficient is 0.949, resulting in a good correlation.

Conclusion

It was possible to determine the elastic modulus of cold compressive strength cylinders using the resonant frequency ratio method. The ratio method identifies resonant

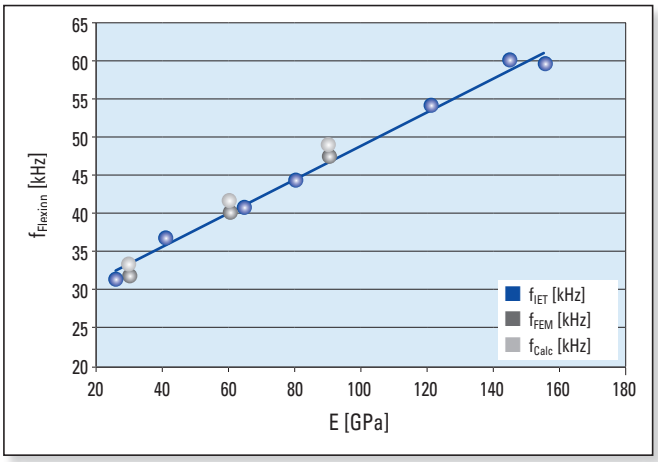

Figure 8. *Flexural frequencies $f_{Flexion}$ versus Young's modulus E. f_{Calc} is calculated using the equation (7), f_{FEM} is determined using finite element simulation and f_{IET} is measured by the IET method on cylindrical samples.*

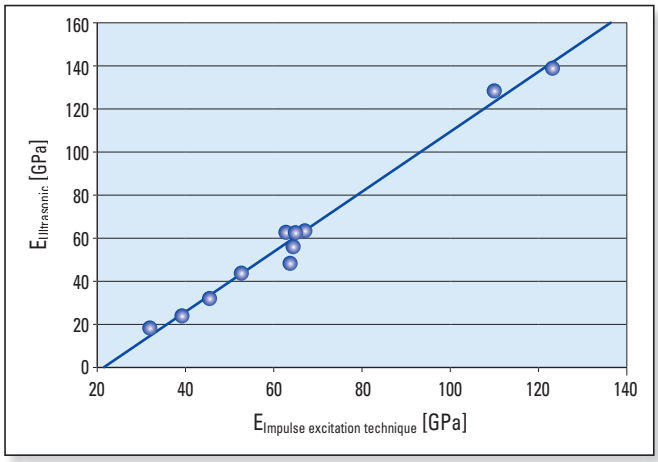

Figure 10. *Ultrasonic Young's modulus versus frequency ratio based IET longitudinal Young's modulus determination.*

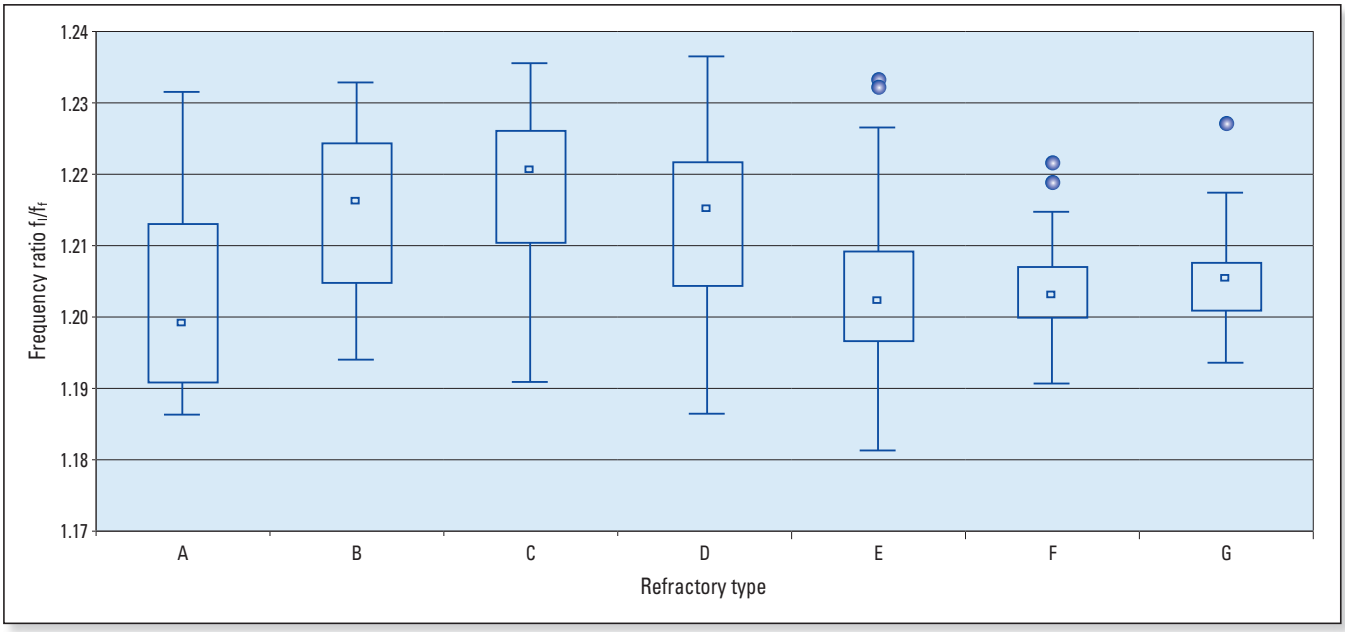

Figure 9. *Box plot of frequency ratios f_l/f_f of 7 refractory types with a total number of 178 cylinders.*

frequencies in the frequency spectrum which was determined by the impulse excitation technique.

The resonant frequency method determines the Young's modulus of the whole CCS cylinder volume in a nondestructive test. The destructive CCS test also determines the cold compressive strength of the whole cylinder volume. The volume based analysis allows for a better comparison between the nondestructive and the destructive measurement method and ensures that samples selected for round robin testing are as homogeneous as possible.

Another result of the resonant frequency relation method was the possibility to estimate the Poisons ratio of a CCS cylinder. The resonant frequency relation method saves money at the RRT sample production procedure because the measurement time and the determination uncertainty of the Young's modulus in comparison to the ultrasonic transmission method were decreased.

Within the ReStaR project the resonant frequency relation method was successfully applied to obtain a similar material parameter distribution for each sample batch for the round robin tests.

References

[1] Dannert, C. ReStaR – Collaborative R&I in the European Refractory Sector to Review and Improve Testing Standards. *Refractories WORLDFORUM*, Vol. 5, Issue 4, 2013.

[2] Urbanek, G. and Uhlig, S. Importance, organization and evaluation of interlaboratory tests. 56th International Colloquium on Refractories 2013, EUROGRESS, Aachen, Germany, September 25–26, 2013.

[3] ISO 10059-2:2003. Dense, shaped refractory products – Determination of cold compressive strength. International Organization for Standardization, Geneva, Switzerland. http://www.iso.org/iso/catalogue_detail.htm?csnumber=36154

[4] ASTM C830-00, Standard Test Methods for Apparent Porosity, Liquid Absorption, Apparent Specific Gravity, and Bulk Density of Refractory Shapes by Vacuum Pressure, ASTM International, West Conshohocken, PA, 2000, www.astm.org

[5] Manhart, C. and Urbanek, G. Investigation and Verification of the Ultrasonic and Resonant Frequency Measurement Methods for Burned Refractory Products With Original Geometry and an Application Example, Presented at 56th International Colloquium on Refractories 2013– Refractories for Industrials, Aachen, Germany, September 25–26, 2013.

[6] Lord, .J.D, and Morrell, R. Elastic modulus measurement. *Measurement Good Practice Guide*. No. 98, February 2007, National Physical Laboratory, Middlesex, 2007.

[7] Martinček, G. Nedeštruktívne dynamické metódy skúšania stavebných materiálov. (Dynamic non-destructive methods of testing of construction materials) Academia, Bratislava, 1962.

[8] Manhart, C., Schickert, M., and Urbanek, G. Ultrasonic Imaging of Refractories Using Different Coupling Techniques, *RHI Bulletin*. 2013, No. 1, 67–73.

[9] Abaqus 6.14 Analysis User's Guide Volume II: Analysis, Dassault Systèmes, Vélizy-Villacoublay, France. http://www.3ds.com

Authors

Christian Manhart, RHI AG, Technology Center, Leoben, Austria.
Hans Ulrich Marschall, RHI AG, Technology Center, Leoben, Austria.
Gerhard Urbanek, RHI AG, Technology Center, Leoben, Austria.
Bernd Lorenzoni, RHI AG, Technology Center, Leoben, Austria.
Corresponding author: Christian Manhart, christian.manhart@rhi-ag.com

Return to Content

RHI Bulletin > 1 > 2016, pp. 74–77

Thomas L. Drnek

Life Cycle Impact Assessment and Raw Materials

Despite 20 years of research, there remains no robust, globally agreed upon method, or even problem statement, for assessing mineral resource inputs in life cycle impact assessment (LCIA). As a result, inclusion of commonly used methods such as abiotic depletion potential (ADP) in life cycle assessment (LCA)-related evaluation schemes could lead to incorrect decisions being made in many applications.

This paper evaluates the current body of work in LCIA with regard to "depletion potential" of mineral resources. Viewpoints from which models were developed are described and analyzed. The assumptions and data sources that underlie currently used methods have been examined. The use of ore grades, prices, and economic availability in LCIA was reviewed.

Introduction

The tool of life cycle impact assessment was first developed some decades ago. The aim is to analyse or measure the effect of the environmental impact of any consumption or production activity. The focus of the environmental impact is climate change, but other issues can be considered too relevant to disregard. LCA has become an essential tool for industry in a wide variety of sectors to help demonstrate sustainability. The current model exaggerates the environmental consequences of using metals and minerals.

With respect to the impacts on natural resources, the general discussion on the LCIA begins and ends with the issue of depletion, "we will run out of raw materials" similar to the Club of Rome report from the 1970s. Through efforts to make such LCIA results "meaningful", economic data has often been used and the original focus of the LCIA (the environmental impact) has been lost. So the question has become one of availability of raw materials: will we run out of raw materials and/or what potential is left in the short to medium term? Different approaches have been developed, but still need to be verified, accepted for future use in LCIA, or indeed rejected.

For any assessment of availability, we have to start with the analysis of raw material stocks. And when we start there we find different terms: reserves, resources, and occurrences. There are a lot of LCIA models, many of which analyse reserves and resources as the total stock.

From Crustal Content to Mineral Reserves

Identification of mineral reserves is very often done with the approach of CRIRSCO (e.g., the "JORC-Code"). On the one hand, we have the geological information, on the other we have the so called "modifying" factors meaning mainly, but not only, costs. In this case, only occurrences that shows a positive economic result and have a high level of geological confidence will be classified a reserve. The key factor is the assumed price! However the prices of all raw materials fluctuate both in the short term and in the long term. This creates the effect that the reserves/resources data are not sufficiently stable to form a LCIA, (Figure 1).

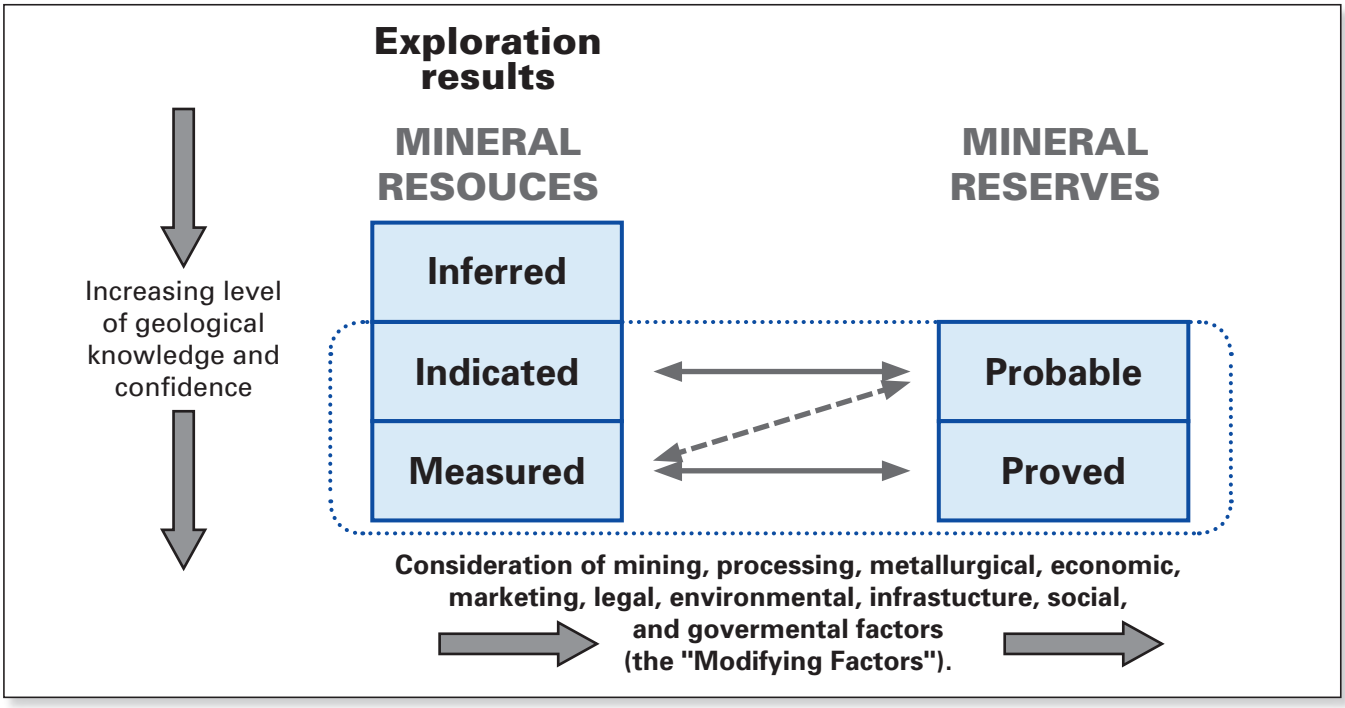

Figure 1. *General relationship between exploration results, mineral resources, and mineral reserves. Source: CRIRSCO.*

When looking beyond the scope of CRIRSCO compliant codes, we find the situation that is shown in figure 2. In the center (the shaded area) the situation is as analysed above. On the upper end is the technosphere and on the lower end the crustal content. The accuracy (or the variability) of the factor differs in the technosphere, (reserves, resources, and the as yet unidentified deposits), such that they can provide no stable basis for further analysis in LCA. The crustal content on the other hand remains constant and has been established, for all elements for roughly a century. This data can be found on any good periodic table. The average values are also known as the "Clarke Values", named after Mr. F. W. Clarke, who performed the initial research in this field. He was head of the Chemistry Department of the USGS and supervised the analysis of approximately 6000 rock samples from 1880 to 1908 to determine the average percentage composition of the earth's crust. The values were further analysed and more data was collected and published however the variation in values is negligible. These values therefore provide an optimal value for any long lived assessment of impacts on the total natural resource [1].

Another approach could be built upon the opportunity cost world view: that says that if the production costs of a particular raw material were to significantly increase over the long term, new opportunities or materials to fulfill their function would arise as a result of the interplay between raw material prices (demand) and production costs (supply). Many such opportunities continuously occur as society continues to innovate, with decisive implications for exploration, extraction, and use of natural resources.

The GDP/GNP is not constantly growing, it generally has a cyclical trend, that starts with an upturn followed by a boom and ends with a recession that can lead to a depression. But the GDP/GNP has a general long term growth trend. In figure 3 the long term production capacity growth is also shown. It is clear, that during a boom shortages can occur, leading to high prices, with the effect that occurrences can become a reserve and in the recession the opposite is true. That can be summarized, by the following points:

>> Price changes with demand in economic cycles.
>> The distance between the GNP line and the capacity of production provides a measure of the availability of the raw material on the market.
>> Market demand and perceptions of this short-term availability determine metal prices and directly affect reported mineral reserves.
>> Raw material prices are directly impacted by technological progress and less predictable socio-economic movements, which do not lend themselves well to characterization in LCA.

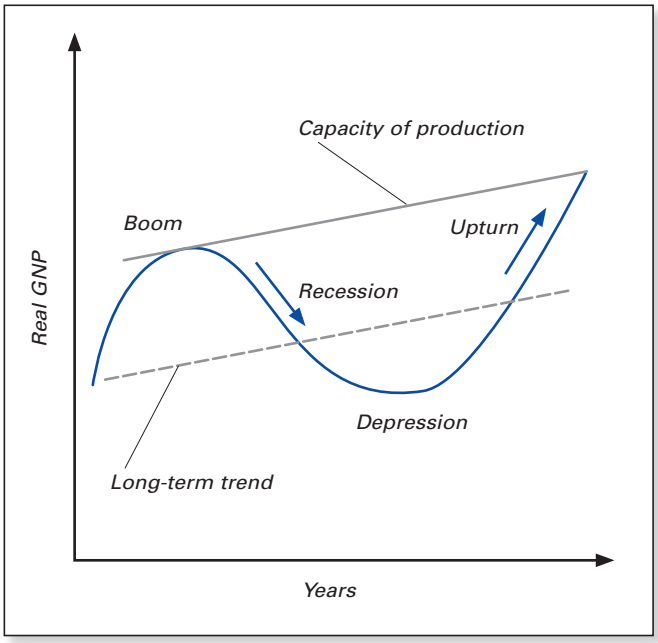

Figure 3. *Metal demand with economic cycles.*

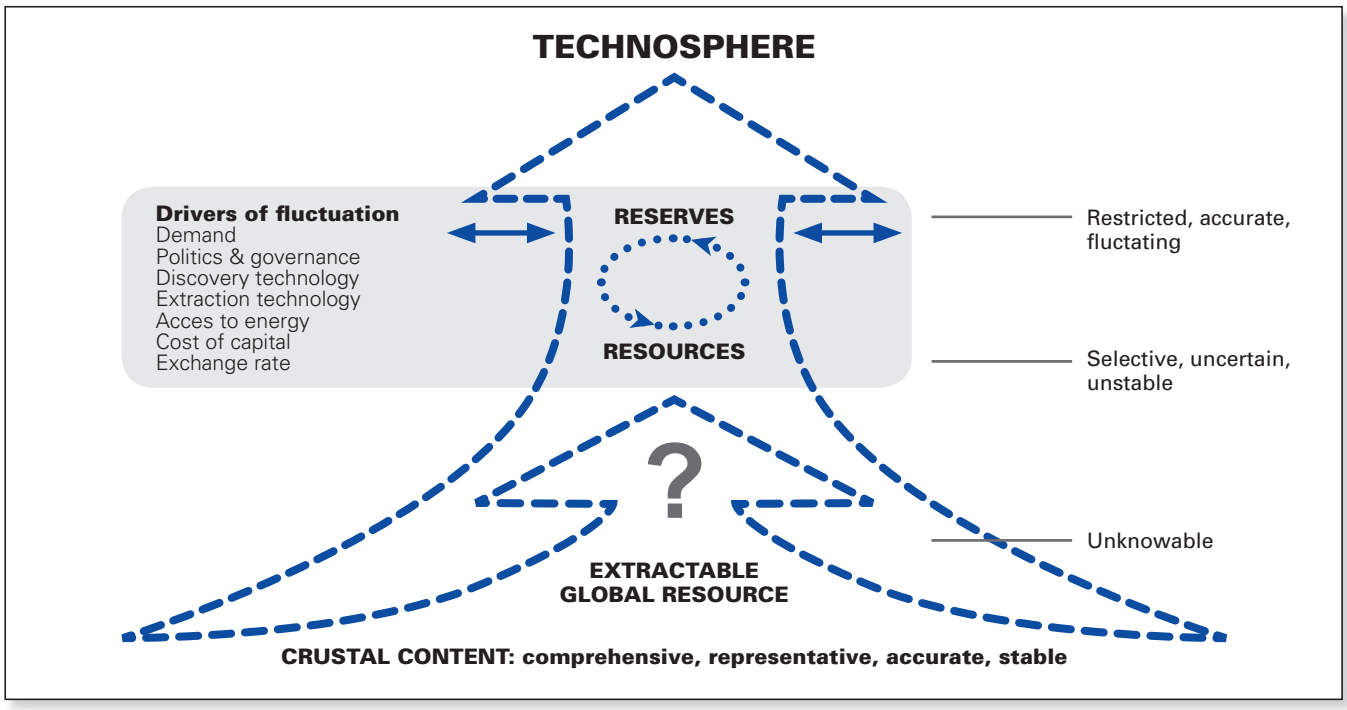

Figure 2. *Depiction of the relationship between crustal content, resources, reserves, and the technosphere [1].*

>> Therefore the contention that observed short-term raw material price trends are evidence of resource depletion cannot be relied upon.
>> It is not possible to reliably estimate the total extractable portion of the crustal content for any metal or mineral.

Economic reserves change annually in response to demand, exploration and supply cycles, politics, and socioeconomic trends [2]. For example:

The iron ore reserve base has fluctuated over recent years, together with market demand as a result of frequent reviews of the estimate; meanwhile, the USGS estimate of total world resources has remained unchanged (Figure 4).

Copper reserve base has continually increased over the same period as a result of frequent reviews of the estimate. Meanwhile, the USGS estimate of total world resources has tripled (Figure 5).

Crustal Content — the "Real" Fixed Stock

"Crustal content is a stable, comprehensive dataset, with which a physical estimate of resource depletion for abiotic resources – if desired and/or useful – could be estimated" [2].

The fixed stock and opportunity cost approaches offer assessments for different timeframes, meaning, when we look at the short term (some years, there is a lot of data available from commercial analysts), when we consider the very long term, meaning centuries, the crustal content provides the best reference (Figure 6). LCIA is traditionally constructed to consider environmental impacts that are relevant at all times and, due to its massive data requirements, is not readily repeatable.

The ongoing discussion (see http://www.euromines.org/events/2015-10-14-mineral-resources-lcia-mapping-path-forward), shows that the focus of LCIA has become lost. It is no longer clear to all, what the purpose currently is or what it should be. In many cases, environmental impact is not analysed – only the question: "can we access the raw materials on today's market?" This is the field of geopolitics and economic availability of raw materials rather than environmental impact assessment.

When considering data, it is easy to see, that the quantities are not constant, they are influenced by many factors (price, geology, etc.). Only the crustal content remains an undisputed environmental fact (Figure 5).

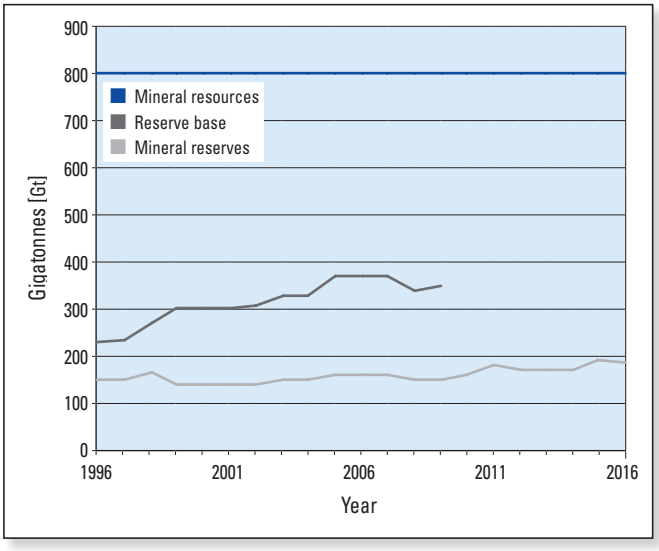

Figure 4. *Comparison of USGS reported data for iron ore.*

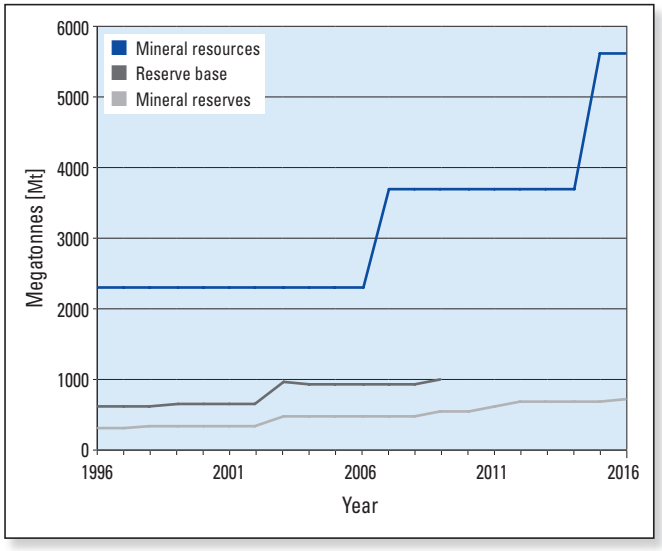

Figure 5. *Comparison of USGS reported data for copper.*

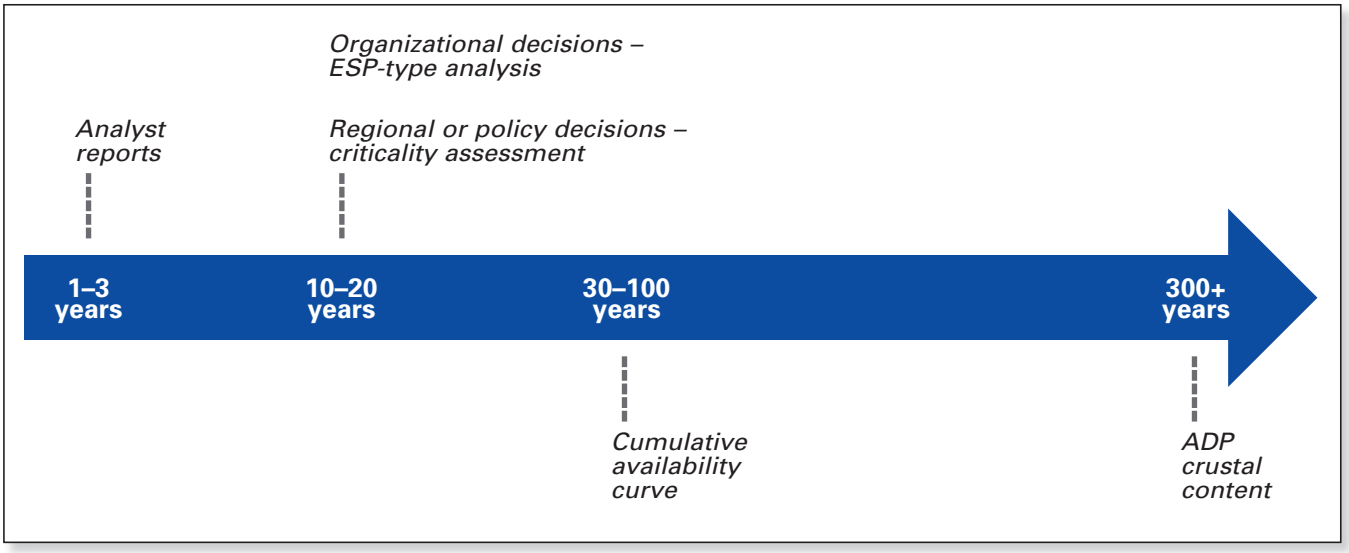

Figure 6. *Depletion and availability assessment tools by applicable time frame [2].*

Conclusions

The economic issue of resource availability should be evaluated in parallel with traditional LCA, not within. LCIA developers should look to economists, the market, and society in general, for broader assessments that consider shorter time periods than the traditional LCIA methods. To do so, the concept of which compartment of the environment (or the economy, or society) should be protected from potential impacts needs to be redefined for Life Cycle Sustainability Assessment (LCSA) to ensure that models estimate what is intended. Ideally, this should contribute to a full "net benefit assessment" of products and processes in economic, environmental, and social terms. Some recommendations regarding mineral resource assessment over various timeframes are provided in the full paper to ensure that future research has a sound basis and practitioners can incorporate the appropriate tools in their work.

References

[1] Clarke F. W. Analyses of Rocks and Minerals from the Laboratory of the United States Geological Survey. 1880 to 1908. USGS Bulletin 419. Department of the Interior, USGS, Washington 1910, p 323.

[2] Drielsma, J. A., Russell-Vaccari, A. J., Drnek, T., Brady, T., Weihed, P., Mistry, M. and Perez-Simbor, L. Mineral Resources in Life Cycle Impact Assessment—Defining the Path Forward. *Int J Life Cycle Assess*, 2015, published online: 09 November 2015.

[3] Weihed, P., Drielsma, J. A., Russell-Vaccari, A. J., Drnek, T., Brady, T., Mistry, M. and Perez-Simbor, L. Life Cycle Impact Assessment of Mineral resources: Potential paths forward and some dead-ends. Presentation: Workshop Mineral Resources in LCIA: Mapping the path forward; http://www.euromines.org/system/files/events/2015-10-14-mineral-resources-lcia-mapping-path-forward/6-drivers-and-needs-vaccari-2015-workshop.pdf.

This article summarises the 2015 International Journal of Life Cycle Assessment article "Mineral resources in life cycle impact assessment—defining the path forward" by Drielsma, J. A., Russell-Vaccari, A. J., Drnek, T., Brady, T., Weihed, P., Mistry, M., and Perez Simbor, L. distributed under the terms of the Creative Commons Attribution 4.0 International License (http://creativecommons.org/licenses/by/4.0/). [2].

Author

Thomas L. Drnek, RHI AG, Breitenau, Austria.
Corresponding author: Thomas L. Drnek, thomas.drnek@rhi-ag.com

Return to Content

RHI GLASS – Reliable partner of the glass industry

An ever increasing number of glass manufacturers trust in the expertise, experience and service of RHI GLASS in order to meet the increasing requirements by the global market.

Based on a comprehensive product portfolio and intensive R&D activities, RHI GLASS offers

- high-grade refractory products and solutions
- dedicated services alongside the furnace campaign
- complete packages from one source

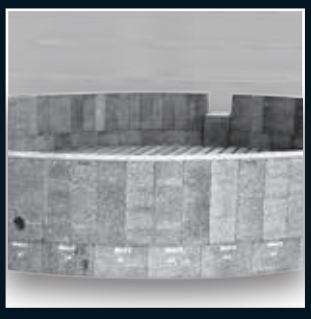

www.rhi-ag.com **EXCELLENCE IN REFRACTORIES**

RHI
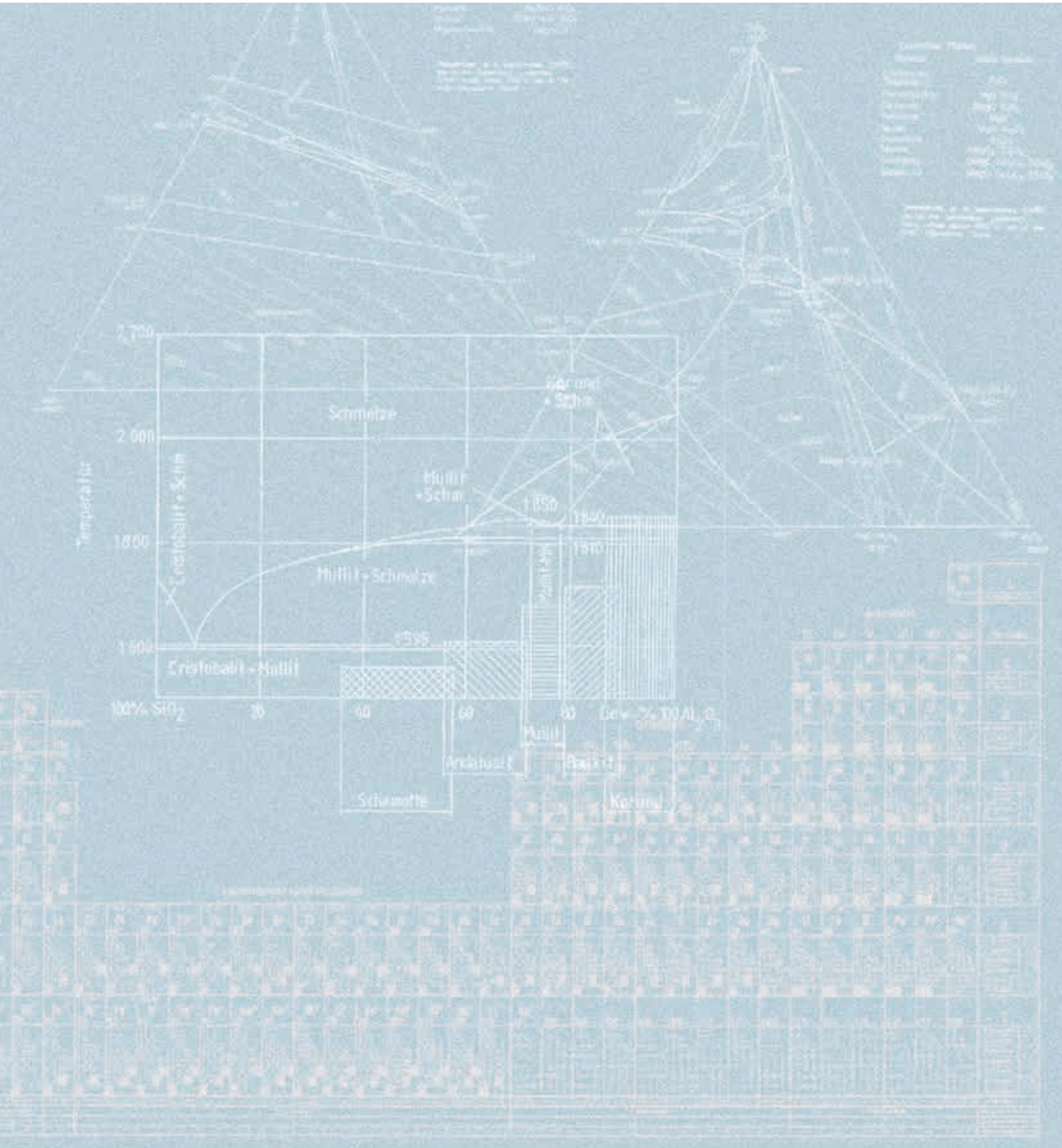
RHI Bulletin >1>2016